



HAL
open science

CONTRIBUTION TO PERSONALIZED FINITE ELEMENT BASED MUSCULOSKELETAL MODELING OF THE LOWER LIMB

Bhriugu Lahkar

► **To cite this version:**

Bhriugu Lahkar. CONTRIBUTION TO PERSONALIZED FINITE ELEMENT BASED MUSCULOSKELETAL MODELING OF THE LOWER LIMB. Biomechanics [physics.med-ph]. HESAM Université, 2020. English. NNT : 2020HESAE070 . tel-03165043

HAL Id: tel-03165043

<https://pastel.hal.science/tel-03165043>

Submitted on 10 Mar 2021

HAL is a multi-disciplinary open access archive for the deposit and dissemination of scientific research documents, whether they are published or not. The documents may come from teaching and research institutions in France or abroad, or from public or private research centers.

L'archive ouverte pluridisciplinaire **HAL**, est destinée au dépôt et à la diffusion de documents scientifiques de niveau recherche, publiés ou non, émanant des établissements d'enseignement et de recherche français ou étrangers, des laboratoires publics ou privés.

**ÉCOLE DOCTORALE SCIENCES DES MÉTIERS DE
L'INGÉNIEUR**
[Institut de Biomécanique Humaine Georges Charpak – Campus de Paris]

THÈSE

présentée par : **Bhriku Kumar LAHKAR**

soutenue le : **14 décembre 2020**

pour obtenir le grade de : **Docteur d'HESAM Université**

préparée à : **Arts et Métiers, Sciences et Technologies**

Spécialité : **Spécialité du diplôme**

Contribution à la modélisation musculosquelettique personnalisée du membre inférieur par éléments finis

THÈSE dirigée par : **Mme SKALLI Wafa**
et co-encadrée par : **Mme THOREUX Patricia et M. ROHAN Pierre-Yves**

Jury

M. Yohan PAYAN , Directeur de Recherche CNRS, Laboratoire TIMC IMAG, Université Grenoble Alpes	Rapporteur et Président
M. Sébastien LUSTIG , Professeur des Universités/Praticien Hospitalier, Service de Chirurgie Orthopédique, CHU Lyon Croix-Rousse, Hospices Civils de Lyon	Rapporteur
Mme Valentina CAMOMILLA , Maître de Conférences, Département des sciences du mouvement, de l'homme et de la santé, Université de Rome "Foro Italico"	Examineur
M. Patrick LACOUTURE , Professeur des Universités, Institut Pprime, UPR 3346 CNRS, Université de Poitiers	Examineur
Mme Wafa SKALLI , Professeur des Universités, Institut de Biomécanique Humaine Georges Charpak, Arts et Métiers, Sciences et Technologies	Examineur
Mme Patricia THOREUX , Professeur des Universités/Praticienne Hospitalière, Hôpital Avicenne et Institut de Biomécanique Humaine Georges Charpak, Arts et Métiers, Sciences et Technologies	Examineur
M. Pierre-Yves ROHAN , Maître de Conférences, Institut de Biomécanique Humaine Georges Charpak, Arts et Métiers, Sciences et Technologies	Examineur

To my parents, my wife Sweta and my sisters Dipshikha and Dibyasree

Declaration

I hereby declare that work done in the thesis entitled, "**Contribution to personalized finite element-based musculoskeletal modeling of the lower limb**" submitted towards partial fulfillment for the award of Doctoral Degree at Institut de Biomécanique Humaine Georges Charpak, Arts et Métiers ParisTech, Paris, France, is an authentic record of work carried out by me under the supervision of Prof Wafa Skalli (PhD), Prof Patricia Thoreux (PhD, orthopedic surgeon) and Pierre-Yves Rohan (PhD).

Date: 14th December, 2020

Bhriku Kumar Lahkar

Acknowledgement

First and foremost, I would like to express my profound exaltation and gratitude to my thesis supervisors Prof Wafa Skalli (PhD), Prof Patricia Thoreux (PhD, orthopedic surgeon), and Pierre-Yves Rohan (PhD) for their candid guidance, constructive propositions, and overwhelming inspiration in nurturing the research. It has been a blessing for me to spend many opportune moments under their direction since the inception of the thesis.

In particular, the present work is a testimony of continuous guidance and motivation from Mme Skalli and Pierre-Yves, which finally led to realize the thesis in its current form. Apart from professional activities, I learned many personal traits during our discourse face-to-face or otherwise. Noteworthy to mention their care and concern when I felt sick during the second year of my thesis. I consider myself fortunate to have worked with such wonderful human beings.

I would like to offer my sincere thanks to other couple of mentors without whom achieving the objectives wouldn't have been possible. Thank you Prof Helene Pillet (PhD), Xavier Bonnet (PhD) and Ayman Assi (PhD), for providing crucial resources and information in the successful completion of this work. I would also like to thank Mme Marine Souq and M. Mohamed Marhoum for their administrative assistance.

I am grateful to *Institut de Biomécanique Humaine Georges Charpak*, BiomechAM chair program and its investors Fondation ParisTech, Société Générale, COVEA for providing financial assistance.

Of course, the pandemic (COVID 19) also deserves some credit. Although it has adversely affected the socio-economic and health structure of all nations and economies, it has taught to remain complacent at a personal level. Thank you for shaping me into a more mature and resilient person.

Finally, I would like to express my sincere gratitude to all who directly or indirectly helped me complete my thesis.

Contents

Declaration	ii
Acknowledgement	iii
Contents	iv
Résumé en français	1
General Introduction	21
1 Musculoskeletal Anatomy of the Lower Limb and Clinical Context	23
1.1 Descriptive anatomy	23
1.1.1 Osseous components	23
1.1.2 Lower limb musculature and connective tissues	25
1.2 Biomechanics of the hip and knee joint	27
1.3 Clinical context	29
1.3.1 Lower limb pathology and prevalence	29
1.3.2 Assessment methods	29
1.3.3 Treatments and outcomes	32
2 Literature Review	35
2.1 FE modeling and analysis of the knee joint	35
2.1.1 Geometry	35
2.1.2 Material properties	38
2.1.3 Boundary and loading condition	40
2.1.4 Verification and Validation	40
2.2 Musculoskeletal modeling	41
2.3 FE-MSK model	45
2.4 Objectives	47
3 Subject-specific finite element model development and evaluation of the knee joint	49
3.1 Fast subject-specific FE mesh generation of the knee joint from biplanar X-ray images	50
3.1.1 Introduction	50
3.1.2 Materials and methods	51

3.1.3	Results and Discussion	54
3.1.4	Conclusions	55
3.2	Development and evaluation of a new procedure for subject-specific tensioning of finite element knee ligaments	58
3.2.1	Introduction	58
3.2.2	Materials and methods	59
3.2.3	Results	64
3.2.4	Discussion	67
4	Soft Tissue Artifact correction in motion analysis	71
4.1	Development and evaluation of a new methodology for Soft Tissue Artifact compensation in the lower limb	72
4.1.1	Introduction	72
4.1.2	Materials and methods	73
4.1.3	Results	79
4.1.4	Discussion	82
4.2	Experimental quantification of soft tissue deformation in quasi-static single leg flexion using biplanar imaging	85
4.2.1	Introduction	85
4.2.2	Materials and methods	86
4.2.3	Results	89
4.2.4	Discussion	92
5	Clinical application: Preliminary investigation	95
5.1	Utility of EOS system in evaluating TKA implant pose	96
5.1.1	Introduction	96
5.1.2	Materials and methods	98
5.1.3	Results	99
5.1.4	Discussion	99
	General conclusion and perspectives	103
	A Sources of errors in gait analysis	106
	B Various TKA alignment state-of-the-art approaches	107
	C Soft Tissue Deformation (STD) with both the schemes	110
C.0.1	Scheme1	110
C.0.2	Scheme2	111
	D Definition of TKA implant coordinate system (CSYS)	112
	Bibliography	114

Résumé en français

Le système musculo-squelettique (MSK) du membre inférieur travaille en synergie pour assurer à la fois stabilité et mobilité. Toute perturbation de la synergie due à des troubles du système MSK peut entraîner des limitations fonctionnelles, ce qui est une cause majeure de handicap sur tous les continents et dans toutes les économies du monde. L'un des troubles du système MSK les plus répandus est l'arthrose, qui touchera 303 millions de personnes dans le monde en 2017 (Stanaway et al., 2019).

L'arthroplastie totale du genou est l'intervention chirurgicale la plus courante pour l'arthrose en phase terminale afin de restaurer la fonction articulaire. Cependant, les patients ne restent que partiellement satisfaits en raison de la performance sous-optimale de l'articulation reconstruite. Il existe des facteurs liés aux techniques chirurgicales, à l'état de santé général des patients et aux caractéristiques de leur appareil MSK individuel qui contribuent au résultat global d'une intervention chirurgicale. Parmi les nombreux facteurs, le mauvais alignement des composants de l'implant est un facteur majeur qui contribue à réduire la survie de l'implant (Schroer et al., 2013).

Pour faciliter l'alignement correct des implants, les chirurgiens s'appuient largement sur les modalités d'imagerie médicale (par exemple, CT, IRM) pour évaluer les informations morphologiques des patients, telles que l'alignement 3D des membres, la forme et la taille des os. Malgré les progrès des techniques d'évaluation, il ne semble pas y avoir de consensus complet sur une procédure particulière qui fonctionne le mieux. Comme la défaillance d'un implant est associée au relâchement et à l'usure de l'implant en raison des fortes contraintes développées à l'interface de l'implant (MacInnes, Gordon et Wilkinson, 2012), il faut donc, pour éviter la dégradation de l'implant, éviter les fortes contraintes articulaires. C'est pourquoi il est nécessaire d'avoir une compréhension objective des charges mécaniques in vivo au niveau de l'articulation.

Il existe des moyens complémentaires pour étudier la mécanique des articulations in vivo (par exemple, la quantification de la cinématique articulaire, la quantification des charges mécaniques transmises via les articulations, etc.) L'analyse de la marche est souvent utilisée pour l'évaluation partielle ou indirecte des altérations du système MSK après une blessure ou pathologie, et des résultats fonctionnels du traitement. Une telle approche permet une évaluation quantitative du schéma de mouvement des patients, mais les charges mécaniques articulaires ne peuvent pas être étudiées directement.

Dans ce contexte, les modèles éléments finis (EF) sont utilisés pour estimer la mécanique locale de l'articulation. Bien que pertinents, l'utilisation en milieu clinique de ces modèles

reste un verrou majeur en raison de l'expertise et le temps nécessaire pour le développement de tels modèles patient-spécifiques et aussi pour la simulation de cas d'usages. Les principaux défis sont la génération rapide et précis d'un maillage en éléments finis à partir d'images médicales et la mise en place d'une approche avec un compromis entre simplicité et pertinence. En outre, les modèles éléments finis représentent, pour la plupart, la réponse mécanique de sujets humains post-mortem en réponse à des chargements passifs ou des efforts musculaires génériques. Comme ce comportement de charge ne représente, que partiellement, des chargements physiologiques spécifiques à chaque individu, l'intégration de tels modèles avec des conditions de chargement physiologiques est indispensable.

Pour définir des chargements mécaniques cliniquement pertinents, la plupart des travaux dans la littérature utilisent des modèles MSK qui incorporent des données issues de l'analyse quantitative du mouvement à partir d'un système de capture de mouvement basé sur des marqueurs cutanés. Mais ces techniques présentent d'importantes limites, dont les « artefacts de tissus mous » (i.e., le mouvement relatif entre les marqueurs cutanés et les os sous-jacents) ce qui introduit une erreur lors du calcul de la cinématique des articulations. Par conséquent, pour estimer avec précision la cinématique des articulations, il est primordial de compenser ces artefacts.

Pour lever ces verrous, l'objectif de ce travail est de contribuer à développer un cadre de modélisation MSK complet pour étudier de manière couplée la mécanique locale (par exemple, la charge de contact de l'articulation) de l'articulation dans des conditions physiologiques limites.. L'objectif général est se compose donc des deux objectifs suivants :

- Développer et évaluer un modèle EF personnalisé de l'articulation du genou en tenant compte de la géométrie spécifique au sujet et des propriétés des matériaux ligamentaires.
- Compenser l'artefact des tissus mous dans l'analyse du mouvement en adoptant une nouvelle approche.

Le travail suivant illustre une approche de modélisation et d'évaluation par éléments finis (EF) de l'articulation du genou pour estimer la cinématique de l'articulation. Dans une première partie, une méthodologie pour la génération rapide et quasi-automatique de maillages d'éléments finis personnalisés de l'articulation du genou à partir d'images radiographiques biplanaires est proposée. Ce travail a fait l'objet d'une conférences Internationale avec acte et comité de Lecture (Lahkar et al., 2018). Dans un deuxième temps, l'évaluation de la réponse mécanique passive des modèles EF personnalisée sous un chargement externe en flexion est décrite. Une nouvelle méthodologie pour calibrer les propriétés des matériaux ligamentaires à partir de données qu'il est possible de collecter en routine clinique est également proposée et évaluée. Ce travail a été publié dans la revue à comité de lecture *Computer Methods in Biomechanics and Biomedical Engineering* intitulée "Development and evaluation of a new procedure for subject-specific tensioning of EF knee ligaments" (Lahkar et al., 2020) Dans une troisième partie, pour contribuer à la mise en place de protocoles permettant de collecter des données sur les conditions aux limites in vivo, une nouvelle méthodologie

pour la compensation des artefacts des tissus mous dans l'analyse quantitative du mouvement par la méthode des éléments finis. Enfin, dans le dernier chapitre, une quantification expérimentale de la déformation des tissus mous lors de la flexion quasi-statique d'une seule jambe à l'aide de l'imagerie biplanaire.

Partie I : Génération rapide d'un Maillage EF personnalisé de l'articulation du genou à partir d'images radiographiques bipanaires De nombreux modèles EF de l'articulation du genou ont été mis au point pour étudier le mécanisme lésionnels du genou (Kiapour et al., 2014), l'évaluation de la chirurgie (Kang et al., 2018 ; Xie et al., 2017) et la cinématique de contact dans l'articulation du genou (Donahue et al., 2002 ; Koo, Rylander et Andriacchi, 2011 ; Ali et al., 2016). Cependant, en raison des coûts de calcul importants requis pour développer et personnaliser les modèles à partir de données de tomodensitométrie ou d'IRM, toutes les études de la littérature ne comprenaient les données que d'un seul individu. Pourtant, la variabilité inter-individuelle ne peut pas être négligée lorsqu'il s'agit d'estimer la réponse mécanique d'un patient, qui est évidemment directement liée à la morphologie des os et le comportement mécanique des différents tissus.. Comme alternative aux données de la tomodensitométrie et de l'IRM, l'utilisation de l'image radiographique biplanaire est prometteuse pour effectuer des reconstructions 3D des structures osseuses (Chaibi et al., 2012) en raison de la faible dose de rayonnement, du temps de reconstruction très court et de la capacité à reproduire facilement des structures osseuses complexes.

La qualité du maillage EF joue un rôle essentiel dans l'obtention de résultats fiables et précis. Traditionnellement, les maillages tétraédriques sont faciles à générer, mais ils réduisent l'ordre de convergence des déformations et des contraintes (Payen et Bathe, 2011) et souffrent de problèmes de stabilité numérique associés au verrouillage en cisaillement et au verrouillage volumétrique (Joldes, Wittek et Miller, 2009 ; Onishi et Amaya, 2014). De plus, un maillage par éléments finis avec des éléments tétraédriques nécessite plus d'éléments que les éléments hexaédriques pour obtenir la même précision de solution, ce qui entraîne un coût de calcul plus élevé (Ramos et Simoes, 2006). Pour éviter ces problèmes, les éléments hexaédriques sont préférés pour la conception de modèles biomédicaux (Gérard et al., 2006 ; Rohan et al., 2017).

La construction automatique d'un maillage EF avec des éléments hexaédriques est un processus long et restrictif (Tautges, Blacker, et Mitchell, 1996). La littérature montre que la majorité des articles traitent de méthodes automatiques rapides et robustes pour générer des maillages tétraédriques de géométries arbitraires (Löhner et Parikh, 1988 ; Yerry et Shephard, 1984). Bien que plusieurs équipes aient contribué à développer des méthodes permettant la génération automatique de maillages hexaédriques à l'aide de différentes techniques, l'utilisation de la génération automatique de maillages hexaédriques est encore limitée en raison de problèmes de robustesse (Rohan et al., 2017).

L'objectif de la présente étude a été motivée par encourageants obtenus pour la modélisation EF personnalisée de la colonne cervicale inférieure (Laville, Laporte et Skalli, 2009). Dans ce travail, une approche spécifique pour générer automatiquement un maillage EF

personnalisé à partir d'images radiographiques biplanaires est proposée pour la structure de l'articulation du genou.

Onze spécimens de membre inférieur sain de cadavres frais, âgés de 47 à 79 ans, ont été utilisés dans ce travail basé sur une étude précédente (Pillet et al., 2016). Chaque spécimen comprend le fémur, le tibia et la rotule avec des structures articulaires passives intactes.

La méthodologie globale de la présente étude suit les étapes suivantes : (a) acquisition d'une image radiographique biplanaire pour les spécimens d'intérêt, (b) reconstruction 3D du fémur, du tibia et de la rotule, (c) génération d'un maillage générique (MG) de toute l'articulation du genou, (d) déformation du MG pour obtenir un maillage personnalisé (MP), (e) évaluation de la qualité du maillage du MP et (f) calcul de la précision de la représentation de la surface.

Tout d'abord, des images radiographiques biplanaires des structures osseuses (fémur, tibia et rotule) pour l'un des spécimens cadavériques (dénommé générique) ainsi que pour les 11 spécimens d'intérêt ont été acquises à l'aide du dispositif d'imagerie à faible dose EOS. Ensuite, à partir des images radiographiques, des modèles numériques 3D de tous les spécimens ont été obtenus en utilisant un algorithme de reconstruction 3D validé par des études précédentes avec un temps de reconstruction de 10 min pour chaque spécimen (Chaïbi et al., 2012 ; Quijano et al., 2013). Pour rappel, le processus de reconstruction 3D commence par l'identification et le marquage de diverses régions anatomiques et de points de repère sur les images biplanaires. Ensuite, sur la base d'inférences statistiques, un modèle paramétrique personnalisé simplifié (SPPM) est généré. Ensuite, le modèle générique 3D morpho-réaliste est déformé vers le MPPP pour obtenir un modèle paramétrique personnalisé morpho-réaliste (MPPM) en utilisant les moindres carrés mobiles et l'interpolation par krigeage (Trochu, 1993). Enfin, ce MPPM est ajusté manuellement jusqu'à l'obtention de la meilleure estimation du modèle spécifique au sujet concerné.

Dans l'étape suivante, la reconstruction 3D générique a été importée dans Geomagic Studio 12.0 (systèmes 3D, Caroline, États-Unis) pour la construction manuelle de patches afin de former des ensembles de cubes déformés dans le modèle. Ensuite, le modèle CAO a été importé dans une routine Matlab personnalisée pour créer un maillage volumétrique. Ici, chaque cube déformé a été discrétisé en ensembles de petits blocs. Cela a été fait en discrétisant les bords du cube déformé, puis les faces suivies par le cube entier. Ainsi, un maillage linéaire hexaédrique générique a été généré pour un cube déformé d'abord, puis pour les autres avec le même procédé.

Enfin, une cartographie (fonction ϕ) des points sources (génériques) aux points cibles (spécifiques au sujet) a été évaluée en appliquant une double interpolation de krigeage (Trochu, 1993). Ensuite, sur la base de la cartographie, le maillage générique de chaque spécimen a été déformé pour obtenir un maillage spécifique au sujet en utilisant une interpolation numérique. La déformation du maillage a été effectuée dans une routine Matlab personnalisée avec un coût de calcul de près de 30 secondes pour chaque spécimen.

Grâce à la méthodologie entièrement automatisée décrite, un maillage spécifique au sujet a été généré pour les 11 spécimens d'articulation du genou. La figure 1 illustre tous les maillages générés à l'aide de cette méthodologie. La qualité du maillage individuel de l'articulation du genou est représentée en termes d'indicateurs de qualité du maillage (% d'avertissement au-dessus de la valeur seuil). Il n'y a aucune erreur dans aucune maille et le pourcentage total d'avertissement est très inférieur de manière satisfaisante, avec une valeur maximale de 0,59% pour le 10e spécimen.

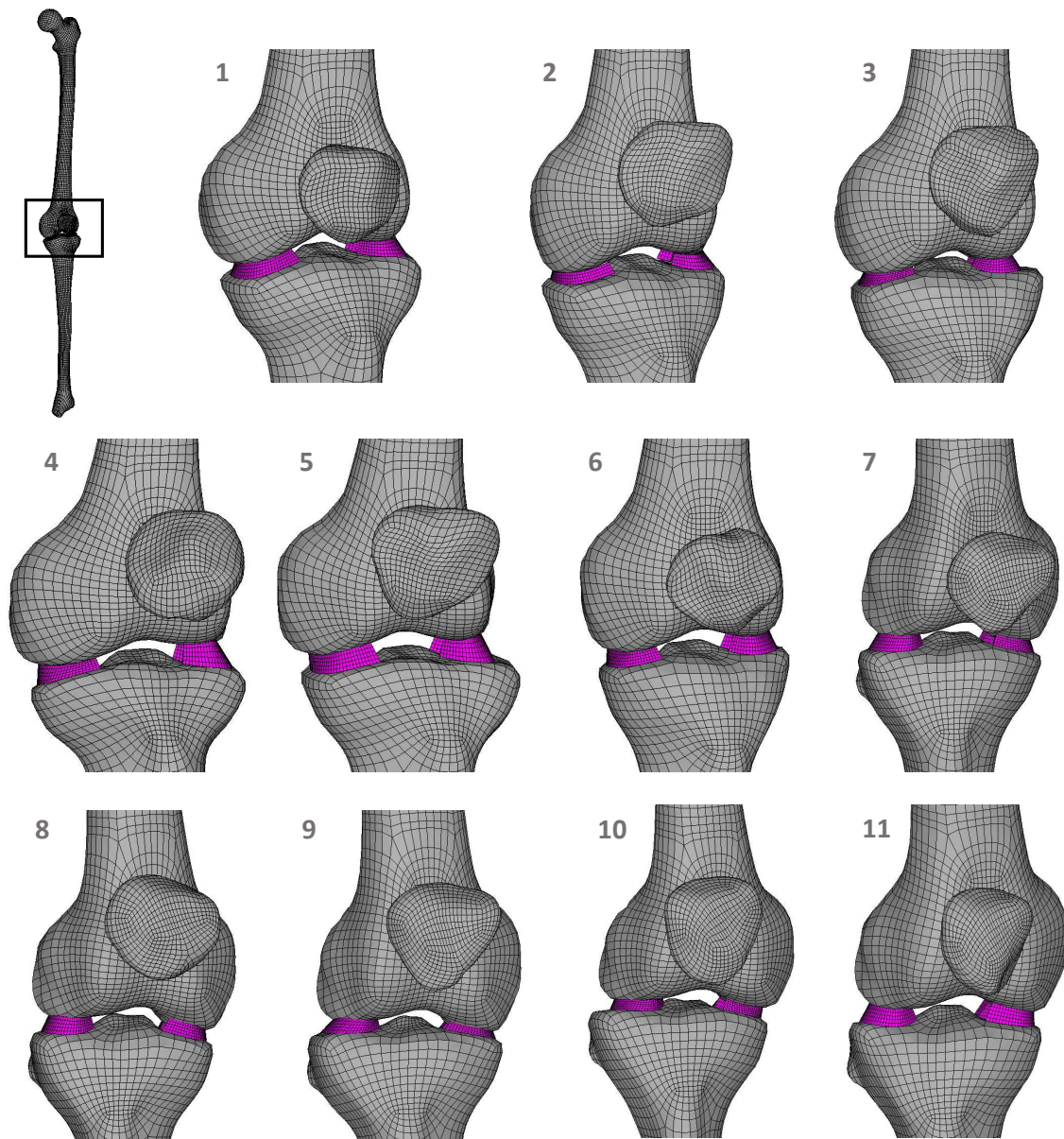


FIGURE 1: Maillage global de l'articulation du genou pour l'ensemble des 11 spécimens. Pour plus de clarté, seule l'épiphyse distale du fémur et l'épiphyse proximale du tibia sont représentées

La méthodologie proposée dans la présente étude repose principalement sur la conception minutieuse d'un maillage EF générique à partir d'une reconstruction 3D de la structure cible avec les caractéristiques anatomiques d'intérêt appropriées. La prudence s'impose

dans les zones fonctionnelles : surface de contact et sites d'insertion des ligaments de l'articulation du genou. Ce travail préliminaire est un effort ponctuel, désormais pour établir la déformation automatique du maillage, du générique au spécifique.

Dans l'ensemble, ce travail a contribué à la génération rapide, précise et semi-automatique d'un maillage EF hexaédrique de l'articulation du genou. En raison de la rapidité et de la spécificité du sujet en termes de géométrie, cette méthodologie a le potentiel d'être mise en œuvre dans la routine clinique pour étudier les caractéristiques personnalisées de l'articulation du genou. Toutefois, dans ce but, la validation du modèle est importante. Une évaluation sera abordée dans la partie suivante.

Partie II: Développement et évaluation d'une nouvelle procédure de mise en tension des ligaments à éléments finis du genou Les modèles EF sont couramment utilisés comme un moyen complémentaire fiable aux études expérimentales fournissant des informations significatives sur la biomécanique de l'articulation du genou. Diverses techniques de modélisation ont été utilisées pour modéliser la structure de l'articulation, en particulier les ligaments. Certaines des stratégies sont guidées par la simplicité, tandis que d'autres se concentrent sur la capture fidèle de l'anatomie spécifique du spécimen avec différents niveaux de fidélité de représentation de l'articulation. Par exemple, certains modèles de la littérature comprenaient des géométries 3D de ligaments ayant un comportement matériau complexe (Kiapour et al., 2014 ; Limbert, Taylor, et Middleton, 2004 ; Orsi et al., 2016 ; Pena et al., 2006). Une telle approche permet d'étudier le comportement d'enveloppement des ligaments et d'analyser la réponse biomécanique locale (par exemple, les contraintes et les déformations 3D à travers les tissus). Néanmoins, les modèles anatomiquement plus complexes nécessitent des informations détaillées basées sur des images des structures des tissus mous considérées. La génération et la simulation de tels modèles nécessitent souvent un temps beaucoup plus long que celui nécessaire pour des modèles plus simples (Bolcos et al., 2018). Par conséquent, les modèles plus simples peuvent être bénéfiques pour les études où un nombre plus élevé de sujets doit être analysé et, en même temps, capable de prédire la mécanique des articulations.

Dans une tentative de simplification du modèle, d'autres auteurs ont proposé de représenter les ligaments sous forme de faisceaux de ressorts ou de câbles de tension uniquement (Adouni et Shirazi-Adl, 2009 ; Baldwin et al., 2012 ; Moglo et Shirazi-Adl, 2005). Bien que les ligaments soient exposés à des états de contrainte en compression et en traction, la contribution de la contrainte de traction est nettement plus élevée que les autres (Pena et al., 2006 ; Orsi et al., 2016). Une telle simplification est donc considérée comme raisonnable et recommandée en particulier pour prédire la cinématique des articulations (Beidokhti et al., 2017). Néanmoins, la personnalisation des propriétés des ligaments (raideur et précontrainte), bien que cliniquement essentielle pour restaurer la stabilité des articulations, représente un défi pour la communauté. Par exemple, il existe un consensus sur le fait que la sous-tension des greffes pourrait entraîner une laxité articulaire, qui est biomécaniquement analogue à celle d'un genou déficient sur le plan ligamentaire (Sherman et al., 2012). En outre, en raison de

la morphologie variable, différents faisceaux d'un ligament (par exemple, deux faisceaux de fibres principales du LCA) peuvent présenter une précontrainte variable en devenant actifs à différents angles de flexion (Girgis, Marshall et JEM, 1975). Du point de vue de la modélisation, il a également été signalé qu'une prétension ligamentaire mal appliquée peut avoir un effet considérable sur la cinématique du genou (Mesfar et Shirazi-Adl, 2006 ; Rachmat et al., 2016). Pour s'attaquer à ce problème, certains auteurs ont utilisé des méthodes inverses pour calibrer le comportement constitutif de certains ligaments. Les auteurs ont utilisé soit des tests de laxité (Baldwin et al., 2012 ; Beidokhti et al., 2017) soit des charges de distraction (Zaylor, Stulberg, et Halloran, 2019) pour estimer les propriétés des ligaments en minimisant les différences entre la cinétique prédite par le modèle et la cinétique expérimentale. Ces calibrations sont toutefois susceptibles d'être coûteuses sur le plan des calculs.

Pour contribuer à lever ce verrou, nous avons proposé un cadre original pour calibrer la tension des ligaments du genou EF personnalisé dans les modèles EF, basé sur des données acquises expérimentalement. L'évaluation du modèle personnalisé a été réalisée en comparant, pour chacun des six spécimens cadavériques testés, la cinématique fémoro-tibiale prédite numériquement en flexion passive avec les données expérimentales de. Nous avons émis l'hypothèse que la méthodologie proposée avec des pré-tensions personnalisées pouvait permettre de prédire la cinématique passive globale de l'articulation du genou.

Nous avons obtenu les réponses cinématiques expérimentales du genou dans une étude précédente (Rochcongar et al., 2016). La procédure expérimentale est brièvement rappelée ci-après. Six échantillons de membres inférieurs fraîchement congelés, prélevés sur des sujets âgés de 47 à 79 ans, ont été testés en flexion-extension passive sur un banc d'essai cinématique préalablement validé (Azmy et al., 2010 ; Hsich et Draganich, 1997). La peau et les muscles ont été enlevés, à l'exception de huit centimètres de tendon du quadriceps et du muscle poplité avant la collecte des données cinématiques. Toutes les autres structures pertinentes des tissus mous des articulations (comme les ligaments, la capsule articulaire) ont été conservées intactes pendant l'acquisition des données cinématiques. Le fémur a été maintenu fixe, et le mouvement de flexion a été introduit dans le tibia par un système de cordes et de poulies. Pendant la flexion, les positions des trois trépieds marqueurs placés sur le fémur, le tibia et la rotule ont été enregistrées à l'aide d'un système optoélectronique. Ces positions enregistrées ont permis d'établir des cadres de référence auxiliaires à partir de $t=0$ (avant l'application de la charge de flexion) jusqu'à la fin de la flexion. Les incertitudes de mesure avec le système optoélectronique ont été évaluées au préalable. Des incertitudes globales de moins de 0,5 mm en translation et de 1° en rotation ont été obtenues (Azmy et al., 2010).

De plus, deux radiographies orthogonales de chaque spécimen ont été acquises à l'aide d'un système de radiographie biplanaire EOS afin d'obtenir des modèles numériques 3D des os et des marqueurs de trépied. À partir des modèles 3D, des cadres de référence anatomiques pour le fémur, le tibia et la rotule ont été définis (Schlatterer et al., 2009). Des cadres de référence auxiliaires ont également été définis à partir des marqueurs de trépied,

ce qui a permis d'établir une relation entre les cadres anatomiques et les cadres auxiliaires. Cette relation a également été utilisée pour convertir les données cinématiques acquises en mouvements relatifs patellofémoraux et tibiofémoraux dans le cadre de référence anatomique du fémur avec la séquence de Cardan ZY'X".

Après l'acquisition des données cinématiques, chaque spécimen a été entièrement disséqué pour identifier les sites d'insertion des ligaments. L'absence de traumatisme et l'intégrité des structures des tissus mous ont été vérifiées pendant la dissection. Un chirurgien expérimenté a identifié l'origine et les sites d'insertion des ligaments suivants : faisceaux antéro-médial (AM) et postéro-latéral (PL) du LCA, faisceaux postéro-médial (PM) et antéro-latéral (AL) du LCP, faisceaux superficiels (MCL) et profonds (MCLd) du LCM, et LCL. Les endroits identifiés ont été marqués avec des peintures radio-opaques, et les os ont été scannés à l'aide d'un scanner de tomographie assistée par ordinateur (Philips, Best, Pays-Bas). Des modèles numériques en 3D de chaque spécimen disséqué ont été acquis à l'aide de MITK-GEM, ce qui a permis d'obtenir des cadres anatomiques et des sites d'insertion des ligaments dans le système de référence du tomodensitomètre. Les modèles numériques 3D et les empreintes numériques des sites d'insertion des ligaments ont ensuite été enregistrés dans la configuration initiale expérimentale. L'enregistrement a été effectué à l'aide de données radiographiques biplanaires. Une fois les coordonnées des sites d'insertion connues, la distance de bout en bout de l'origine des ligaments et du site d'insertion a été calculée dans la configuration initiale expérimentale. Pour des raisons de lisibilité, la distance de bout en bout sera appelée ci-après longueur du ligament.

Le maillage hexaédrique EF personnalisé pour chaque segment osseux a été créé sur la base des modèles numériques basés sur la tomographie assistée par ordinateur (Lahkar et al., 2018). Ensuite, seul le maillage surfacique (élément coques) a été conservé pour représenter les os et le cartilage afin de réduire le coût de calcul (Germain et al., 2016). Ensuite, un lissage du maillage a été effectué au niveau des surfaces articulaires pour améliorer la qualité du maillage (Taubin, 1995).

On a supposé que les os avaient un comportement mécanique isotrope et élastique linéaire avec un module de Young de 12000 MPa (Choi et al., 1990). Comme le schéma de charge dans l'étude est quasi-statique, on a supposé que le cartilage était un matériau isotrope linéaire à phase unique (Eberhardt et al., 1990). Les régions cartilagineuses ont été modélisées en tant que matériau cortico-cartilagineux et affectées d'un module de Young de 250 MPa pour résumer les propriétés matérielles de l'os cortical et du cartilage (Germain et al., 2016). Une très fine bande de matériau entre les os et la région cortico-cartilagineuse a également été modélisée avec des propriétés intermédiaires (2000 MPa) pour limiter la discontinuité mécanique (Germain et al., 2016).

Dans le modèle, les insertions des ligaments croisés et collatéraux ont été basés sur les emplacements déjà identifiés (Rochcongar et al., 2016). Pour les autres ligaments et tendons (ligament fémoro-patellaire, tendon rotulien, tendon du quadriceps, capsule postérieure), des sites anatomiques généraux basés sur une connaissance prima facie de l'anatomiste

ont été utilisés. Chaque ligament croisé a été représenté par 2 faisceaux (Blankevoort et Huiskes, 1991) ainsi que le LCM (profond et superficiel) (Smith et al., 2016). La capsule postérieure et les ligaments fémoro-patellaires étaient représentés par 8 faisceaux chacun (4 faisceaux dans le côté médial et latéral chacun), tandis que le quadriceps et le tendon rotulien étaient représentés par 4 faisceaux chacun (Germain et al., 2016) et le LCL par un seul faisceau (Meister et al., 2000). Tous les ligaments et tendons ont été représentés comme des éléments de câble point à point, en tension uniquement, car leur contribution en tension est beaucoup plus élevée que celle en compression (Baldwin et al., 2009 ; Harris et al., 2016). Trois paires de contact surface-surface sans frottement ont été considérées : le cartilage tibia-fémur (médial et latéral) et le cartilage fémur-patella.

Trois cas de valeurs de précontrainte ligamentaire ont été considérés pour les ligaments croisés et collatéraux. Aucune valeur de précontrainte pour les autres ligaments n'a été prise en compte et les valeurs de rigidité (k) pour tous les ligaments ont été adoptées ou estimées à partir de notre étude précédente (Germain et al., 2016). Il est à noter que des valeurs de rigidité constantes ont été appliquées à tous les spécimens.

Cas 1 : Propriétés génériques des matériaux. Les valeurs de prétension ont été adoptées à partir d'une étude précédente (Germain et al., 2016).

Cas 2 : Précalcul automatique à partir de données expérimentales. Pour chaque spécimen, les précontraintes spécifiques des ligaments et des faisceaux ont été automatiquement calculées à partir des longueurs expérimentales des ligaments.

Cas 3 : Combinaison d'un pré-calcul automatique et d'un ajustement manuel supplémentaire.

Lors de la mise en œuvre des propriétés génériques des ligaments (cas 1), seuls deux modèles EF sur six ont atteint une convergence complète.

La cinématique prédite a montré un grand écart par rapport à l'expérimentation, tant en termes d'ampleur que de tendance. En utilisant les propriétés des matériaux ligamentaires calculées automatiquement, 5 modèles sur 6 ont atteint une convergence sur 60° de flexion.

Grâce aux propriétés des matériaux ligamentaires calculées automatiquement et à l'ajustement manuel, tous les modèles de genou EF sont restés stables sur toute la plage de flexion. La durée d'exécution individuelle était d'environ 13 minutes par spécimen.

TABLE 1: Différence moyenne RACINE DE L'ERREUR QUADRATIQUE MOYENNERACINE DE L'ERREUR QUADRATIQUE MOYENNE \pm ECART-TYYPE entre la cinématique expérimentale et celle prédite par le modèle

Flexion	Cas	A/A(°)	I/E(°)	P/A(mm)	I/S(mm)	L/M(mm)
	1	-	-	-	-	-
0-60°	2	2.4 \pm 1.3	6.3 \pm 6.2	5.0 \pm 3.5	1.9 \pm 1.8	1.2 \pm 1.1
	3	1.5 \pm 1.3	5.3 \pm 5.1	3.4 \pm 2.3	1.2 \pm 0.8	2.0 \pm 1.9

A/A: Abduction/Adduction, I/E: Interne/Externe, P/A: Postérieur/Antérieur, I/S: Inférieure/Supérieure, L/M: Latéral/Médial

Dans cette étude, nous avons mis en place une nouvelle méthodologie pour la construction de modèles personnalisés du genou, avec une géométrie basée sur la tomodensitométrie et évalué une nouvelle procédure de calibrage spécifique au sujet de la prétension des ligaments à partir de données radiographiques biplanaires. La cinématique fémoro-tibiale prédite de chaque modèle a été comparée à la réponse in vitro correspondante pour trois cas différents de propriétés ligamentaires (prétension). Tout d'abord, nous avons cherché à savoir si les modèles EF avec des valeurs génériques de prétension peuvent saisir la variabilité inter-individuelle de la cinématique in vitro. Ensuite, des pré-souches obtenues expérimentalement ont été recrutées dans les modèles EF et la cinématique prédite a été observée (cas 2). Troisièmement, la cinématique du modèle a été observée en ce qui concerne les propriétés calibrées des ligaments basées sur la combinaison de précontraintes pré-calculées et d'autres ajustements (cas 3).

Bien qu'il soit difficile de comparer directement les prédéformations estimées avec des études similaires dans la littérature en raison de la variabilité de la géométrie des ligaments et des propriétés des matériaux, les valeurs des prédéformations ont été trouvées dans la fourchette confirmée par d'autres (Amiri et al., 2006 ; Wismans et al., 1980 ;). En outre, la plupart des ligaments ont été trouvés en état de tension en extension complète, à l'exception du LCP, ce qui est globalement en accord avec la littérature (Blankevoort et Huiskes, 1991 ; Guess, Razu et Jahandar, 2016 ; Moglo et Shirazi-Adl, 2005). De même, la réponse cinématique prédite a également montré une bonne correspondance avec les résultats expérimentaux pour tous les spécimens. Les différences numériques expérimentales constatées dans cette étude étaient comparables à celles d'études similaires rapportées dans la littérature (Beidokhti et al., 2017 ; Harris et al., 2016).

La procédure de calcul de la prétension ligamentaire directement à partir de données expérimentales (cas 3) a fourni une première estimation satisfaisante, basée sur un modèle dont la cinématique estimée était déjà en bon accord avec les données expérimentales. Comme cette approche semble être peu coûteuse sur le plan des calculs (15-20 secondes pour obtenir une prétension ligamentaire spécifique pour un seul modèle de genou) et simple sur le plan méthodologique, elle peut servir d'alternative fiable pour estimer les valeurs de prétension ligamentaire spécifiques au sujet. Il convient de noter qu'aucune évaluation directe des tensions ligamentaires n'a été réalisée dans la présente étude. La décision de mettre en œuvre la technique actuelle comme alternative doit être prise avec prudence. Pour une mise en œuvre réussie de cette technique dans le cadre clinique, une évaluation exhaustive du modèle dans diverses conditions de charge est nécessaire, y compris la tension ligamentaire et la tension de contact.

En conclusion, comme il s'agissait d'une première étude visant à appliquer directement des valeurs de précharge sur des modèles directement issus de l'expérience, qui peuvent trouver des portées dans les études cliniques basées sur des modèles, telles que la planification de l'équilibrage ou de la reconstruction des ligaments car elle réduit la complexité du développement des modèles (en particulier l'étalonnage des ligaments) ainsi que le coût de calcul, tout en maintenant une bonne correspondance avec les données expérimentales.

Dans ce but, une évaluation plus poussée du modèle serait nécessaire pour les échantillons de plus grande taille et dans d'autres scénarios cliniquement pertinents.

Dans l'ensemble, cette partie a permis d'aborder deux défis importants dans l'élaboration de modèles et les approches d'évaluation, comme l'a expliqué la revue de la littérature. La méthodologie quasi-automatique employée dans la première partie a permis de générer un maillage EF de l'articulation du genou spécifique au sujet, avec une qualité de maillage et une précision de représentation de surface satisfaisantes.

Partie III: Développement d'une nouvelle méthodologie pour la Compensation des artefacts des tissus mous dans l'analyse quantitative du mouvement par la méthode des éléments finis Une évaluation précise de la cinématique *in vivo* est essentielle pour obtenir des informations sur le fonctionnement normal des articulations (Akbarshahi et al., 2010) et pour étudier la pathologie des articulations des membres inférieurs (Andriacchi et Alexander, 2000). La capture de mouvement basée sur les marqueurs cutanés (SM) est la technique la plus répandue utilisée pour estimer la cinématique du squelette du membre inférieur. Toutefois, la précision de cette technique est affectée par le mouvement relatif des tissus mous par rapport à l'os sous-jacent, un biais communément appelé "artefact des tissus mous" (STA). S'il n'est pas compensé, le STA peut entraîner des erreurs cinématiques moyennes allant jusqu'à 16 mm en translation et 13° en rotation pour l'articulation du genou (Benoit et al., 2006). Ces erreurs peuvent avoir une influence significative sur l'évaluation de la pathologie ou les effets du traitement dans l'analyse clinique de la marche (Seffinger et Hruby, 2007).

Différentes méthodes ont été proposées dans la littérature pour réduire l'effet de la STA sur l'estimation de la pose osseuse. Parmi celles-ci, la MBO, qui s'appuie sur un modèle cinématique prédéfini avec des contraintes articulaires spécifiques, est de plus en plus utilisée. Au départ, des contraintes cinématiques simples telles que les articulations à charnière ou sphériques étaient considérées comme représentant l'articulation de la hanche et du genou (Lu et O'connor, 1999 ; Reinbolt et al., 2005). Plus tard, des contraintes anatomiques sur les articulations (mécanisme parallèle, courbes de couplage) ont été introduites, ce qui a encouragé la cinématique 3D car elles ont permis des déplacements articulaires (Gasparutto et al., 2015 ; Richard et al., 2016). Cependant, quelles que soient les contraintes articulaires imposées, les cinématiques génériques (non personnalisées) dérivées de modèles se sont révélées inexactes (erreur cinématique du genou jusqu'à 17° et 8 mm) car ces modèles ne pouvaient pas s'adapter à la géométrie spécifique du patient, en particulier dans des conditions pathologiques (Clément et al., 2017).

La simplification conjointe a des conséquences indirectes sur la précision prédictive des modèles musculo-squelettiques du corps rigide (MSK) et des modèles MSK basés sur la FE. Les études qui ont utilisé des modèles FE-MSK pour prédire la mécanique locale des articulations en utilisant la cinématique articulaire *in vivo* (Shu et al., 2018 ; Xu et al., 2016), ont supposé que l'articulation du genou avait un DoF de 1. Cela pourrait entraîner une

propagation des incertitudes sur la cinématique prédite et affecter la réaction articulaire ainsi que les forces musculaires et ligamentaires.

Dans les contextes susmentionnés, l'estimation fiable de la cinématique du squelette à l'aide de données de mouvement basées sur la SM reste un défi majeur (Richard, Cappozzo et Dumas, 2017). Dans une étude précédente, un modèle conceptuel EF a été proposé pour la compensation de la STA (Skalli et al., 2018). L'objectif de la présente étude était de développer le modèle conceptuel pour le membre inférieur et de le mettre en œuvre sur des volontaires sains en tenant compte des modèles spécifiques au sujet.

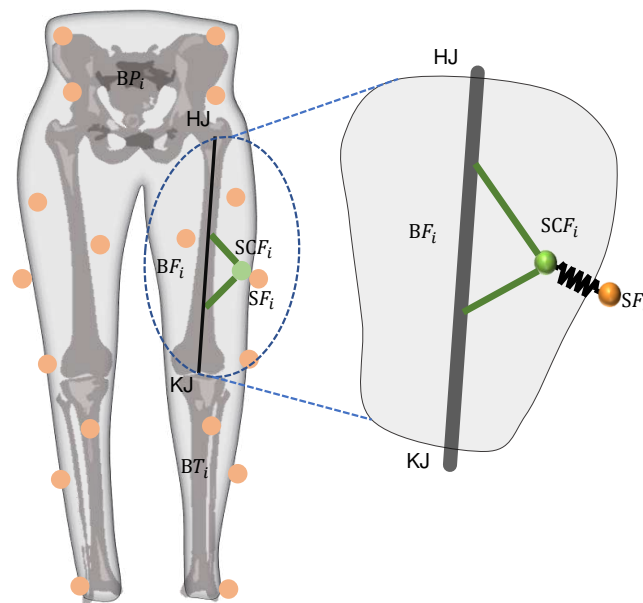


FIGURE 2: Illustration schématique du modèle conceptuel de l'EF des membres inférieurs.

Le modèle conceptuel du membre inférieur est constitué de segments osseux, de nœuds représentant des marqueurs cutanés et sous-cutanés, d'éléments articulaires et d'éléments qui relient les marqueurs cutanés aux os correspondants. Les segments osseux sont représentés par un ensemble de faisceaux à haute rigidité. Les articulations entre les segments sont représentées par des liens rigides, permettant des rotations libres au niveau de l'articulation et des déplacements contrôlés. Pour simplifier la modélisation des tissus mous, tout l'effet de déformation des tissus mous est rapporté au niveau sous-cutané. Par conséquent, la connexion entre un marqueur cutané et le segment osseux correspondant est représentée par une combinaison de ressorts reliant le marqueur cutané au marqueur sous-cutané et de faisceaux reliant les marqueurs sous-cutanés aux segments osseux (figure 2).

Les déplacements des marqueurs cutanés mesurés tout au long du cycle de la marche sont considérés comme des données d'entrée dans le modèle d'EF, ce qui permet de déterminer les emplacements des marqueurs osseux et sous-cutanés et la cinématique des articulations.

66 volontaires sains ont été inclus (tranche d'âge : 18-60 ans ; poids : $71,3 \pm 15$ Kg ; taille

: 170 ± 10 cm) dans cette étude. Les seuls critères d'exclusion étaient les antécédents de chirurgie orthopédique des membres inférieurs.

L'analyse quantitative du mouvement a été effectuée sur un système d'analyse optoélectronique comprenant 7 caméras vidéo (Vicon Motion System Ltd., Oxford Metrics, UK). Les marqueurs optoélectroniques ont été positionnés selon la méthode de la Plug-in Gait (Davis III et al., 1991), et les participants ont été invités à effectuer une marche en palier à une vitesse choisie par eux-mêmes. Des radiographies biplanaires ont ensuite été acquises à l'aide du système EOS (EOS Imaging, France). Des modèles numériques 3D des os ont été obtenus à l'aide d'un algorithme de reconstruction 3D validé par des études antérieures (Chaibi et al., 2012). L'emplacement des marqueurs cutanés a également été calculé à partir de radiographies biplanaires.

À partir des modèles numériques 3D des os, des points de repère anatomiques spécifiques au sujet ont été identifiés, ce qui a permis d'obtenir les coordonnées nodales de chaque os. La distance entre la peau et les marqueurs sous-cutanés a été arbitrairement choisie comme étant de 1 mm (c'est-à-dire la longueur du ressort). Sur la base du déplacement moyen en translation de l'articulation du genou trouvé dans notre précédent travail expérimental *in vitro* (Germain et al., 2016), la longueur de l'articulation du genou a été fixée à 20 mm. Pour la hanche, la longueur articulaire a été fixée à 1 mm sur la base de données non publiées sur le déplacement en translation de la hanche quantifié à l'aide de rayons X biplanaires.

Les déplacements des marqueurs mesurés à partir de la capture du mouvement ont été progressivement introduits dans le modèle comme une condition limite prescrite, et les positions des marqueurs osseux et sous-cutanés résultants tout au long du cycle de marche ont été calculées à l'aide du logiciel commercial ANSYS.

La figure 3 illustre la cinématique de rotation et de translation estimée à l'aide de mesures de marqueurs cutanés et d'un modèle de EF intégrant le modèle d'articulation à 6 DoF pour l'articulation du genou.

Pour l'articulation du genou, la valeur maximale du dROM ($12,5^\circ$) a été observée pour la rotation Int/Ext suivie de la rotation Flex/Ext ($-6,3^\circ$) et Abd/Add ($1,5^\circ$) respectivement. Un maximum de 20 mm de déplacement de l'articulation a été noté dans la direction (Post/Ant), tandis que les autres DoFs ont montré jusqu'à 9 mm (Med/Lat) et 3 mm (Inf/Sup) pour la cinématique STAC. Ces résultats ont montré jusqu'à 30,5 mm, 12,5 mm et 21 mm respectivement pour la cinématique basée sur le SM.

Des schémas cinématiques qualitativement similaires ont été observés entre les résultats cinématiques de la STA compensée (STAC) basée sur la SM et la EF pour les articulations de la hanche et du genou, avec des différences dans la portée ROM pour tous les DoFs. Les cinématiques basées sur la SM étaient comparables à celles de la littérature (D'Isidoro, Brockmann et Ferguson, 2020 ; Fiorentino et al., 2017).

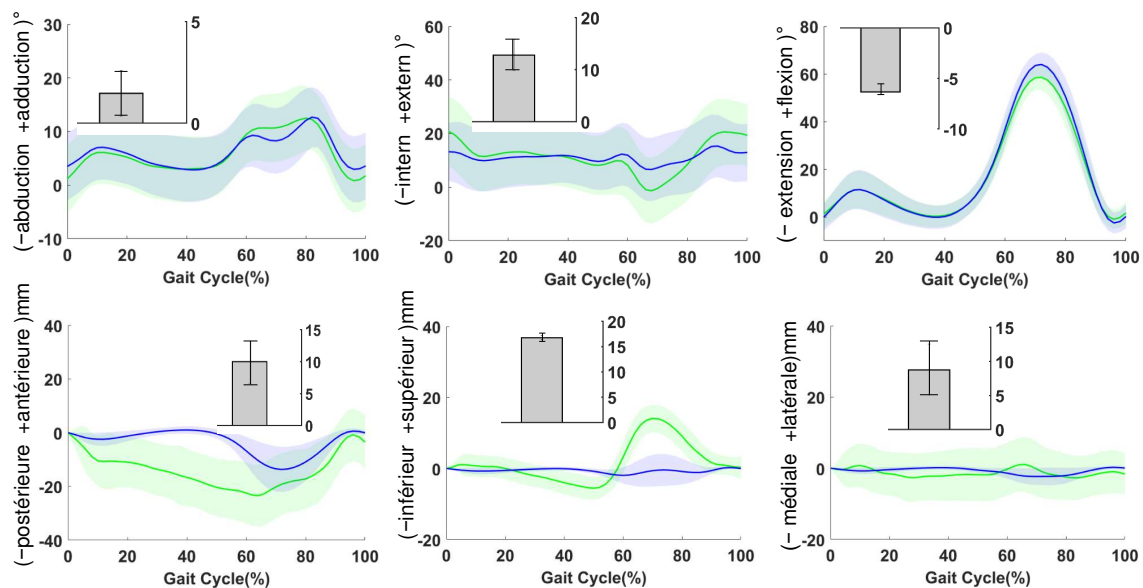


FIGURE 3: La cinématique de l’articulation du genou pendant la marche est présentée comme Mean \pm 1SD. Les valeurs moyennes pour les résultats basés sur les marqueurs cutanés (vert) et les résultats prévus par le modèle EF (bleu) sont présentées sous forme de lignes continues, tandis que l’écart-type est présenté dans des tons plus clairs.

L’approche proposée peut servir dans deux grands domaines d’application : i) dans l’analyse de la marche pour la recherche, où la personnalisation des modèles à l’aide de l’imagerie médicale (par exemple, CT, IRM, rayons X biplanaires) n’est généralement pas effectuée. Toutefois, il est possible de compenser l’ATS par des techniques classiques de mise à l’échelle du modèle, tout en étant capable de différencier les paramètres de rigidité des tissus mous entre différents sous-groupes. ii) dans l’analyse clinique de la marche, où la personnalisation du modèle par imagerie médicale pourrait permettre de saisir les détails anatomiques des articulations saines ou dégénérées.

En conclusion, nous avons présenté un modèle conceptuel de EF du membre inférieur pour la compensation de la STA et l’avons testé avec succès sur une population de 66 sujets de morphologies différentes. Le modèle s’est avéré satisfaisant pour la compensation de l’ATS et polyvalent, facilitant les paramètres nécessaires à la personnalisation du modèle. La méthodologie développée et évaluée dans cette étude peut améliorer la précision des prédictions cinématiques, ce qui est essentiel pour les modèles MSK ainsi que pour la prise de décisions cliniques.

Dans cette partie, nous avons observé que le modèle proposé basé sur l’EF du membre inférieur pouvait effectivement compenser l’ATS et les résultats observés étaient conformes à la littérature. Cependant, lors de l’élaboration du modèle, des valeurs de rigidité arbitraires ont été attribuées aux ressorts car aucune information sur la déformation des tissus mous à chaque emplacement de marqueur n’était disponible. Cela a conduit à étudier expérimentalement le modèle de déformation des tissus mous au niveau du membre inférieur pendant le mouvement. Cette contribution est incluse dans la partie suivante.

Partie IV: Quantification expérimentale de la déformation des tissus mous lors de la flexion quasi-statique d'une seule jambe à l'aide de l'imagerie biplanare L'analyse du mouvement basée sur les marqueurs de peau (SM) est la méthode non invasive la plus courante pour estimer la position et l'orientation du squelette dans l'espace 3D. La précision de cette méthode est principalement limitée par le mouvement relatif entre les tissus mous et l'os sous-jacent, communément appelé artefact des tissus mous (STA). Afin de compenser ce mouvement et d'estimer avec précision la position du squelette in vivo pendant le mouvement, il est essentiel de connaître le schéma de déformation des tissus mous (STD) pendant le mouvement (Benoit et al., 2006 ; Stagni et al., 2005).

Plusieurs études invasives et radiologiques ont été proposées pour caractériser les STD lors de différentes tâches motrices. La plupart de ces études ont conclu que les STD dépendent d'un sujet individuel, du type d'activité exercée, de la configuration des marqueurs ainsi que des lieux. Par exemple, peu d'études ont constaté que l'erreur cinématique due à une STD est plus importante à la cuisse qu'à la jambe, ce qui suggère un schéma spécifique à la localisation et au segment pour compenser l'artefact (Akbarshahi et al., 2010 ; Stagni et al., 2005 ; Benoit et al., 2006). Néanmoins, ces études se sont principalement concentrées sur la quantification des erreurs cinématiques causées par les STD plutôt que sur les STD elles-mêmes.

À la connaissance des auteurs, il n'existe qu'une seule étude dans la littérature traitant de la quantification des STD à différents emplacements et directions de marqueurs chez 20 volontaires sains (Gao et Zheng, 2008). Mais, en raison de limitations techniques empêchant l'accès à la position des os, la quantification des STA a été rapportée comme un mouvement inter-marqueurs au lieu d'un mouvement des marqueurs par rapport à la position réelle des os. Par conséquent, on manque encore de données de référence sur les STD spécifiques au sujet, à l'endroit et à la direction, qui pourraient fournir des indications pour des stratégies efficaces de compensation de la STA pour l'analyse des mouvements basée sur la SM.

Parmi les différentes méthodes mises au point pour compenser la STA, la méthode MBO (pour Multi-Body Optimisation) est de plus en plus utilisée. Elle attribue généralement une matrice de poids reflétant la distribution des erreurs STA parmi les marqueurs adhérent à un segment (Lu et O'connor, 1999). En marge de ces méthodes, une nouvelle approche basée sur l'EF pour compenser la STA du membre inférieur a été évaluée avec succès dans une population de 66 sujets. Le modèle EF permet d'incorporer la rigidité de correction de STA à chaque emplacement de marqueur, et la rigidité peut être calibrée sur la base des informations sur les STD locales à chaque emplacement de marqueur et le long de chaque direction anatomique. Toutefois, en raison du manque de données sur les STD, des valeurs arbitraires ont été attribuées aux paramètres de rigidité.

L'étude actuelle vise donc à quantifier la déformation des tissus mous du bassin, de la cuisse et de la tige à chaque emplacement de marqueur et dans trois directions anatomiques lors de la flexion quasi statique d'une jambe du genou à l'aide d'une radiographie biplanare à faible dose. Les données rétrospectives incluses dans l'étude ont recruté dix volontaires

(tranche d'âge : 23-40 ans ; tranche de poids : 63-89 kg, tranche de taille : 1,7-1,9 m). Les sujets ont été équipés d'un total de 20 marqueurs cutanés rétro-réfléchissants (bassin : 4, cuisse : 8 et tige : 8) selon la méthode Plug-in Gait (Davis III et al., 1991). Trois paires de radiographies biplanaires (EOS Imaging, France) ont été acquises dans trois configurations pour chaque sujet (figure 4.7). Tout d'abord, une paire de radiographies a été prise en position debout. Ensuite, deux paires séquentielles de radiographies à environ 20° et 40° de flexion du genou ont été acquises alors que chaque sujet effectuait une flexion quasi statique du genou sur une seule jambe. Par souci de clarté, trois postures séquentielles seront ci-après désignées respectivement comme la pose 1, la pose 2 et la pose 3 pour la position debout, 20° et 40° de flexion du genou.

Données radiographiques biplanaires et modèles 3D

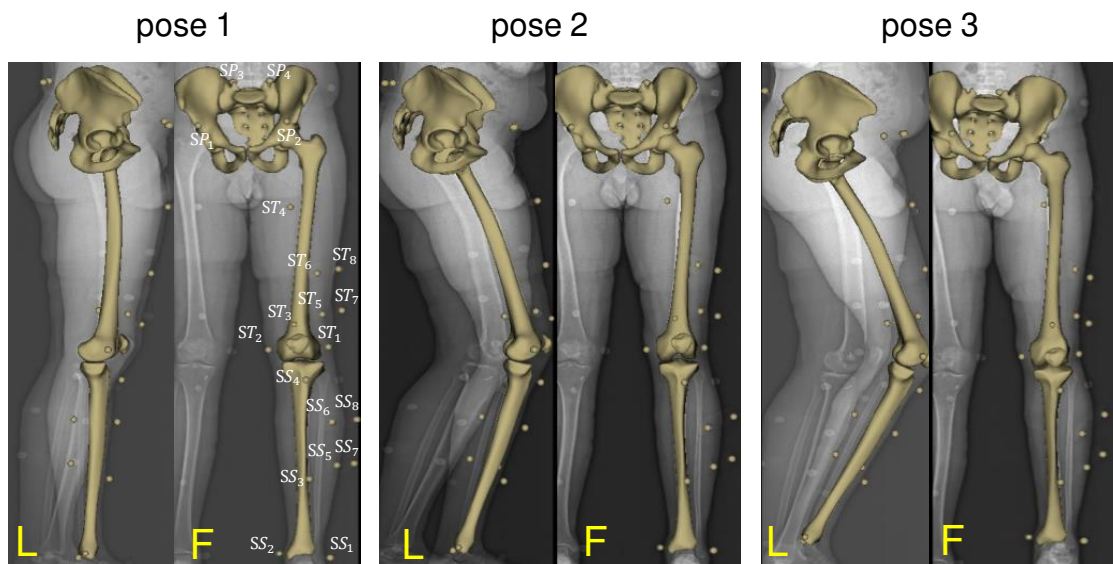


FIGURE 4: Modèles numériques 3D du bassin, du fémur et du tibia et de leurs marqueurs respectifs collés à la peau aux positions : pose 1 (en pose libre), pose 2 (flexion du genou à 20°) et pose 3 (flexion du genou à 40°) construites à partir de radiographies orthogonales

Les modèles numériques 3D des os (bassin, fémur et tibia) ont d'abord été obtenus en position debout à l'aide d'un algorithme de reconstruction 3D développé précédemment par (Chaibi et al., 2012) pour le fémur et le tibia et (Mitton et al., 2006) pour le bassin. Les modèles 3D ont ensuite été projetés sur les radiographies frontales et latérales. Les positions des contours osseux ont été ajustées manuellement jusqu'à ce que les contours correspondent exactement à ceux des radiographies à chaque pose. Les positions 3D des marqueurs cutanés à chaque pose ont également été calculées à partir des radiographies biplanaires en utilisant la même procédure.

La quantification des STD sur le bassin, la cuisse et le jarret a été réalisée sous la forme d'un élément des tissus mous (ETM) :

La position 3D des marqueurs cutanés dans toutes les poses a d'abord été calculée à partir des données radiographiques biplanaires et exprimée dans les cadres de référence osseux

respectifs. À partir des marqueurs cutanés, un ensemble de marqueurs virtuels, appelés marqueurs sous-cutanés, a été défini 1 mm sous le marqueur cutané. Tout l'effet de déformation des tissus mous au niveau du marqueur est rapporté à l'ETM, qui relie le marqueur cutané au marqueur virtuel. On a supposé que la connexion entre le marqueur virtuel et le segment osseux correspondant était rigide. En raison de l'hypothèse de rigidité, les emplacements des marqueurs sous-cutanés dans le cadre anatomique sont restés les mêmes dans toutes les poses. Ainsi, les différences absolues entre la peau et les emplacements des marqueurs sous-cutanés dans les poses 2 et 3 ont été calculées et exprimées dans les cadres anatomiques osseux dans les directions x , y et z .

Dans l'ensemble, la déformation des tissus mous a montré une similarité intersujets chez la plupart des sujets présentant un profil de STD similaire. Bien qu'une telle observation soit en contraste avec l'idée qui prévaut actuellement selon laquelle les STD sont spécifiques à un sujet, elle a néanmoins été trouvée en accord avec une étude qui expliquait l'éclipse de la similarité par la dissimilitude chez quelques sujets (Gao et Zheng, 2008). Deuxièmement, on a observé que les STD spécifiques à un segment présentaient la déformation la plus importante au niveau de la cuisse, suivie du bassin et de la jambe (Akbarshahi et al., 2010 ; Walker, 2015). Une observation similaire a également été rapportée dans des études qui ont mesuré une erreur cinématique plus élevée à la cuisse (Sangeux et al., 2006 ; Stagni et al., 2005).

La STA s'est produite dans les trois directions de l'os encastré dans les cadres anatomiques, mais pas de manière uniforme pour la cuisse et le jarret en particulier. La déformation des tissus mous dans la direction proximale-distale de la cuisse et du tronc était nettement plus importante. Cela est probablement dû à l'orientation de la structure musculaire de la cuisse et du fémur, qui se contracte et se détend lors des mouvements sur sa longueur. La déformation dans la direction médio-latérale était la plus faible. Une observation similaire a également été rapportée dans la littérature (Gao et Zheng, 2008). La STD quantifiée est une conséquence à la fois de la contraction musculaire et du glissement de la peau. Actuellement, d'autres méthodes existantes, telles que les attaches invasives et les mesures fluoroscopiques, se sont révélées utiles pour quantifier la déformation des tissus mous. Mais les méthodes invasives sont susceptibles de modifier le mouvement libre des tissus mous et peuvent donc avoir un impact sur leurs résultats. La fluoroscopie n'est pas non plus efficace pour capturer l'ensemble du membre inférieur, bien qu'elle soit efficace pour les observations locales en dynamique. Par conséquent, l'EOS, associée à des marqueurs cutanés, peut servir de référence pour localiser la position réelle des os et quantifier les STD pour une amplitude de mouvement limitée.

Les conclusions de l'étude pourraient ouvrir la voie à des stratégies efficaces de compensation des STA pour l'analyse du mouvement basée sur les SM. Au lieu d'assigner une rigidité de correction STA arbitraire, les sujets ayant des modèles de STD similaires peuvent être regroupés pour assigner la même rigidité de correction. De plus, pour ces activités quasi-statiques, tous les marqueurs du bassin peuvent être regroupés pour attribuer les mêmes valeurs de rigidité. Il en va de même pour la tige. Pour la cuisse, les emplacements des marqueurs où la STD a été observée le plus haut peuvent être assignés avec la rigidité la

plus faible et vice versa. Il convient de noter que lors de l'attribution des valeurs de rigidité pour la cuisse et le fémur, des valeurs de rigidité différentes doivent être définies selon la direction anatomique. En conclusion, bien que les données sur les STD fournies dans cette étude puissent être utiles pour les futures approches de compensation des STA, une étude plus approfondie serait nécessaire dans différentes activités dynamiques.

Conclusion générale Pour conclure, la première phase de la thèse s'est concentrée sur la génération rapide d'un maillage par éléments finis spécifique au sujet de l'articulation du genou à partir d'images radiographiques biplanaires. Cette étude a permis de générer un maillage hexaédrique pour le fémur, le tibia et la rotule à partir de la reconstruction 3D de 11 spécimens cadavériques. L'ensemble de la procédure, de la reconstruction 3D à la génération du maillage, a pris 12 minutes de temps de calcul par spécimen. La qualité du maillage et la précision de la représentation de la surface ont été très satisfaisantes. Cette contribution a ouvert la voie à une étude fiable de la variabilité inter-individuelle des éléments passifs de l'articulation du genou et de son effet sur la cinématique de l'articulation. En estimant la cinématique de l'articulation du genou spécifique à un sujet en flexion passive, cette étude a été confrontée à un défi important de personnalisation des propriétés des tissus mous, en particulier les ligaments. Comme les approches d'optimisation existantes sont coûteuses en termes de calculs, une nouvelle procédure pour estimer les propriétés des matériaux ligamentaires spécifiques à un sujet (prétension) a été proposée et évaluée sur 6 échantillons cadavériques. Les valeurs de précontrainte spécifiques au sujet et au ligament ont été directement calculées à partir de l'étude expérimentale et mises en œuvre dans les modèles d'EF correspondants pour estimer la cinématique des articulations. L'évaluation du modèle spécifique au sujet a été réalisée en comparant la cinématique fémoro-tibiale prédite avec la réponse in vitro des spécimens correspondants. L'accord expérimental-numérique a été jugé très satisfaisant et conforme à la littérature. La validation in vitro des modèles de EF a servi d'étape intermédiaire nécessaire pour transformer davantage le modèle vers des charges in vivo. Cette contribution a ouvert des portes pour utiliser des stratégies de développement de modèles simplifiées mais pertinentes vers une modélisation personnalisée des éléments finis. La deuxième phase du doctorat s'est concentrée sur le développement et l'évaluation d'une nouvelle approche de compensation des STA basée sur les FE. Dans ce contexte, un modèle d'EF conceptuel du membre inférieur a été proposé pour démontrer la capacité du modèle à minimiser la STA. Le modèle était mis en œuvre sur 66 sujets, et les résultats des modèles d'EF personnalisés se sont révélés prometteurs et en accord avec la littérature. La caractéristique unique du modèle est sa polyvalence qui permet de prendre en compte la déformation des tissus mous spécifique au sujet, à la tâche et à l'emplacement du marqueur, soulignant ainsi la nécessité d'une bonne compréhension de la déformation des tissus mous à différents emplacements du marqueur afin de faciliter de meilleures stratégies de compensation. C'est pourquoi, dans le prolongement des travaux susmentionnés, une quantification expérimentale de la déformation des tissus mous a été réalisée à l'aide de l'imagerie biplanar. Cette contribution a permis de mieux connaître la répartition de la déformation des tissus mous entre les individus et les différents emplacements des marqueurs. Lorsqu'elles

sont intégrées dans le régime d'indemnisation des STA, ces informations perspicaces sur la déformation des tissus mous peuvent fournir des résultats plus fiables et cliniquement pertinents.

Dans l'ensemble, les objectifs entrepris pendant le doctorat sont apparus nécessaires pour développer un cadre complet de modélisation EF-MSK. Néanmoins, pour développer un modèle EF-MSK à part entière, l'intégration des muscles au modèle existant est essentielle pour piloter le modèle avec des muscles actionnés suivant le pipeline des dynamiques inverse et directe. Dans cette direction, des travaux futurs seront nécessaires et le cadre développé pour la modélisation EF-MSK dans l'étude actuelle fournira une base solide.

General Introduction

The musculoskeletal (MSK) system of the lower extremity combinedly acts as a pillar and propulsion system when we stand, walk, or perform an activity. The bones, ligamentous structure, and muscles all together work in synergy to provide both stability and mobility. Any disturbance in the synergy due to MSK disorders, may lead to functional limitations, which is a major cause of disability in all continents and economies. One of the highly prevalent MSK disorders is osteoarthritis (OA), affecting 303 million people globally in 2017 (Stanaway et al., 2019).

Total Knee Arthroplasty (TKA) is the most common surgical intervention for end-stage OA to restore joint function. Yet, patients remain partially satisfied due to sub-optimal performance of the reconstructed joint. There are factors related to surgical techniques, patients' general health condition and characteristics of their individual MSK apparatus that contribute to the overall outcome of a surgical intervention. Out of numerous factors, malalignment of implant components is a major contributor to the reduced implant survival (Schroer et al., 2013).

To facilitate proper implant alignment, surgeons largely rely on medical imaging modalities (e.g., CT, MRI) to assess patients' morphological information, such as 3D limb alignment¹, bone shape and size. Despite the advancement of assessment techniques, there seems no complete consensus on a particular procedure that works the best. As implant failure is associated with implant loosening and wear due to high stress developed at the implant interface (MacInnes, Gordon, and Wilkinson, 2012), therefore, to avoid implant degradation, high joint stresses have to be avoided. This motivates the need for an objective understanding of the *in vivo* mechanical loads at the joint.

There are complementary means to investigate *in vivo* joint mechanics (e.g., joint kinematics, joint load etc.). Gait analysis is often used for partial or indirect assessment of potential alternations of MSK properties after injury/pathology, and functional outcomes of treatment. Such approach although allows quantitative assessment of patients' motion pattern, however, joint mechanical loads cannot be investigated directly.

In the aforementioned context, Finite Element (FE) models are traditionally popular in estimating local mechanics of the joint. Yet, translating models to clinics remains a major bottleneck due computational burden associated with model development and simulation. The key challenges are fast and accurate generation of finite element mesh from images

¹three dimensional alignment of bone segments (e.g., femur and tibia) with respect to each other

and, adopting a approach with a decent trade-off between simplicity and relevance. Moreover, conventional FE models are mostly representative of the *in vitro* specimens working under either passive load or generic muscle loads. As such loading behavior cannot represent subject-specific physiological loads, integrating FE models with physiological loading conditions is indispensable.

To define clinically relevant loads, MSK models are widely used that generally incorporate motion data acquired from skin marker-based motion capture system. Such motion data inherently constitutes an artifact commonly known as Soft Tissue Artifact (STA), which directly introduces error while computing joint kinematics. Therefore to accurately estimate joint kinematics, compensating for STA is paramount.

Based on the aforementioned series of challenges, it appears that there is still a need for developing a comprehensive MSK modeling framework to understand local mechanics (e.g., joint contact load) of the joint under physiological boundary conditions.

To explore such possibilities, the BiomecAM chair program on subject-specific MSK modeling was initiated at *Institut de Biomécanique Humaine Georges Charpak*. The program seeks to develop computational models for clinical research in order to help diagnosing disease entities, treatment planning, and monitoring. Experimental facilities such as motion capture system and *in vitro* test rig are available that go hand-in-hand with computational modeling and evaluation framework. Presence of imaging resource like biplanar low dose X-Ray system (EOS[®], EOS-imaging, France) works as a focal point in the institute, which facilitates fast image acquisition of the whole body skeleton. Overall, the entire amenities available at the institute offer a holistic approach in developing MSK models.

To exploit such facilities available at the institute towards developing clinically relevant MSK models, the overall aim of the PhD thesis is thus set as “*contribution to personalized finite element based musculoskeletal modeling of the lower limb*”. The overall aim is motivated by the need to understand native knee joint biomechanics in daily activities and eventually to translate the model in clinical practice for surgery planning and assessment.

The manuscript is organized as follows-

The first chapter includes overview of the general anatomy of the lower limb with a specific attention to the knee joint, and its clinical contexts. The second chapter contains review of relevant literature concerning finite element models, gait analysis and associated MSK models to highlight the current challenges. The third chapter focuses on development of personalized finite element models dealing with both geometry and material properties of the ligaments, and validation with experimental results. In the fourth chapter, a novel approach for soft tissue artifact compensation is proposed and evaluated. The fifth chapter contains an opening towards clinical application, where utility of the low dose biplanar X-ray system is briefly explored in evaluating TKA implant alignment.

Chapter 1

Musculoskeletal Anatomy of the Lower Limb and Clinical Context

The lower limb musculoskeletal system consists of connective tissues of the articulated bony skeleton and the skeletal ligaments and muscles that act across the articulations. It is specialized to support the body's weight, locomotion and maintenance of the overall stability of the body. This chapter briefly overviews the musculoskeletal anatomy of the lower limb and the clinical context with a specific attention to the knee joint.

1.1 Descriptive anatomy

1.1.1 Osseous components¹

(i) Pelvis The pelvis is large, irregular and constricted centrally. The bony pelvis is composed of 4 bones : the two hip bones, the sacrum and the coccyx. The two hip bones articulate with each other anteriorly at the symphysis pubis and posteriorly with the sacrum at the sacro-iliac joints. The hip bones consist of ilium, ischium and pubis bones which fuse at the deep hemispherical socket forming the acetabulum. The **hip joint** is the articulation between the femur head and the acetabulum of the hip bone. Each of pelvic bones has unique landmarks (i.e. tuberosities and notches), such as anterior/posterior superior iliac spine (figure 1.1(A)). The primary function of the pelvis is to transfer the load of the upper body onto the lower limb during walking, standing or other motor tasks and to provide a strong and stable connection between the trunk and the lower extremities.

(ii) Femur The femur is the longest bone in the human body and articulates on its upper part with the acetabulum (hip joint) and on its lower part with the tibia, fibula and patella altogether to form the knee joint. Its shaft has a general forward convexity. Proximally, the femur consists of a head, neck and greater and lesser trochanters. The distal extremity of the femur is wider and more substantial acting as a bearing surface for transmission of weight to the tibia. It bears two large condyles (medial and lateral) that articulate with the tibial plateaus forming the **femorotibial joint**. The two most prominent points of the condyles

¹(Burgess and Lui, 2019; Gray, 2009; Snell, 2010)

are medial and lateral epicondyles. The condyles are separated by the intercondylar fossa (figure 1.1(B)).

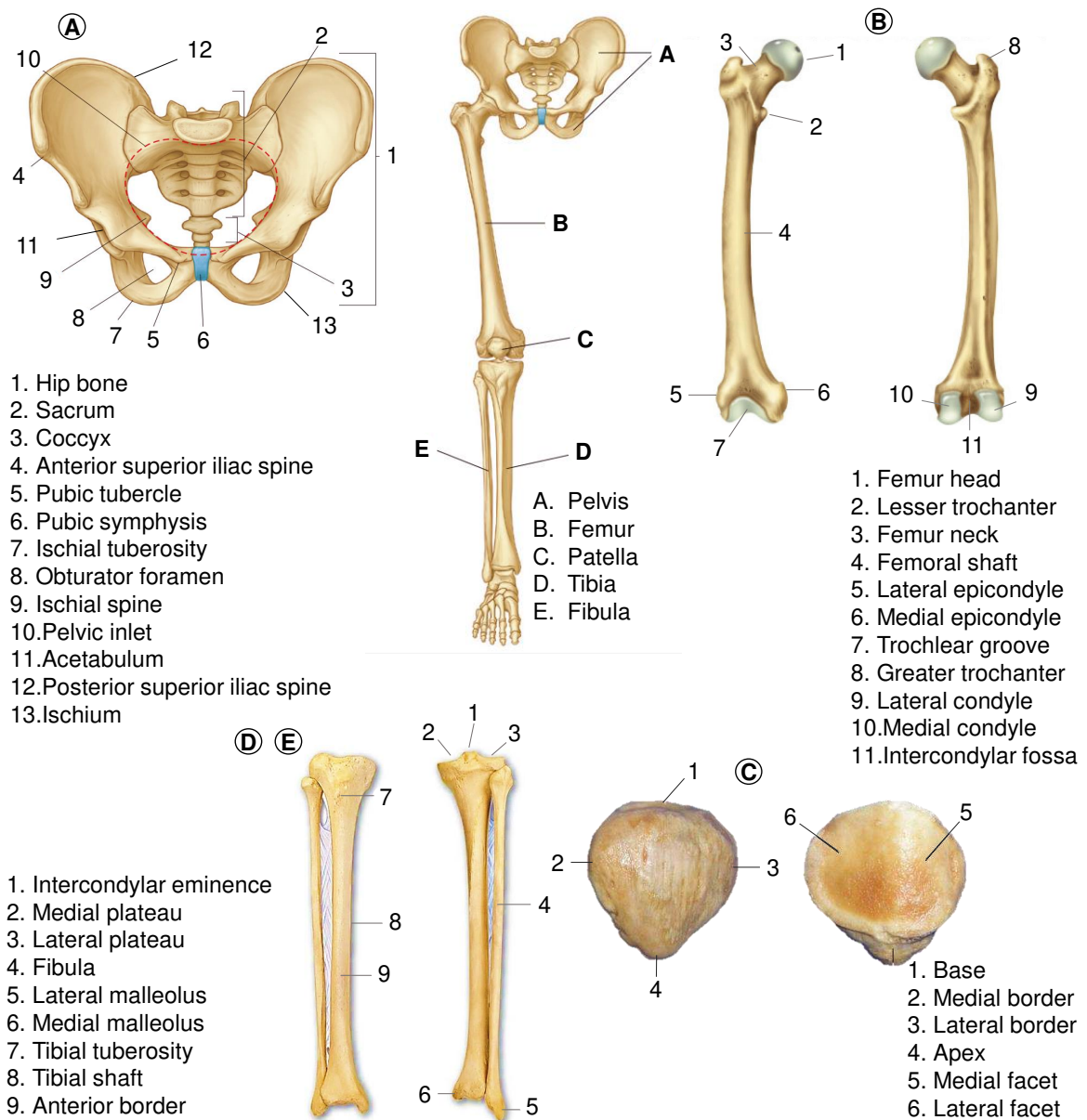


FIGURE 1.1: Lower limb bone segments and their respective landmarks for the (A) pelvis, (B) femur, (C) patella, (D) tibia and (E) fibula (figures adopted from (Gray, 2009) anatomy)

(iii) Patella The patella is the largest sesamoid bone lying anterior to the distal femur (figure 1.1(C)). It is flat, distally tapered and proximally curved. It has three borders and an apex. The thick superior border (also known as base) slopes anteroinferiorly. The medial and lateral borders are thinner and converge distally. The articular surface of patella extends onto the anterior surfaces of both the femoral condyles forming the **femoropatellar joint**.

(iv) Tibia The tibia lies medial to the fibula (figure 1.1(D)). The tibial shaft is triangular in cross-section and has expanded ends. The expanded proximal end bears the weight

transmitted through the femur and has asymmetric articular facets called medial and lateral plateaus. The medial tibial plateau is normally concave, whereas the lateral plateau has an anteroposterior convexity with large subject-to-subject variations (Hashemi et al., 2008). The plateaus are separated by intercondylar eminence. The slightly expanded distal end is laterally rotated compared to the proximal. The tibial tuberosity is the truncated apex of a triangular area divided into distal rough and proximal smooth region, where the patellar ligament is attached.

(v) **Fibula** The fibula is more slender than the tibia and has an irregular shaped head, a narrow neck, a long shaft and a distal lateral malleolus (figure 1.1(E)). The fibular collateral ligament (FCL) (also known as lateral collateral ligament (LCL)) is attached to the fibular head.

1.1.2 Lower limb musculature and connective tissues²

(i) **Muscles** The muscles of the anterior compartment of the thigh include sartorius, rectus femoris, vasti medialis, intermedius and lateralis (figure 1.2(A)). Vasti and rectus femoris extend towards the knee joint through a common tendon, collectively referred to as quadriceps tendon and they act as an extensor muscle of the knee.

The muscles of the medial compartment of the thigh include gracilis, pectineus, adductor longus, adductor brevis and adductor magnus. These muscles primarily act as adductors of the thigh.

The posterior compartment consists of long and short heads of biceps femoris, semitendinosus and semimembranosus. These are collectively termed as 'hamstrings' and they act as hip extensor and knee flexor (figure 1.2(B)).

(ii) **Menisci and ligamentous structure** The menisci (medial and lateral) of the knee joint are roughly semi-lunar in shape. Their proximal surfaces are concave shaped and articulate with the cartilage of the femoral condyles. The distal surfaces are generally flat shaped, resting on the tibial plateaus.

The menisci act as shock absorbers and protect the joint from the considerable forces generated during motion. They also provide stability by maintaining congruity with the articular surfaces. Other functions are lubrication, nutrition and proprioception (Cameron and Macnab, 1972).

The capsular and ligamentous assembly of the knee joint along with articular surfaces and muscles play a fundamental role in providing stability to the joint. As per general anatomical sites, the **cruciate ligaments**, ACL (anterior cruciate ligament) and PCL (posterior cruciate ligament) are inserted into the intercondylar femoral recess on one side, and respectively on pre-spinal and retro-spinal areas of the tibia on the other side (figure 1.2(D))

²(Capkin et al., 2017; Gray, 2009)

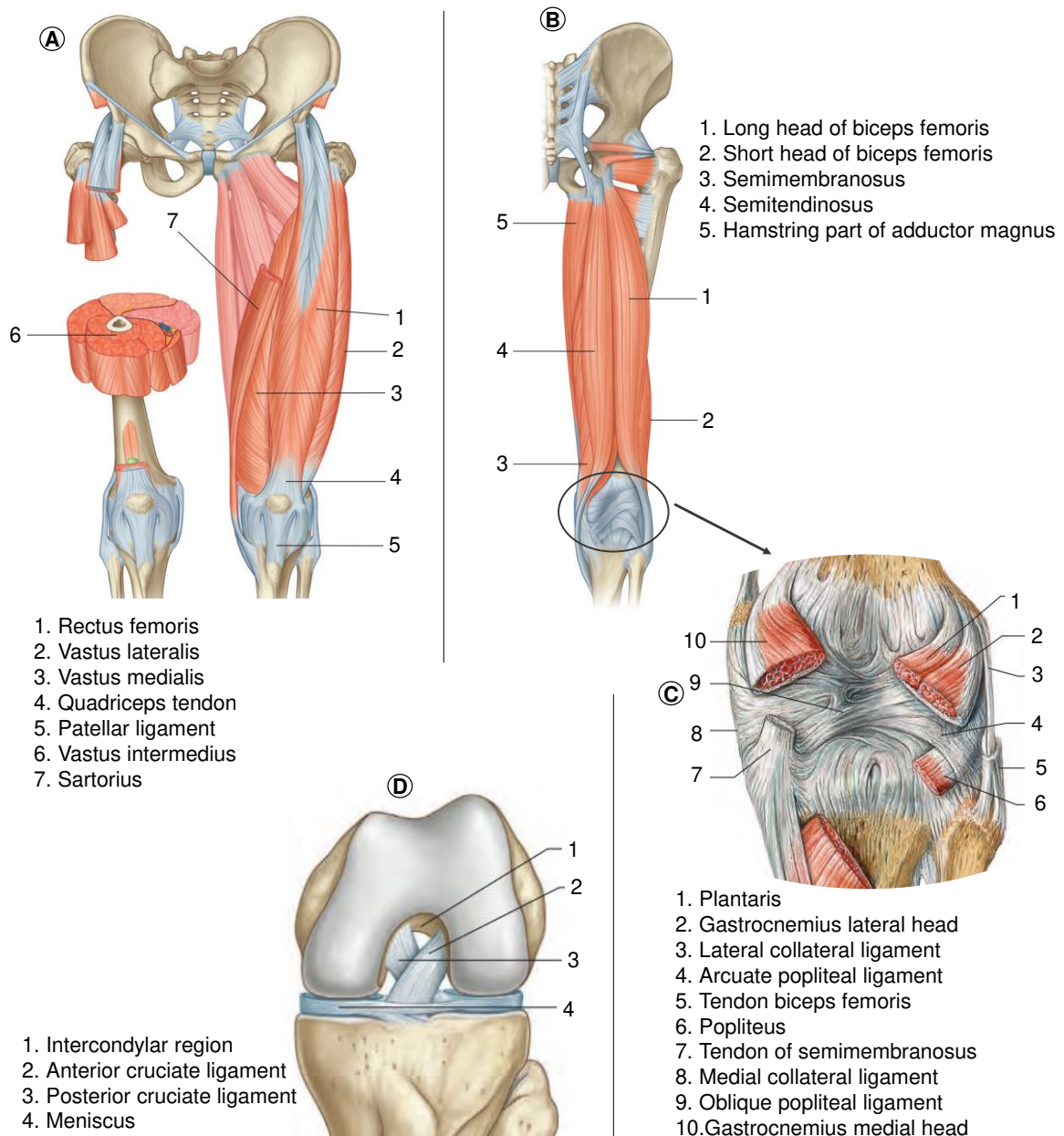


FIGURE 1.2: Lower limb muscle and ligamentous structure responsible for knee motion and stability. (A) Muscles of the anterior compartment of the thigh, (B) muscles of the posterior compartment of the thigh, (C) Posterior aspect of the knee with capsule intact and (D) anterior aspect of the knee in full flexion (figures adopted from (Gray, 2009) anatomy)

(Gray, 2009). They both stabilize the joint anteroposteriorly by restricting excessive movement of drawer (anterior and posterior translation), and limit internal rotation by winding each other (Zlotnicki et al., 2016). The ACL is mainly formed of two functional bundles, AM (anteromedial) and PL (posterolateral), and the PCL is formed of AL (anterolateral) and PM (posteromedial) (Logterman, Wydra, and Frank, 2018; Petersen and Zantop, 2007). The **collateral ligaments**, MCL (medial collateral ligament) and LCL (lateral collateral ligament) are inserted on the epicondyles of the femur on one side, and below to the tibial medial condyle

and the head of the fibula respectively on the other side (figure 1.2(C)) (Gray, 2009). They restrict lateral and medial movements and limit external rotation (Abulhasan and Grey, 2017). The MCL comprises of two (or possibly three) functional bundles, namely deep, superficial, and intermediate bundles. The patellar ligament is inserted on one side on the lower part of the patella and on the other on the anterior tuberosity of the tibia. It plays a fundamental role in the kinematics of the femoropatellar joint. The femoropatellar ligaments and the distal attachments of the quadriceps femoris muscle are mainly responsible for the stabilization of the patella. They (medial and lateral) originate from the femoral epicondyles and attach to the patellar borders. Other ligaments, such as popliteofibular, oblique popliteal ligament and arcuate act as complementary stabilizers on the posterior aspect of knee.

1.2 Biomechanics of the hip and knee joint³

The most frequent motion in the hip and knee joint occurs during locomotion. The movements of the lower limb in level walking activity can be broadly divided into "swing" and "stance" phases. When the leg swings, the knee flexes and the hip extends to avoid dragging the toes on the ground. At the end of swinging, the leg approaches the ground by extending the knee and flexing the hip in synergy. As the medial femoral condyle size is normally higher than the lateral one, the tibia rotates laterally towards the end of knee extension. This kinematic phenomenon is well known as 'screw-home' mechanism (Goodfellow and O'Connor, 1978) (figure 1.3).

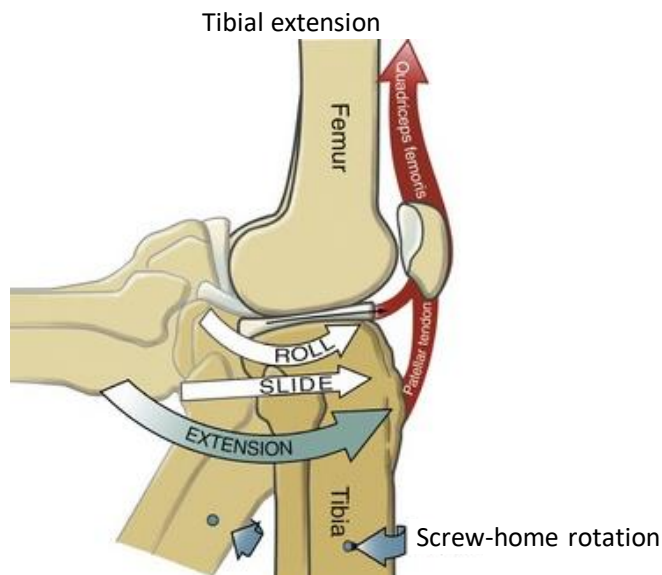


FIGURE 1.3: Screw-home rotation of the tibia towards the end of extension (Tocks et al., 2018)

At the terminal extension, the knee joint can be slightly hyperextended (although variable from subject-to-subject) and is locked by tightening the soft tissues. However, Thus, the knee joint maintains a stable configuration prior to weight bearing when the leg forwards

³(Gray, 2009)

for the heel-strike. At this point, the knee acts like a single link, and the hip rotates laterally moving forward. After the leg impacts the ground, the knee flexes allowing the tibia to rotate medially, and the soft tissues relax to deform and absorb energy. Conversely, the knee extends towards the toe-off allowing the tibia to rotate laterally and the foot becomes a rigid lever for pushing the body forward.

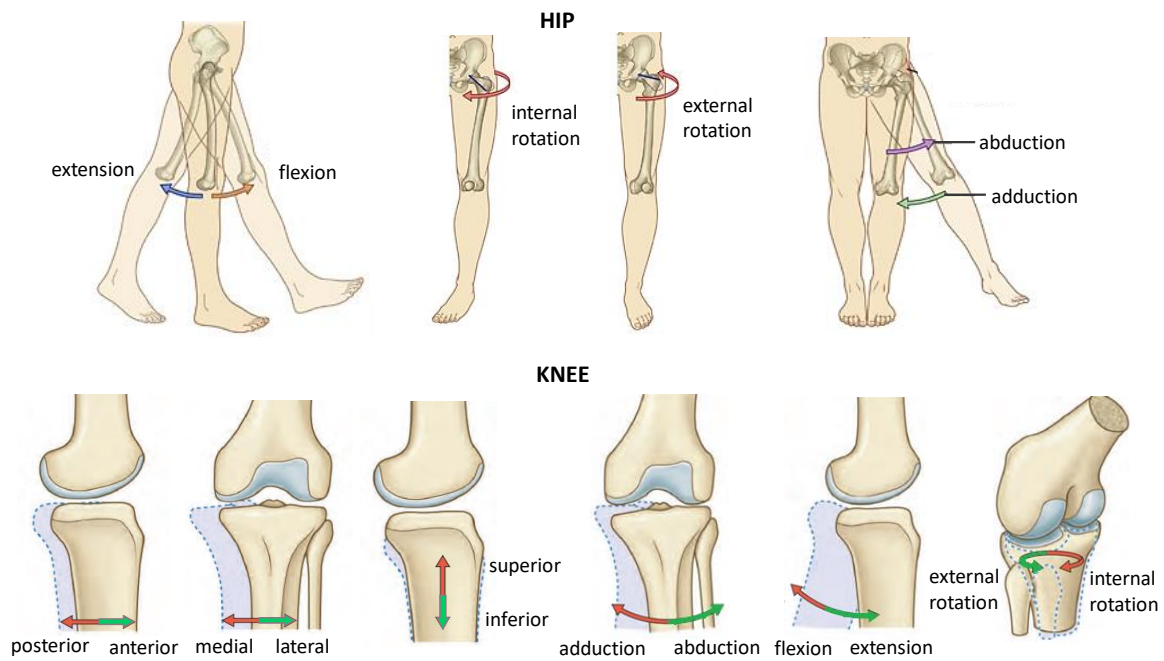


FIGURE 1.4: The hip and knee joint motions in three dimensions (figure for the hip adopted from *basic medical*) and for the knee from (Gray, 2009))

Hip joint is comparatively stable as it is closely fitted to the acetabulum. During motion, it normally goes into unrestricted motion in 3 rotational Degrees of Freedom (DoF) (figure 1.4). The relative translations between the femoral head and acetabulum surfaces are innately limited for healthy individuals, and therefore commonly referred to as 'ball and socket' joint (Molini et al., 2011). For the knee joint, both mobility and stability are achieved by the interactions of the joint surfaces, passive stabilizers, and muscles crossing the joint. Because of relatively incongruent nature of the articular surfaces, the joint is considerably mobile in comparison to the hip joint. The knee joint experiences motion in 6 DoF (3 rotational and 3 translational), although the primary motion i.e., flexion/extension is in the sagittal plane. Abduction and adduction motion of both the joints occur in the coronal/frontal plane, whereas medial-lateral (also known as internal-external) motion takes place in transverse plane. These motion patterns for both the hip and knee joint are subjected to vary from subject to subject depending on the articular geometry, soft tissue properties and muscle loads.

1.3 Clinical context

1.3.1 Lower limb pathology and prevalence

Lower limb pathological conditions are common burdens of individual health affecting around 303 million of individuals globally in 2017 (Stanaway et al., 2019).

Among different pathological conditions, osteoarthritis (OA) is highly prevalent characterized by loss of joint articular cartilage resulting in disability and increased morbidity. Although OA can affect any joint, it mostly occurs at the knee joint, and it is mainly driven by mechanical factors (Brandt et al., 2006). For instance, knee ligament laxity or rupture decreases the stability of the knee joint by increasing tibial translation and thereby may increase the risk of OA up to 4 times (Blagojevic et al., 2010). Therefore for proper assessment of the joint stability and associated risks, understanding the relationship between ligament behavior and its effect on the joint mechanics may be beneficial.

1.3.2 Assessment methods

Medical imaging Medical imaging techniques such as Magnetic Resonance Imaging (MRI), Computed Tomography (CT) and X-ray play a vital role in diagnosing and monitoring joint disorders and treatment.

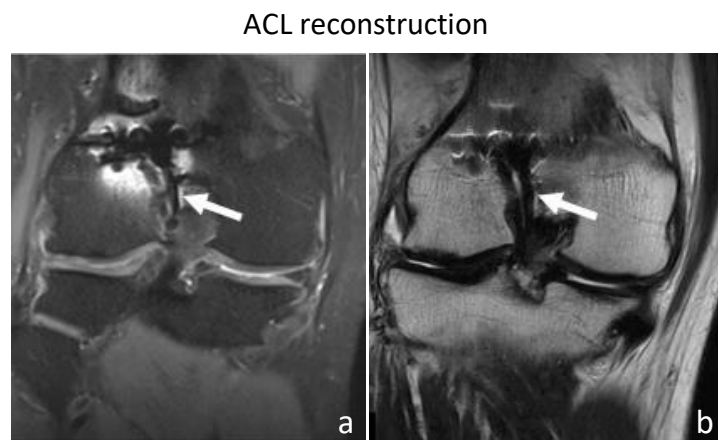


FIGURE 1.5: Coronal MR images of ACL double bundle reconstruction (Viala et al., 2016)

Magnetic Resonance Imaging (MRI) is often used to analyze the status of menisci and ligaments, integrity and performance of the muscles. It provides high resolution soft tissue contrast and multiplanar tomographic display. As because there is no risk of radiation exposure, it is a popular choice in diagnosing traumatic soft tissue injury. However, as it can interact with metals, it is not safer for patients with pacemakers and other metallic implants. It can also be used for examining ligament reconstructions (figure 1.5).

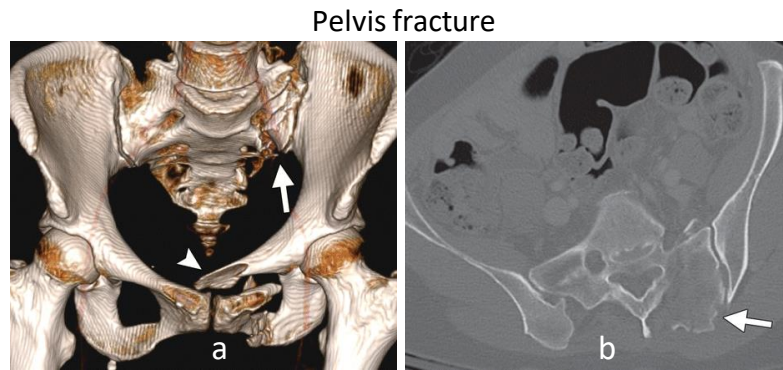


FIGURE 1.6: Lateral and vertical shear injury of the pelvis (a) 3D volume rendered CT image with cranially displaced sacral fracture (arrow), (b) axial CT images showing oblique fracture (arrow) (Khurana et al., 2014)

In CT scan, a series of X-ray images taken at different angles are combined together to produce cross-sectional slices of the bones, soft tissues and blood vessels. It generally provides detailed and accurate information than plain X-ray images. It is normally used for reliable examination of internal organ injuries/pathologies and MSK disorders. For instance, CT scan can better assess the degree of subtle pelvis fractures (Wedegaertner et al., 2003) (figure 1.6). Moreover, medical stuffs (surgeons, radiologists) can also analyze the images in 3D reconstruction for preoperative planning. Nevertheless, CT scans are more expensive than X-rays and readily not available in all kinds of hospitals and clinics. During scanning the patient is also exposed to harmful radiations similar to conventional X-ray.

An X-ray is the quickest and most accessible form of imaging. It is generally used to spot fractures, joint dislocations and misalignment. It is also considered reliable to detect OA in later stages, although not suitable to detect different forms of subtle tissue injuries.

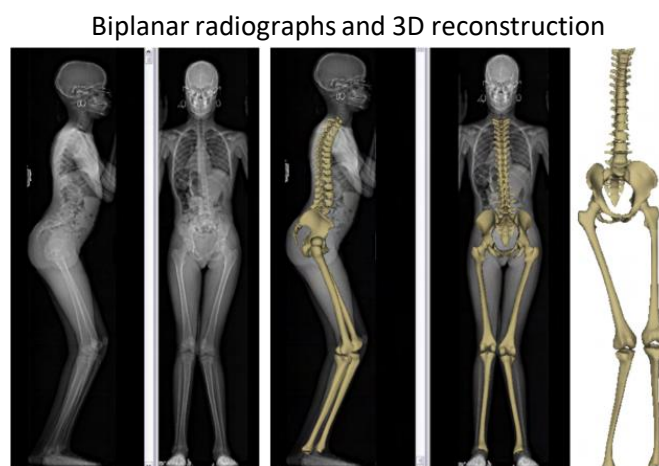


FIGURE 1.7: 3D skeleton of a cerebral palsy patient (Dubousset et al., 2010)

Biplanar low dose X-Ray system (EOS[®], EOS-imaging, France) is effectively used in routine clinics. As it allows simultaneous acquisition of antero-posterior and lateral images of

the whole body, 3D surface reconstruction of the bones can be obtained. This particularly helps a clinician to examine bone deformities and misalignment by computing different clinically relevant parameters in 3D (e.g., femorotibial mechanical angle, femoral and tibial torsion, femoral neck shaft angle etc.) (figure 1.7). Unlike other imaging modalities, the EOS system can be used in physiological weight-bearing position. Furthermore, the radiation doses with EOS are 800 to 1000 times lower than CT scans (Dubousset et al., 2010).

All the above mentioned medical imaging techniques are helpful in diagnosing different types of lower limb disorder and monitoring treatment. However, such evaluations are only performed in static conditions and not sufficient for functional evaluations during dynamic activities. In this context, gait analysis is widely used as a complementary means.

Gait analysis Gait analysis is used in clinical assessment of human locomotion that displays dynamic posture and coordination during movement. It is particularly useful in partial or indirect assessment of any potential alternations at the joint or outcome of a surgery. It is also sometimes used for selecting among various treatment options, monitoring progress and to predict prognosis (Brand, 1989; Baker, 2006). This is achieved by performing rigorous trials. Although gait analysis is widely used in multiple research areas such as orthopedics, rheumatism, neurological disorder, rehabilitation, product design and sports biomechanics, it is still variably implemented for clinical assessment purposes.

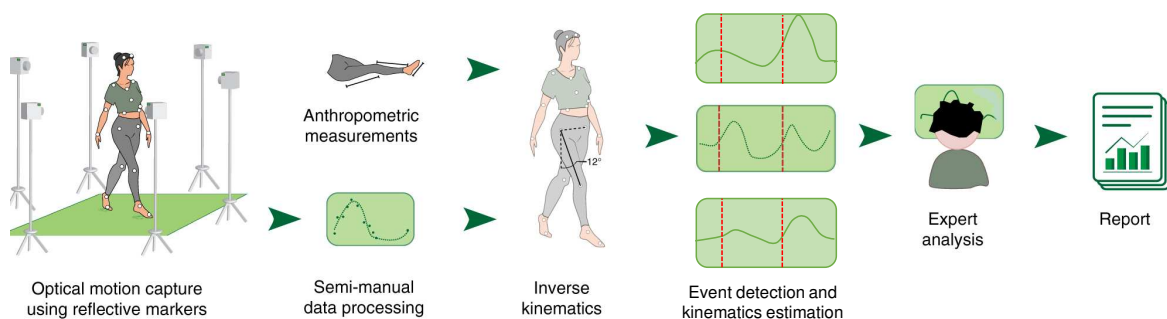


FIGURE 1.8: A general clinical workflow of gait analysis. A clinician first places the reflective markers on the subject based on anthropometric measurements. Several cameras track the locations of the markers that are later reconstructed into 3D position time series. Then using inverse kinematic approach relevant joint angles are computed and various gait events (toe-off, heel strike) are detected. Finally based on expert analysis, a report is prepared for clinical decision. making (Kidziński et al., 2020)

Currently, skin marker-based motion capture system is widely used in gait analysis. In this technique, retro-reflective markers are placed on the skin, and their instantaneous positions are obtained using stereophotogrammetry and optoelectronic sensors (figure 1.8). External forces are measured with force plates and electrical activity of muscles with electromyography (EMG). Anthropometric quantities are obtained either using a scale or calipers, or more modern techniques such as 3D scanners. An anthropomorphic model consisting of a kinematic chain of links is used to derive parameters (e.g., kinematics, kinetics) that are

not directly observable. Each link in the model represents a segment comprising the bony part and soft tissues.

Throughout the process, from marker attachment to estimation of kinematics and kinetics, three sources of errors affect the analysis. The first one is *instrumental error*, which appears as a result of instrumental noise and volume calibration inaccuracies. The second source of error arises from difficulty in placing the markers accurately in regards to specific anatomical landmarks. These two sources of errors and methodologies to minimize them is briefly explained in appendix A.

The third source of error is considered the most invalidating source, commonly referred to as Soft Tissue Artifact (STA). STA originates due to relative movement of muscles and skin to the underlying bone. This relative movement is a result of soft tissue deformation associated to skin sliding, muscle contraction, gravitational and inertial effects (Leardini et al., 2005). As this error has the same frequency content as that of the bone motion, distinguishing this error from actual bone motion is not possible with filtering methods (Stagni et al., 2005). STA directly introduces error in computing skeletal kinematics, because of which, direct usage of gait data for clinical assessment and decision-making is debatable. This motivates the need for exploring effective STA compensation strategies.

1.3.3 Treatments and outcomes

To restore joint stability and to regain functional mobility of the joint, different surgical procedures are recommended at different levels of impairment from a standard menu of options.

For example, to restore joint stability due to ligament rupture, ligament reconstruction is widely used. In such surgical technique, the ruptured ligament (e.g., ACL) is generally replaced by a graft tissue harvested from the patient (autograft) or sometimes from a donor (allograft) by inserting it through a drilled tunnel of femur and tibia. Normally, ACL reconstruction is considered as an effective surgery with 75-90% patients reporting good to excellent outcomes (Miller and Cole, 2004). Yet, 10-25% patients require a revision causing great concerns among surgeons. Failure to ligament reconstructions is primarily attributed to technical faults (around 70%) such as non-anatomic tunnel placement and improper graft tensioning (George, Dunn, and Spindler, 2006). Improper graft tensioning often leads to either under-constraining (lax ligaments) or over-constraining of the knee. Therefore, to properly optimize tensioning for ligament reconstruction, knowledge of native ligament mechanical behavior is critical. This motivates the need for geometric and mechanical modeling of the knee joint to properly understand how ligament tensioning effects the native knee stability.

Secondly, in the case of OA, Total Knee Arthroplasty (TKA) is an often recommended as final operative management. It is among the most frequently employed orthopedic surgeries, estimating a demand for primary TKA to grow by 673% by 2030 (Kurtz et al., 2007).

While planning for TKA implantation, clinicians preoperatively assess the knee in the three spatial planes for successful implant positioning. There are several options available for proper implant positioning (detailed in Appendix B). For instance, one popular principle is to position the implant components by aligning to the mechanical axis of the knee joint (Jeffery, Morris, and Denham, 1991). Conversely, others recommend anatomical alignment of implants, which reported better implant durability (Kim et al., 2014). Few others also advocate on kinematic alignment and patient specific instrumentation for longer implant survivorship (up to 10 years) and functional outcomes (Howell et al., 2001; Yaffe et al., 2014; Zhu et al., 2017). Despite such aforementioned geometric alignment approach for better functional outcomes, no complete consensus on a particular technique has been achieved yet, as "one size fits none" for many treatments (Fregly, Boninger, and Reinkensmeyer, 2012). For better functioning of the implant, along with optimal choice of implant design and alignment, a precise balancing of the soft tissues is also critical (Vaienti et al., 2017).

As overall functional stability of the knee joint is achieved by inter-dependent interaction of various constituents of the joint (e.g., articular surface, capsule, menisci, ligaments and muscles), it is clinically difficult to differentiate variability of influence on TKA performance. Therefore, a comprehensive understanding of these elements in a native knee is important for surgery planning. Personalized computational modeling could be one possible avenue for objective assessment of subject-specific properties.

Synthesis

This chapter highlighted that

- Personalized computation modeling such as FE modeling could be helpful for understanding native knee joint mechanics and for surgery planning. Therefore first part of the next chapter will be focused on salient FE models and their model development and evaluation strategies.
- We also observed that for proper assessment of functional outcomes of an intervention, gait analysis is essential as it offers physiological loading conditions. It is also important for prescribing clinically relevant boundary conditions for computational models (e.g., musculoskeletal models). However, direct usage of gait data is error prone because of soft tissue artifact (STA). Therefore the second part of the next chapter will be focused on different STA compensation strategies. Also different complementary means for assessing joint biomechanical behavior under *in vivo* loading conditions will be explored.

Chapter 2

Literature Review

The illustration of the musculoskeletal (MSK) anatomy and broader clinical context in the previous chapter echoed that personalized finite element (FE) models seem to be beneficial for better understanding the local biomechanical behavior of the joint elements (e.g., ligament, articular geometry) and their interactions.

2.1 FE modeling and analysis of the knee joint

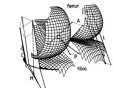
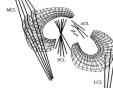
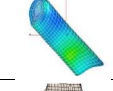
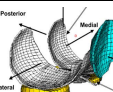
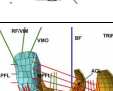
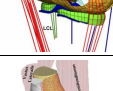
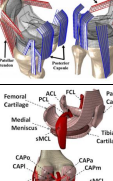
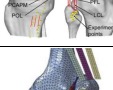
A variety of FE models have been developed in the literature in order to study various quantities of interest, and the degree of model complexity varies with the purpose of study. The level of complexity leads to various sets of challenges that can be observed while developing the geometry, assigning material properties, prescribing boundary conditions and in model validation/verification processes. In this regard, various studies are synthesized in table 2.1 and will be commented below.

2.1.1 Geometry

One of the key challenges in obtaining subject-specific FE mesh for the bones lies in mesh generation approaches based on different medical imaging modalities. For instance, (Bendjaballah, Shirazi-Adl, and Zukor, 1997) developed a FE model consisting of bones, and cruciate and collateral ligaments. The bone geometry was developed from CT data. Similarly in another sets of studies to investigate joint biomechanics under various quadriceps force (Mesfar and Shirazi-Adl, 2005), knee jury mechanism (Kiapour et al., 2014), have acquired bone geometry from CT data. MRI was also used in other studies (Baldwin et al., 2012; Beidokhti et al., 2017; Harris et al., 2016). Although such imaging modalities considered to be the best suited for viewing bone morphology, however, in addition to inherent disadvantages (e.g., radiation dose and non-weight bearing position), 3D model reconstruction from the sets of images is a cumbersome process, due to which most of the studies are restricted to a single specimen only (Adouni and Shirazi-Adl, 2009; Bendjaballah, Shirazi-Adl, and Zukor, 1997; Mesfar and Shirazi-Adl, 2005). More recently use of biplanar X-ray imaging is shown to be promising in daily clinical practice (Dubousset et al., 2010). Introduction of this alternative approach has improved the reconstruction techniques in terms of time, ease

and flexibility of application (Chaibi et al., 2012). Such remarkable techniques, developed at *Institut de Biomécanique Humaine Georges Charpak*, indicate a possibility of generating fast and accurate subject-specific FE models.

TABLE 2.1: Synthesis of most relevant FE models

Author, year	FE model	Imaging modality	Ligaments		Specimens	Boundary conditions	Validation/Verification	Routine clinical use
			Geometry	MP				
(Blankevoort and Huiskes, 1996)		Roentgen-stereophotogrammetry	ACL, PCL, MCL and LCL (non-linear line elements)	Literature (K kept constant, %ε subject specific)	4	Axial torque on tibia	One-to-one	NO
(Bendjaballah et al., 1997)		CT	ACL, PCL, MCL and LCL (Non-linear springs)	Literature	1	Varus valgus moment	Literature	NO
(Limbert et al., 2004)		Direct measurement	ACL	Literature	1	Passive flexion as displacement	Literature	NO
(Peña et al., 2005)		MRI	ACL, PCL, MCL and LCL (continuum)	Literature (Non-linear hyperelastic fibered material)	1	Axial load to the tibia	Literature	NO
(Peña et al., 2006)		MRI	ACL, PCL, MCL and LCL (continuum)	Literature (%ε subject specific)	1	Combined compressive and AP tibial load	Literature	NO
(Mesfar and Shirazi-Adl, 2005)		CT	ACL, PCL, MCL, LCL, PT, MPFL and LPFL (Non-linear springs)	Literature	1	Angular displacement at different Q-force	Literature	NO
(Adouni and Shirazi-Adl, 2009)		CT	ACL, PCL, MCL, LCL, PT, MFPL, LFPL, Quadriceps and Hamstring muscle group (non-linear springs)	Literature	1	Angular displacement on tibia	Literature	NO
(Dhaheer et al., 2010)		NA	ACL, PCL, MCL, LCL, PT, QT, MFPL and LFPL (continuum)	Literature	1	Angular displacement with muscle loading	Literature	NO
(Baldwin et al., 2012)		MRI	PT, QT, LFPL, MFPL	Non-linear tension only springs in a deformable 2D mesh	3	Internal/external and Varus/valgus torque	One-to-one	NO
(Kiapour et al., 2013)		CT, MRI	ACL, PCL, MCL, LCL, MFPL, LFPL, PFL, PT, Capsule, Quadriceps and Hamstring muscle group (continuum)	ACL, PCL, MCL, LCL (Incompressible, anisotropic and Hyperelastic) Others (non-linear spring)	16	Various loading conditions with simulated muscle load	With average experimental data of all specimens	NO
(Harris et al., 2016)		MRI	ACL, PCL, MCL, LCL, POL, PFL and ALS (non-linear springs)	Optimized K and %ε	4	Torque in different DoF	One-to-one	NO
(Naghbi Beidokhti et al., 2017)		MRI	ACL, PCL, MCL, LCL, PT and Quadriceps muscle tendons (continuum and non-linear spring)	Literature, Optimized	3	Internal/external and varus/valgus torque	One-to-one	NO

To include ligaments in the models according to their subject-specific anatomical attachment sites, studies either did not explicitly mention the procedure (Pena et al., 2005; Pena et al., 2006), or used MRI data (Baldwin et al., 2012; Harris et al., 2016; Kiapour et al., 2014). Few others also attempted to implement personalized insertion sites based on CT data, but was partially successful because of poor visibility of soft tissues in the images (Adouni and Shirazi-Adl, 2009; Mesfar and Shirazi-Adl, 2005). Notably, all these studies agreed that implementing accurate subject-specific ligament attachment sites in the models is essential to avoid undesired influence on ligament loads and eventually in joint kinematics. In this context, (Rochcongar et al., 2016) at *Institut de Biomécanique Humaine Georges Charpak*, introduced an original technique to identify ligament attachment sites accurately based on CT images of dissected knee joint. Such insights could be a strong ground for subject-specific joint modeling.

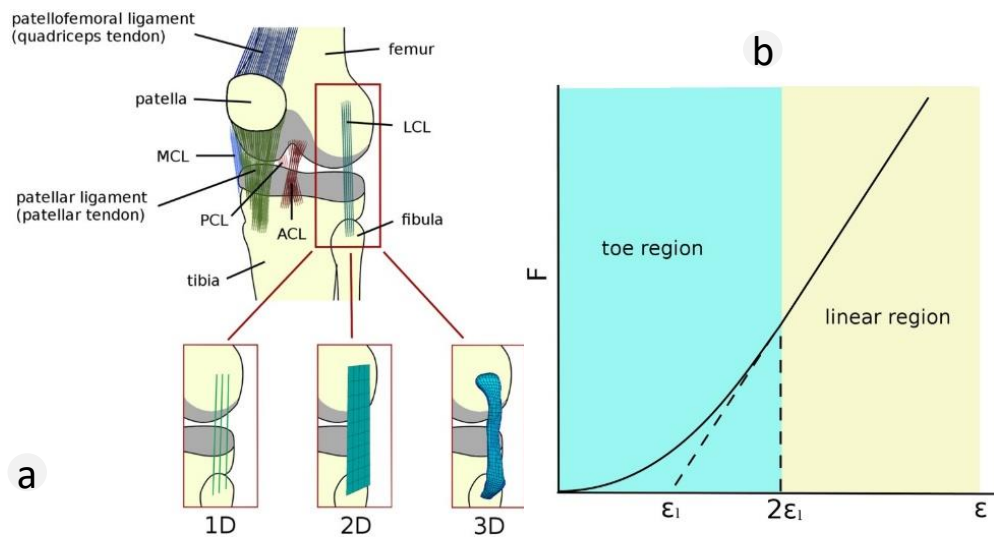


FIGURE 2.1: (a) Schematic representation of the knee ligaments (ACL, PCL, MCL and LCL) as 1D, 2D and 3D elements adopted from (Galbusera et al., 2014) (b) force(F) - strain(ϵ) behavior of a ligament adopted from (Blankevoort and Huijskes, 1991). $2\epsilon_1$ is the threshold strain indicating toe to linear region

With regards to modeling of the ligaments, traditionally both 1D and higher dimensionality (2D, 3D) elements have been equally used (figure 2.1a). As because the ligaments are not able to sustain compression load, 1D elements such as cables/springs, trusses are commonly used either as bundles of elements (Bendjaballah, Shirazi-Adl, and Zukor, 1997; Mesfar and Shirazi-Adl, 2005) or as a single bundle (Yu, Walker, and Dewar, 2001). Such elements are advantageous for easy implementation and computationally inexpensive. While detailed representation (e.g., solid elements) of the ligaments could be interesting for studying force distribution on the ligaments (Bendjaballah, Shirazi-Adl, and Zukor, 1997), such models require detailed image-based information resulting in high computational cost in developing and simulating them. Moreover, neglecting 3D behavior of ligaments does not dramatically impact other parameters such as joint kinematics (Blankevoort and Huijskes, 1991). In this aspect, simpler representation may be beneficial for studies where higher number of subjects need to be analyzed and, at the same time, capable of predicting joint mechanics (Beidokhti

et al., 2017; Galbusera et al., 2014).

To represent other soft tissues (e.g., cartilage, menisci) in the model, wide range of possible choices can be observed. The level of detailing varies according to research question and specific application of it. Some models concentrate on faithful capture of specimen-specific anatomy using CT and MRI imaging to investigate mechanical role of the components in a tissue. For example, one study included main articular soft tissue structures of the knee joint, featuring cartilage layers and menisci with complex material behavior (Pena et al., 2006) to study combined role of ligaments and menisci. Such type of models can potentially provide new insights into surgery performance such as meniscectomy, and disease progression such as OA. Conversely, some other strategies are steered by simplicity, where all the joint soft tissues are not explicitly modeled. For instance, the same group referred earlier excluded cartilage and meniscal geometry in the model that was aimed to study effect of graft tensioning in ACL reconstruction (Pena et al., 2005). This study concluded that "influence of menisci and cartilage with regards to the main objective of the study is not very important". These studies underlined the importance of a proper decision-making on inclusion of relevant joint elements in the model.

Overall, all the above studies and their methodology of representing the joint, particularly the passive structures, highlighted several challenges. These can be broadly tailored into two categories. First, generation of fast and accurate subject-specific FE mesh and second, a proper balance between relevance and simplicity to represent the joint structure.

2.1.2 Material properties

When it comes to assigning material properties of the bones, depending on the scale of hierarchy and purpose of study, varieties of material modeling are chosen. At mesoscale, bones are investigated either at osteon level embedded in the cortical bone or at the porous network in the spongy bone (Sabet et al., 2016). At the macroscale or at the whole bone level, bones are differentiated between cortical and trabecular/spongy bones. This differentiation is largely based on distinction of porosity of the bones (Morgan, Unnikrisnan, and Hussein, 2018). Such differentiation helps studies to investigate bone fracture mechanism (Keyak et al., 2001), to estimate bone strength following treatments of osteoporosis (Burr, 2016). At this level, anisotropy, inhomogeneity, viscoelasticity and nonlinearity can be introduced. Even multiscale models are used to understand cascade of mechanisms at different levels within the bone (Sabet et al., 2016). However, to investigate quasistatic response at the joint, considering bone as linear elastic is reasonable. Elastic modulus of cortical bone has been reported roughly in the range 10 GPa to 32 GPa, when measured with different test methods such as destructive, ultrasound and non-indentation method (Choi et al., 1990; Hunt et al., 1998). The Poisson's ratio varies in the range 0.15 to 0.45, however it is classically set to 0.3 (Rupin et al., 2008). Since the elastic modulus of bone is considerably higher than the surrounding soft tissues, the bones are considered rigid more often (Beidokhti et al., 2017; Halloran, Petrella, and Rullkoetter, 2005; Pena et al., 2005). The choice of bones as rigid is also motivated by reduced computational time.

Quantitative estimation of material properties of soft tissues is extremely challenging. The properties are known to vary with subject, posture, loading condition and time (Zheng and Mak, 1999). The properties can also be different depending upon whether measured *in vivo*, *in vitro* or *in situ*. However, *in vitro* methods are more popular for detailed investigation of both the physiological and mechanical behaviors of tissue. Therefore, constitutive laws assigned to soft tissues are conveniently acquired from various *in vitro* experimental studies available in the literature.

For representing cartilage, varieties of material representation can be seen in the literature. To understand cartilage mechanics and influence of cartilage structure on the knee joint, some authors used depth-dependent cartilage properties with fibril networks (Halonen et al., 2016; Shirazi, Shirazi-Adl, and Hurtig, 2008). A few included multi-scale modeling of cartilage (Tanska, Mononen, and Korhonen, 2015; Halloran et al., 2012). Cartilage as linear elastic material has been commonly used due to its equivalence between incompressibility and short-time biphasic nature (Ateshian, Ellis, and Weiss, 2007; Kiapour et al., 2014). One study at *Institut de Biomécanique Humaine Georges Charpak* also showed the possibility of defining cartilage and bone together as a homogeneous bone-cartilage material with equivalent material properties of bone and cartilage (Germain et al., 2016). Although, such consideration may not be sufficient for estimating cartilage mechanics, yet can be considered relevant for predicting kinematic behavior of the knee joint. Similar is the case for the meniscus, where a detailed representation was required to understand role of meniscus in response to loading and damage progression (Halonen et al., 2014; Kiapour et al., 2014).

Ligaments, based on their representation, different constitutive laws have been traditionally assigned. For 1D type of elements, non-linear force-strain behavior is assigned to the ligaments with quadratic toe region and linear forward (Blankevoort and Huijsskes, 1991) (figure 2.1b). Bi-linear form of force-strain behavior has also been used by linearizing the toe region (Shin, Chaudhari, and Andriacchi, 2007). In 3D representation of ligaments, they are commonly defined as incompressible material behavior (Beidokhti et al., 2017; Dhaher, Kwon, and Barry, 2010). In either case, whether 1D or 3D, the elements representing the ligaments can only sustain tension and offer no resistance to compressive load (Galbusera et al., 2014). Moreover, knee ligaments (particularly ACL, LCL and MCL) are known to be at strained state, already sustaining tensile load at full extension (Guess, Razu, and Jahandar, 2016; Pena et al., 2006). The PCL normally stays in slack condition at the full extension (Blankevoort and Huijsskes, 1991). This strain at the fully extended position of the knee is commonly referred to as prestrain or reference strain or initial strain.

Deriving prestrain values confronts numerous hurdles. Challenges are mostly linked to both measurement and modeling issues. Measurement challenges are related to identification of accurate ligament attachment sites and determination of ligament characteristics during motion (Belvedere et al., 2012; Gardiner, Weiss, and Rosenberg, 2001; Rochcongar et al., 2016). Owing to such difficulties, FE models generally adopt prestrain values from other studies (Adouni and Shirazi-Adl, 2009; Bendjaballah, Shirazi-Adl, and Zukor, 1997; Mesfar

and Shirazi-Adl, 2005). However, such approach cannot be considered as subject-specific as prestrain values do not correspond to the specimen under study.

In an attempt for assigning subject-specific prestrain values, laxity tests on cadaveric specimens are normally used to indirectly estimate prestrain values based on optimization methods (Baldwin et al., 2012; Harris et al., 2016; Beidokhti et al., 2017), which aim for minimizing a cost function (experimental-numerical kinetic/kinematic difference) in subsequent iterations. All these studies concluded that subject-specific prestrain values offer accurate kinematic and kinetic prediction. Nevertheless, such methods are likely to be computationally expensive up to 400-600h per specimen depending upon complexity of the models as reported by (Beidokhti et al., 2017). In such context, any alternative approach which can circumvent high computational cost could be beneficial for clinical translation.

2.1.3 Boundary and loading condition

In FE models representing *in vitro* specimens, boundary and loading conditions are normally based on corresponding controlled *in vitro* studies. Such studies mostly focused on reproducing *in vitro* experiments. For instance, passive flexion load as displacement was applied on the tibia in a study to understand the behavior of stressed and stress-free ligament (Limbert, Taylor, and Middleton, 2004). Other studies also attempted to implement *in vivo* alike dynamic loads. To observe detailed biomechanics (e.g., joint kinematics, ligament and extensor muscle forces) of the knee joint in various closed kinematics chain exercises, (Mesfar and Shirazi-Adl, 2005) introduced flexion load at the tibia under various quadriceps force by keeping the femur fixed. Based on the results, this study advocated the use of squat exercises in post-ligament reconstruction period. In a similar fashion, (Baldwin et al., 2012) and their subsequent works used a whole joint knee simulator (Kansas Knee Simulator) to apply dynamic loads on the joint of a cadaveric specimen. Then the experimental loading profile was implemented to evaluate the FE model of the knee joint. Although such models based on cadaveric specimens are admirable in increasing knowledge on interaction between passive stabilizers of the joint, yet debatable for muscular activity in the absence of physiological loading conditions. Moreover, such implemented loads are largely generic as same loading pattern were applied for different specimens, whereas the knee joint is subjected to variable loading conditions during daily life activities such as walking. *In vivo* based computational models such as musculoskeletal models seem to be an efficient alternative since such models can embody physiological loading conditions based on motion analysis data.

2.1.4 Verification and Validation

Traditionally, *in vitro* models are considered relatively simple to validate with corresponding experimental study in comparison to *in vivo* models. This is particularly true for validating joint kinematics, where reasonably accurate kinematics can be obtained by rigidly attaching markers to the bones. In this aspect, a kinematic test bench was developed at *Institut de Biomécanique Humaine Georges Charpak* (Azmy et al., 2010). This experimental set up uses a servo-actuator to place the quadriceps tendon under traction and a rope and

pulley system to continuously mobilize the knee in flexion/extension by introducing passive load at the tibia, while keeping the femur fixed. Then, with the help of bone-attached retro-reflective tripod markers and an optoelectronic device, spatial bone positions can be deduced. Subsequently, this set up has been used in several other studies to acquire joint kinematics and parallelly served in model validations (Dagneaux et al., 2015; Germain et al., 2016). However, substantial variabilities can be observed regarding model validation. In some scenarios, models were validated against average experimental data (Germain et al., 2016; Kiapour et al., 2014) representing general trends. These studies, although build confidence in the ability of FE models to represent general trends, such evidence may not be sufficient to capture inter-individuality of knee specimens. Here, direct validation (one-to-one) of model-predicted response against corresponding cadaveric results could be crucial for proper model validations before translating the model to *in vivo* loading conditions.

Synthesis 1

After reviewing various literature on *in vitro* FE models, it is evident that despite significant advancements over recent years, translating models to clinics remains a major challenge. The challenges are mainly linked to-

- Fast and accurate methods for building subject-specific FE models.
- Adopting a modeling approach with decent trade-off between relevance and model simplification to accelerate computational time.
- Calibration of ligament material properties.

2.2 Musculoskeletal modeling

To noninvasively investigate relationship between locomotion and internal biomechanical quantities, musculoskeletal (MSK) modeling represents a valuable method in a wide range of physiological and pathological conditions. Traditionally, such models have been used to study wide variety of biomechanical investigations such as mechanisms of MSK disorder (Eltoukhy et al., 2017; Neptune, Zajac, and Kautz, 2009), effects of surgery (osteotomy (Brand, 1997; Schmidt et al., 1999), tendon transfer (Fridén and Lieber, 2002; Murray et al., 2002; Herrmann and Delp, 1999; Delp, Komattu, and Wixson, 1994), tendon lengthening (Delp, Statler, and Carroll, 1995; Delp and Zajac, 1992), ligament reconstruction (Pena et al., 2005), total joint replacement (Delp, Komattu, and Wixson, 1994; Delp et al., 1996; Piazza and Delp, 1996)). Models have also been used to analyze muscular coordination in dynamic activities to understand normal (Anderson and Pandy, 2003) and pathological movement (Piazza and Delp, 1996).

The usual pipeline of MSK model development approach are accompanied by inverse kinematics, inverse dynamics and forward dynamics (figure 2.2). In the inverse kinematics, skin marker based motion data is usually used as input to estimate joint kinematics. Then,

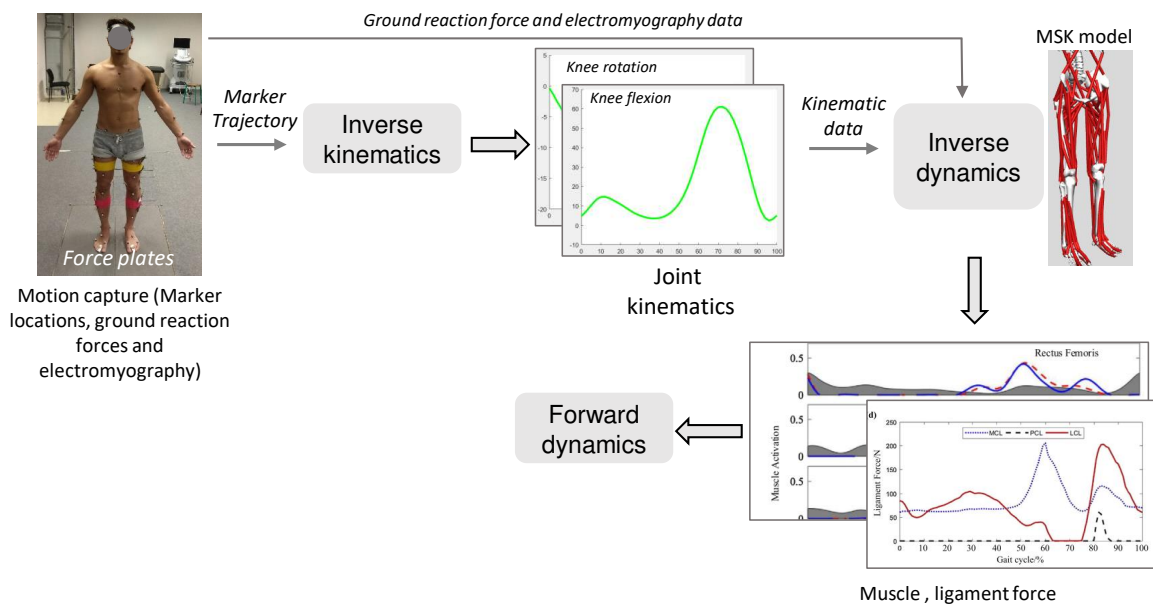


FIGURE 2.2: Skin marker trajectories are fed to the inverse kinematics analysis to estimate joint kinematics. The estimated kinematics along with ground reaction force (GRF) and electromyography data are input to the inverse dynamics analysis to calculate muscle forces. Activated muscles are then used in the forward dynamics analysis to drive the model (MSK model adopted from open sim and muscle and ligament force curves from (Shu et al., 2018))

in inverse dynamics, the model is driven by GRF¹ and computed joint kinematics data to estimate muscle actuation. Then, in the forward dynamics, actuated muscle drives the model to produce the motion pattern conforming to the recorded motion data. Thus contribution of different muscles in producing a definite movement pattern can be estimated. However, while doing so, all the studies based on skin marker-based motion data confront a major sources of error, commonly referred to as Soft Tissue Artifact (STA) as already mentioned in Chapter 1 (subsection 1.3.2). STA is known to be dependent on subjects, performed tasks and marker configuration (Petersen and Zantop, 2007). If not compensated for, STA can lead to biased outcomes resulted from bone interference while assessing skeletal kinematics (Dyrby and Andriacchi, 2004; Benoit et al., 2006; Stagni et al., 2005). For example, in walking, the average absolute rotational and translational error can range 2.4°-4.4° and 3.3-13 mm, respectively (Benoit et al., 2006).

Various methods exist in the literature reporting attempts to reduce the effect of STA on bone pose estimation. Some of the most relevant STA compensation methods are presented in table 2.2. Initially, a pure segmental approach was implemented considering the segments (pelvis, thigh, shank) separately, known as single-body optimization (Veldpaus, Woltring, and Dortmans, 1988). Later on, double anatomical landmark calibration (Cappello et al., 1997), point cluster technique (Andriacchi et al., 1998) were introduced. These

¹Ground Reaction Force

TABLE 2.2: Synthesis of salient STA compensation methods. (MBO: Multibody Optimization)

Author, year	Objective	Method	Motor task	Verification/Validation	Remarks
(Veldpaus et al., 1988)	To estimate translation and rotation matrix of a moving body from spatial marker coordinates	Least square algorithm	-	-	- First method - Segmental approach - Cannot correct rotational error
(Lu and O'Connor, 1999)	Bone pose estimation from skin marker locations	Global Optimization method (MBO)	-	-	- An enhanced method - Spherical joint constraint (3 DoF)
(Reinbolt et al., 2005)	Tuning of multibody kinematic model to experimental data	MBO	Walking	-	- Two level optimization - 3 DoF for hip, 1 DoF constraint for the knee
(Duprey et al., 2010)	To evaluate influence of joint constraint on kinematic estimation	MBO	Level walking	-	- Knee and ankle kinematics depends on joint constraint - Hip kinematics independent of constraint - Parallel mechanism provides physiologic motion
(Bergamini et al., 2011)	To provide ligament lengthening constraint as a plausible method in MBO	MBO	-	-	- A subject specific approach - Ligament length should be considered in the MBO models
(Clément et al., 2015)	To develop and validate knee joint model with anatomical and subject-specific kinematic constraint	MBO	Quasistatic squat	Biplanar radiographs	- MBO models can be improved with subject-specific models
(Gasparutto et al., 2015)	To validate MBO model with ligament constraint	MBO	Running	Bone pin	- Recommended introduction of anatomical constraint in MBO - Personalization of geometry should be considered
(Richard et al., 2016)	Knee joint kinematic estimation with a joint stiffness matrix	MBO	Stair climbing	Biplanar fluoroscopy	- Demonstrated feasibility of deformable joint - Recommended soft constraint as an alternative
(Clément et al., 2017)	To evaluate if generic models can estimate joint kinematics of osteoarthritic knee	MBO	Quasistatic squat	Stereo-radiography	- Generic models exhibited inaccurate kinematics
(Potvin et al., 2017)	To reduce STA error using adaptive kinematic constraint	Adaptive kinematic constraint	Gait trial	Bone pin	- Valid representation of joint kinematics with adaptive constraint
(Richard et al., 2017)	To compare different knee joint models for STA compensation	MBO	Level walking, cutting, hopping	Bone pin	- Most satisfactory results with no joint constraint - Spherical or hinge joint didn't significantly reduce STA - MBO cannot be considered as fully reliable method
(Nardini et al., 2020)	To validate a subject-specific knee model based on parallel mechanism	MBO	Knee flexion	Video-fluoroscopy	- Recommended medical imaging to personalize models

methods were partially successful in compensating STA by estimating bone position satisfactorily. But couldn't estimate the orientation of the bones properly. Consequently, multi-body optimization (MBO) methods were used as an alternative to compensate for STA (Lu and O'connor, 1999). This method relies on a predefined kinematic model, which entails searching for the best possible overall pose by minimizing the distances between the measured and model estimated marker trajectories in least square sense and respecting joint constraints. This method considers revolute (Reinbolt et al., 2005) or spherical (Charlton et al., 2004; Lu and O'connor, 1999; Reinbolt et al., 2005) joint kinematic constraints as the most common choices to represent hip and knee articulation. Although such approximation provides a satisfactory balance between complexity of the models and accuracy of the synthesized motion, yet such constraints do not allow joint displacement and therefore limit its performance in reducing STA (Stagni et al., 2005). For subjects with lesions at the joint structure, more anatomical description at the joint level is required.

Later on, different sets of joint anatomical constraints such as parallel mechanism, coupling curves, ligament length variation, elastic joint were implemented particularly in the knee joint to facilitate joint displacement (Bergamini et al., 2011; Duprey, Cheze, and Dumas, 2010; Gasparutto et al., 2015; Richard et al., 2016). These studies showed that anatomical constraints could offer physiological motion, such as limited abduction-adduction with femoral rollback. However, such constraints were also shown inaccurate (kinematic error up to 17° and 8 mm) and inadequate for clinical application as these models could not adapt patient-specific geometry, particularly in the case of OA patients (Clément et al., 2017). In opposed to the remarks of (Duprey, Cheze, and Dumas, 2010), who observed parallel mechanism as a better choice, (Richard, Cappozzo, and Dumas, 2017) obtained accurate result with no constraint. The later study also concluded that MBO cannot be considered as a fully reliable method. Recently, use of medical imaging is also recommended to personalize models (Nardini et al., 2020).

Despite such significant advancement in compensating for STA, MBO methods still lack the versatility of implementing subject-specific characteristics. In that support, an experimental study on quantification of soft tissue deformation (STD) concluded that for reliable STA compensation, knowledge of marker location-specific STD is essential (Gao and Zheng, 2008). With such information better STA compensation strategy can be devised. This indicates a need for adaptable modeling approaches that can account for subject-, task-, and marker location dependent STA.

In light of the aforementioned contexts, the use of FE models appears to be a better strategy as it shows good capacity of implementing subject-specific morphology of the bones acquired from CT or biplanar radiograph data (Lahkar et al., 2018). In that direction, at *Institut de Biomécanique Humaine Georges Charpak*, (Skalli et al., 2018) proposed a FE based novel approach to compensate for STA. The model consists of rigid beam elements to represent bony structures (pelvis, femur and tibia) and compliant springs to account for soft tissue deformation effect. This simple yet versatile model provides ample scope to further investigate

the soft tissue deformability and represent the joint with more complex and anatomically relevant model.

Apart from the lacking of a proper approach in compensating for STA, musculoskeletal (MSK) models also confront other two critical challenges. **Firstly**, the MSK multibody model, comprising of rigid body segments (bones) connected by ligaments and Muscle-Tendon Units (MTU), can consider the individual characteristics of the subjects for biomechanical analysis and simulation (Erdemir et al., 2007; Saraswat, Andersen, and MacWilliams, 2010). Nonetheless, the contribution of muscle and ligament forces at the joint levels and the effects of prosthesis design on human movement cannot be easily studied using MSK models owing to the simplification (spherical, revolute joint consideration) of the joint as elaborated previously (Shu et al., 2018). Moreover, to predict local biomechanical parameters (e.g., contact stress) of the joint, a rigid body MSK model is not suitable. **Secondly**, a usual practice for personalizing the MSK models are based on scaling methods (Correa and Pandy, 2011; Valente et al., 2015). Here a generic model is scaled to fit the dimensions of the subject using certain anatomical landmarks. This technique considers only overall anthropometry of a subject, ignoring the distinctive features of the joint (e.g., ligament insertion sites, articular geometry) (Smale et al., 2019). Therefore, the model may not accurately replicate the subject's anatomy and eventually may impact its kinematic estimations. In this aspect, a group in their series of studies showed considerable differences between MRI-based models and scaled models while estimating muscle tendon length, moment arm and on gait kinematics (Scheys et al., 2008a; Scheys et al., 2008b; Scheys et al., 2011).

In this context, probably the better strategy would be to use concurrent FE-MSK (finite element based musculoskeletal) models to overcome the obstacles (computational burden of FE models and oversimplification of MSK models) of each modeling domain, while improving the quality of the analysis.

Synthesis 2

- STA compensation is paramount for accurate estimation of skin marker-based motion data.
- Simplified joint constraints are currently incapable of representing detailed knee joint structure, particularly in joints with lesion.
- Medical image-based model personalization is essential to replicate subject-specific morphology.
- A versatile approach for STA compensation could be valuable which can take subject-, task-, and marker location-specific STA into account.

2.3 FE-MSK model

FE-MSK modeling approaches have been recently become popular to study local mechanics of the joint under *in vivo* loading conditions (refer to table 2.3). One study reported influence

of deformable joint on muscle parameters, and highlighted the importance of integrated framework for predicting muscle forces (Hume et al., 2018). Other studies also advocated the use of FE-MSK models that aimed for estimating various biomechanical response (cartilage stress (Adouni, Shirazi-Adl, and Shirazi, 2012; Halonen et al., 2016), muscle force (Navacchia et al., 2019), TKR response (Shu et al., 2018)). While, in principle, these methods appear attractive, there are several bottlenecks.

TABLE 2.3: Synthesis of relevant FE-MSK models

Author, year	Objective	Imaging Modality		Material Property	Boundary condition	Validation/ Verification (Subjects)	Review remarks
		Bone	Soft tissue				
(Yang et al., 2010)	Protocol for subject specific knee model	MRI	MRI	literature	Force and moments	Literature (3)	- No STA compensation
(Adouni et al., 2012)	Muscle force and Cartilage stress estimation	CT	CT	literature	Kinematics and GRF	Literature (1)	- Not subject specific - No STA compensation
(Halonen et al., 2016)	Importance of patella and cartilage response during gait	MRI	MRI	literature	Rotation, forces and moments	In-vivo (1)	- No STA compensation - Not robust w.r.t. subject specificity - Spherical joint assumption at knee
(Xu et al., 2016)	To evaluate effect of load carriage on tibia during walking	CT	CT	literature	Force and moments	Literature (1)	- Spherical joint assumption at hip - Knee and ankle as revolute joints
(Fuhao et al., 2017)	Investigation of active muscle force on Knee-Thigh-Hip injury	CT	MRI	literature	Impact load	In-vitro and In-vivo (1)	- Active 3D muscle implementation - Not subject specific
(Sharifi et al., 2017)	Mechanical stability study at early stance in gait	CT	CT	literature	Kinematics and kinetics	Literature (1)	- Not subject- specific - No STA compensation
(Hume et al., 2018)	Influence of muscle force on knee kinematics	CT	MRI	literature	Muscle actuated	In-vivo (12)	- Not subject specific - Model verification against experimental corridor
(Shu et al., 2018)	Mechanics analysis of TKR	CT	CT	literature	Muscle tendon force, GRF	EMG, In-vivo (1)	- 1 DoF assumption - Partial STA compensation
(Navacchia et al., 2019)	To estimate muscle forces	CT	MRI	literature	Muscle tendon force	EMG (2)	- 3 DoF joint at hip - 1 DoF at the knee - Joint deformation affects muscle parameters

First, fast and accurate model FE development approaches in terms of subject-specific morphology and material properties, simplified modeling strategies to foster clinical translation and model validation/verification approaches.

Second, alike rigid body MSK models, most of the FE-MSK models either neglected STA (Yang et al., 2010; Adouni, Shirazi-Adl, and Shirazi, 2012; Halonen et al., 2016; Sharifi, Shirazi-Adl, and Marouane, 2017) or partially compensated it by simplifying the joint. For instance, (Shu et al., 2018) assumed the knee joint as 1 DoF to estimate joint kinematics, and then estimated kinematic data were used to compute muscle parameters (muscle moment, muscle length, muscle velocity). Undoubtedly, such consideration will manifest error propagation in the subsequent steps. A similar methodology was followed in (Xu et al., 2016) study. Hence, solving the STA problem seems to be a common challenge for both the model types, rigid body MSK and FE-MSK models.

Based on the systematic review on various computational modeling strategies, it can be summarized that although a large body of work has been performed in the literature, it highlights enormous complexities in developing a FE-MSK framework for the lower limb, in particular the knee joint. Therefore, it appears that there is still a need for a comprehensive framework of subject-specific FE-MSK modeling by taking the above mentioned challenges into account.

2.4 Objectives

The overall aim of the PhD thesis was thus set as a '**Contribution to personalized FE-based musculoskeletal modeling of the lower limb**' with the purpose of bridging the gap between current state-of-the-art approaches for musculoskeletal modeling and their applicability towards clinics.

Based on the overall aim, manifold sub-objectives were defined as

- To develop and evaluate personalized FE model of the knee joint by taking subject-specific geometry and ligament material properties into account. This objective will be addressed in Chapter 3.
- To compensate for Soft Tissue Artifact in motion analysis by adopting a novel approach. This will be tackled in Chapter 4.
- Finally, a clinical application was briefly explored in the context of utility of the low dose biplanar X-ray system in evaluating Total Knee Arthroplasty (TKA) implant alignment. This will be addressed in Chapter 5.

Chapter 3

Subject-specific finite element model development and evaluation of the knee joint

This chapter illustrates an approach for subject-specific finite element (FE) modeling and evaluation of the knee joint to estimate joint kinematics. The first section includes a methodology for fast and quasi-automatic subject-specific FE mesh generation of the knee joint from biplanar X-ray images, which has been published in a conference proceedings (CMBBE, 2018) (Lahkar et al., 2018). The second section includes evaluation of the subject-specific FE models under passive response. Here, a novel approach for calibrating ligament material properties has been proposed and evaluated. This work has been submitted to the peer-reviewed journal *Computer Methods in Biomechanics and Biomedical Engineering* entitled "Development and evaluation of a new procedure for subject-specific tensioning of FE knee ligaments."

3.1 Fast subject-specific FE mesh generation of the knee joint from biplanar X-ray images

Abstract An accurate and fast computational mesh generation is a prerequisite to perform personalized FE analyses. Traditionally, both triangular/tetrahedral and quadrilateral/hexahedral FE elements are used for 3D mesh generation. But because of distinct numerical advantages, hexahedral elements are preferred to avoid numerical instability. Here, we propose a methodology to develop fast and automatic subject-specific mesh for knee joint from biplanar X-ray images. This methodology first involves building 3D reconstruction from biplanar radiographic image and then generating generic linear hexahedral mesh for the femur, tibia and patella. The generic mesh (GM) for individual bony structure is then deformed to obtain subject specific mesh (SSM) based on kriging interpolation. Meshing of both the meniscus follows a different approach where the surface nodes of the femur and tibia are used to generate linear hexahedral elements mesh. This complete methodology was successfully tested on 11 cadaveric specimens with approximately 12 min computational time for each out of which 3D reconstruction time was nearly 10 min. Numerical cost involved in deforming mesh for each specimen was 30 sec and generating mesh for both the meniscus was nearly 1 min. Mesh quality was assessed using standard ANSYS mesh quality indicators (aspect ratio, parallel deviation, maximum angle, Jacobian ratio and warping factor). For each specimen the value of total warnings above threshold showed in the range of 0.38-0.59% with no error. Surface mesh accuracy was evaluated as the point-to-surface distance between 3D reconstruction and subject-specific mesh and the mean RMS values were reported. For all specimens, mean (RMS) errors in mm were respectively less than or equal to 0.2 (0.3), 0.3 (0.55) and 0.0 (0.1) for femur, tibia and patella which are less than the uncertainties of 3D reconstruction.

Keywords: FEM, 3D reconstruction, subject specific mesh, knee joint, biplanar X-ray

3.1.1 Introduction

Numerous FE models of the knee joint have been developed to investigate knee injury mechanism (Kiapour et al., 2014), surgery assessment (Kang et al., 2018; Xie et al., 2017) and contact kinematics at knee joint (Haut Donahue et al., 2002; Koo, Rylander, and Andriacchi, 2011; Ali et al., 2016). However, because of extensive computational effort required for preparing subject specific model from CT-scan or MRI data, most of the models in literature are done only for one or very few subjects. This results in poor validation of the model while dealing with patient specific estimation of tissue response as well as studying effect of morphological inter-subject variability. As an alternative to CT scan and MRI data, use of biplanar X-ray image is promising to perform 3D reconstructions of bony structures (Chaibi et al., 2012) because of low radiation dose, very little reconstruction time and ability to replicate complex bony structure with ease.

The quality of FE mesh plays vital role in obtaining reliable and accurate results. Traditionally, tetrahedral meshes are easy to generate but it reduces order of convergence for

strains and stresses (Payen and Bathe, 2011) and suffers numerical stability issues associated to shear locking and volumetric locking (Joldes, Wittek, and Miller, 2009; Onishi and Amaya, 2014). Moreover, a FE mesh with tetrahedral elements require more elements as compared to hexahedral elements to achieve same solution accuracy leading to higher computational cost (Ramos and Simoes, 2006). To avoid these issues, hexahedral elements are preferred for designing biomedical models (Gérard et al., 2006; Rohan et al., 2017).

Building automatic FE mesh with hexahedral elements is time consuming and restrictive (Tautges, Blacker, and Mitchell, 1996). Literature shows majority of articles deal with fast and robust automatic methods to generate tetrahedral mesh of arbitrary geometries (Löhner and Parikh, 1988; Yerry and Shephard, 1984). Though, very few teams reported on automatic generation of hexahedral meshes using different techniques, the use of automatic hexahedral mesh generation is still limited due to robustness issues (Rohan et al., 2017).

The objective of the present study was motivated by previous successful implementation of subject specific FE modelling on lower cervical spine (Laville, Laporte, and Skalli, 2009). Here, a specific approach to automatically generate subject specific FE mesh from biplanar X-ray images is proposed for knee joint structure.

3.1.2 Materials and methods

Eleven healthy lower limb cadaveric specimens aged between 47 and 79 years were used in this work based upon a previous study (Pillet et al., 2016). Each specimen includes femur, tibia and patella with joint passive structures intact.

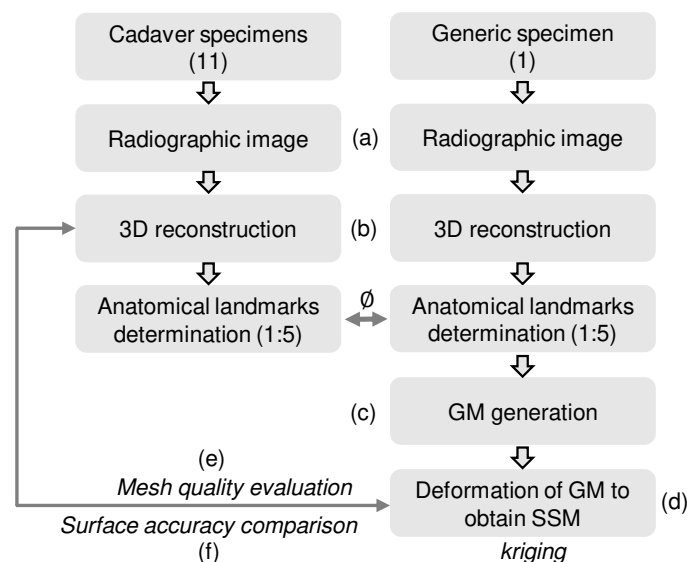


FIGURE 3.1: Overall workflow of subject specific mesh generation for bony structures. The process follows (a) acquisition of radiographic image for knee specimens, (b) 3D reconstruction of bony structures and anatomical landmark determination for each, (d) generation of generic mesh (GM), (d) GM deformation to obtain subject specific mesh (SSM) by numerical interpolation, (e) mesh quality evaluation of the SSM and (f) surface accuracy comparison between the SSM and 3D reconstruction

The overall methodology of the current study uses following steps: (a) acquisition of biplanar radiographic image for specimens of interest, (b) 3D reconstruction of femur, tibia and patella, (c) generation of generic mesh (GM) of whole knee joint, (d) deformation of GM to obtain subject-specific mesh (SSM), (e) mesh quality evaluation of SSM and (f) surface representation accuracy computation. The work flow of this approach is represented in figure 3.1 and is restricted to the mesh generation of the bony structures only. A different methodology is followed to generate mesh for meniscus.

Mesh generation of bony structures

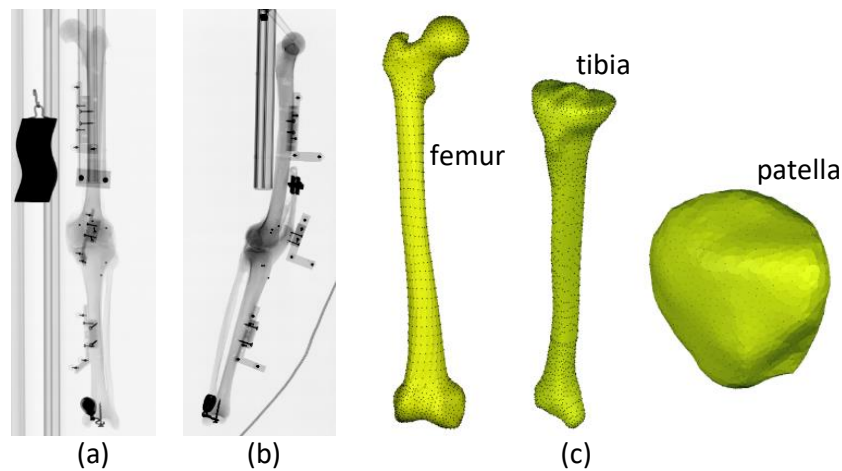


FIGURE 3.2: An example of radiographs in (a) frontal, (b) sagittal view and its (c) 3D reconstruction model of the femur, tibia and patella

First, biplanar radiographic images of bony structures (femur, tibia and patella) for one of the cadaveric specimens (named as generic) as well as all the 11 specimens of interest were acquired using EOS low dose imaging device (EOS[®], EOS-imaging, France). Then from the radiographic images, 3D digital models of all specimens were obtained using 3D reconstruction algorithm validated by previous studies with reconstruction time of 10 min for each specimen (Chaibi et al., 2012; Quijano et al., 2013). As a reminder, 3D reconstruction process begins with identification and labelling of various anatomical regions and landmarks on the biplanar images. Next, based on statistical inferences a simplified personalized parametric model (SPPM) is generated. After that, the morpho-realistic 3D generic model is deformed towards the SPPM to obtain morpho-realistic personalized parametric model (MPPM) using moving least square and kriging interpolation (Trochu, 1993). Finally, this MPPM is manually adjusted till the best estimate of the respective subject specific model (figure 3.2).

In the following step, the generic 3D reconstruction was imported into Geomagic Studio 12.0 (3D systems, Carolina, USA) for manual patch construction so as to form sets of deformed cubes in the model. Then the CAD model was imported to a customized Matlab[®] (Mathworks, Massachusetts, United States) routine to create volumetric mesh. Here, each deformed cube was discretized into sets of small blocks. This was done by discretizing the

edges of the deformed cube, then the faces followed by the whole cube. Thus, generic linear hexahedral mesh was generated for 1 deformed cube first and then for the remaining with the same process. Figure 3.3 shows generic FE meshed model development process for femur. Similar approach was implemented for generic tibia and patella.

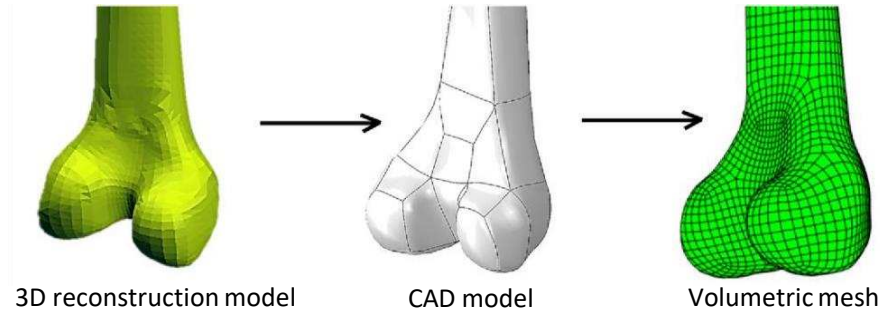


FIGURE 3.3: Generic meshed model development sequence for femur (only distal epiphysis is shown for clarity)

Finally, a mapping (ϕ , as drift and fluctuation) from source (generic) to target (subject specific) points was evaluated by applying dual kriging interpolation (Trochu, 1993). Then, on the basis of the mapping, the generic mesh of individual specimen was deformed to obtain subject-specific mesh using numerical interpolation. Mesh deformation was done in a customized Matlab routine with computational cost nearly 30 sec for each specimen.

Mesh generation of meniscus

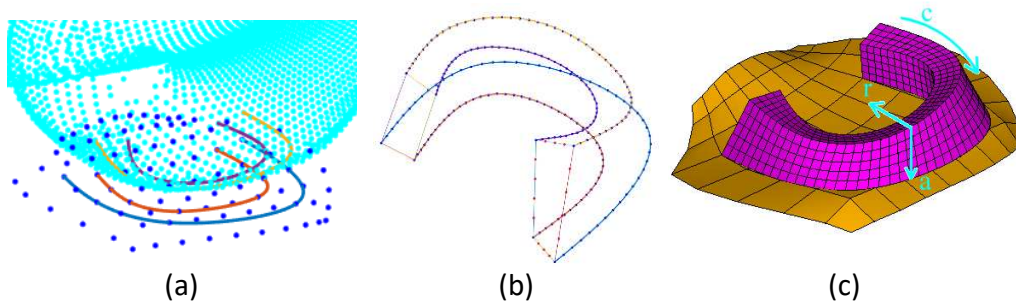


FIGURE 3.4: Mesh generation process of meniscus (a) Spline construction through the surface nodes of femoral condyle and tibial plateau, (b) discretization of splines and connecting lines and (c) volumetric mesh generation (shown for only medial meniscus)

At first, 2 splines were constructed through the selected nodes of the surface meshes of medial tibial plateau (figure 3.4(a)). Then, the nodes on tibial splines were used for searching nearest nodes on the medial femoral condyle using nearest-neighbor interpolation. Another 2 splines were constructed through these searched nodes on femoral condyle. These splines were then connected with straight lines at the extreme nodes. Finally, these splines and the lines were discretized into respectively 50, 5 and 4 no of divisions circumferentially (c), radially (r) and axially (a) (figure 3.4(b)). Then by establishing element connection volumetric mesh (linear hexahedral) was created for the meniscus (figure 3.4(c)). Similar procedure was

followed to generate mesh for the lateral meniscus with numerical cost less than 1 min in a custom made Matlab routine.

Mesh quality evaluation

Mesh quality was assessed using standard ANSYS mesh quality indicators: aspect ratio, parallel deviation, maximum angle, Jacobian ratio and warping factor. The default warning (error) threshold values for linear hex elements are 20 (1000000), 70 (150), 155 (179.9), 30 (1000) and 0.2 (0.4) respectively.

Surface representation accuracy

The accuracy of subject specific mesh for each specimen was compared against respective 3D reconstruction model by registering point-to-surface distance. This was done in a custom made Matlab routine by projecting the subject specific mesh on the 3D model and the error computed (mean, RMS) was also visualized.

3.1.3 Results and Discussion

With the fully automated methodology described, subject specific mesh for all 11 knee joint specimens were generated. Figure 3.5 illustrates all the generated meshes using this methodology.

Mesh Quality

Quality of individual knee joint mesh is represented in table 3.1 in terms of mesh quality indicators (warning % above threshold value). Maximum warnings can be seen in the case of maximum angle followed by aspect ratio. There are no occurrence of errors in any mesh and total warning percentage is satisfactorily very less with a maximum value of 0.59% for specimen 10.

Surface representation accuracy

Table 3.2 represents surface accuracy of individual specimen. For femur and tibia mean (RMS) error in mm varies in the range of 0.1-0.2 (0.2-0.3) and 0.2-0.3 (0.4-0.55) respectively, whereas in the case of patella no mean error can be seen with RMS error varying in the range 0.05-0.1. Overall, subject specific mesh of patella showed highest closeness to the 3D reconstruction model followed by femur and tibia.

Surface representation accuracy for the entire geometry of femur, tibia and patella of each specimen were visualized and as an example illustrated in figure 3.6 for specimen 1. Close-up view in the functional region of knee joint are shown for the femur and tibia.

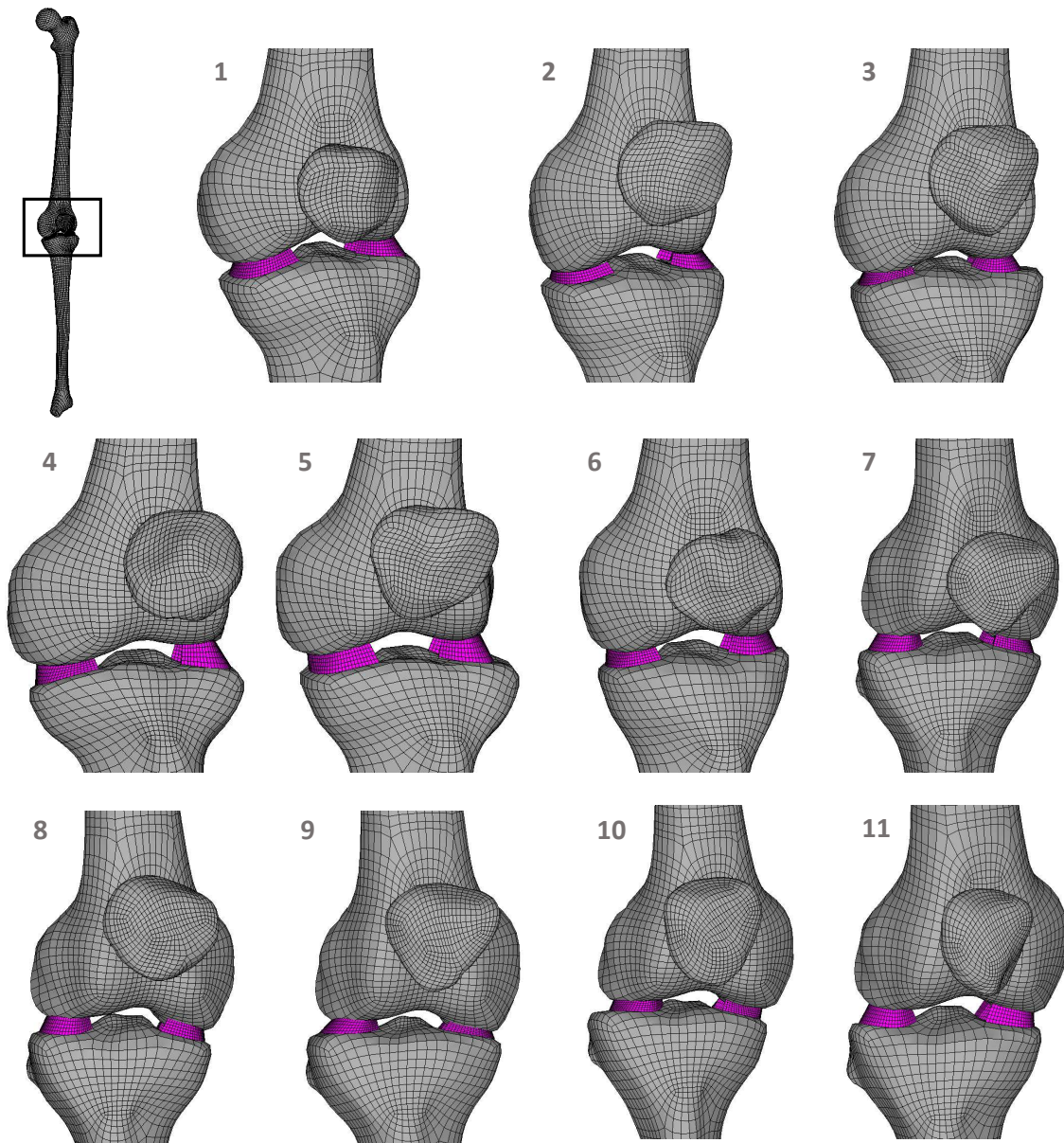


FIGURE 3.5: Global mesh of knee joint for all the 11 specimens. For clarity only the distal epiphysis of femur and proximal epiphysis of tibia is shown

3.1.4 Conclusions

The scientific issue addressed in this study is one of the prevailing challenges faced by the researchers and clinicians to account for inter-subject variability in their investigations. While referring to morphological variations between subjects, the technical hurdles often arise are the automatic generation of hexahedral mesh for individuals with minimum possible time and without compromising mesh quality. The majority of the existing methods require a substantial amount of time to generate patient-specific hexahedral mesh for individual geometry. This is mainly due to the time involved in manual segmentation of images acquired from CT or MRI data.

TABLE 3.1: Mesh quality of each specimen in terms of warning percentage above threshold. Here the warning percentage in each indicator signifies the number of warning counts above threshold divided by total number of elements in percentage

FE model	AR	PD	MA	JR	WF
S1	0.12	0.03	0.25	0.01	0.04
S2	0.20	0.03	0.16	0.01	0.05
S3	0.16	0.03	0.21	0.01	0.04
S4	0.14	0.03	0.36	0.01	0.04
S5	0.18	0.03	0.21	0.01	0.04
S6	0.12	0.04	0.17	0.01	0.04
S7	0.13	0.05	0.22	0.01	0.04
S8	0.21	0.02	0.25	0.01	0.04
S9	0.16	0.03	0.25	0.01	0.04
S10	0.20	0.04	0.30	0.01	0.04
S11	0.12	0.04	0.23	0.01	0.04

AR: Aspect Ratio, PD: Parallel Deviation, MA: Maximum Angle, JR: Jacobian Ratio, WF: Warping Factor

TABLE 3.2: Surface representation accuracy of individual specimen

FE model	Mean (RMS) error in mm		
	Femur	Tibia	Patella
S1	0.2 (0.30)	0.3 (0.50)	0 (0.10)
S2	0.1 (0.25)	0.2 (0.50)	0 (0.10)
S3	0.1 (0.25)	0.3 (0.50)	0 (0.10)
S4	0.1 (0.20)	0.2 (0.40)	0 (0.05)
S5	0.1 (0.20)	0.2 (0.45)	0 (0.05)
S6	0.1 (0.25)	0.3 (0.50)	0 (0.10)
S7	0.1 (0.25)	0.3 (0.50)	0 (0.00)
S8	0.1 (0.25)	0.2 (0.50)	0 (0.05)
S9	0.1 (0.25)	0.3 (0.55)	0 (0.05)
S10	0.1 (0.25)	0.2 (0.40)	0 (0.05)
S11	0.1 (0.25)	0.3 (0.50)	0 (0.10)

Our methodology proposed in the current study mainly relies on careful design of a generic FE mesh from 3D reconstruction of the target structure with proper anatomical features of interest. Proper caution requires in the functional areas: contact surface and ligament insertion sites of the knee joint. This preliminary work is a one-time effort, henceforth to establish automatic mesh deformation from generic to subject-specific.

In all the studied specimens, 3D reconstruction time was nearly 10 min for individuals which is in contrast to the approach with CT or MRI. In all the FE models the regularity of the subject specific mesh is preserved without excessive distortion. Mesh quality of individual mesh is very good with above threshold warning percentage in the range of 0.38-0.59%.

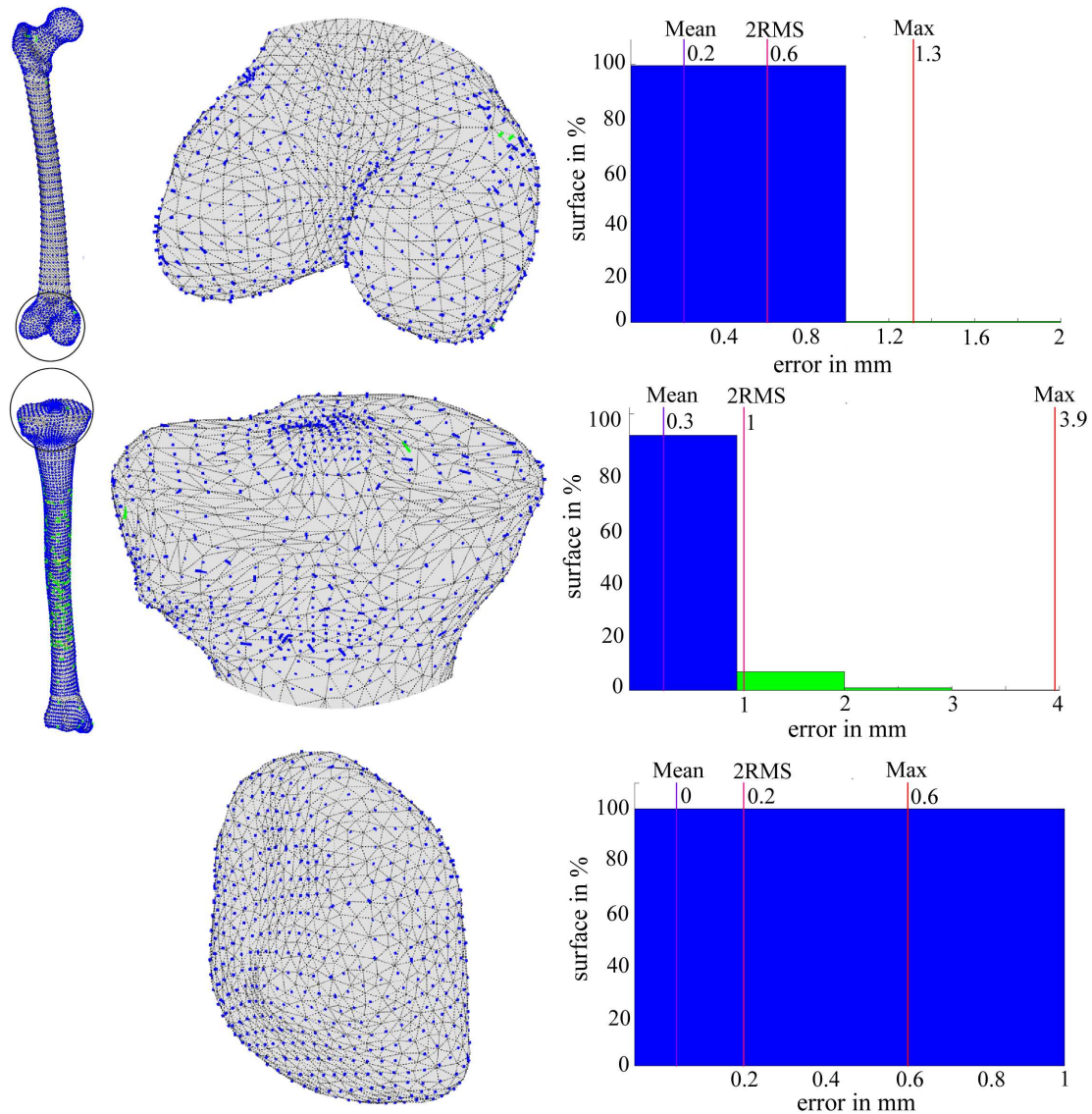


FIGURE 3.6: Surface representation accuracy as point-to-surface distance for (a) femur, (b) tibia and (c) patella

Again, the algorithm employed in the current methodology was able to closely replicate the bony structures of individuals maintaining satisfactory surface representation accuracy. To our best knowledge, no such methodology is developed till now especially for knee joint which can allow generation of nearly accurate mesh from 3D reconstruction for any number of specimens.

Overall, this section of the chapter 1 contributed to fast, accurate and semi-automatic hexahedral FE mesh generation of the knee joint. Because of fastness and subject specificity in terms of geometry, this methodology has the potential to be implemented in clinical routine to investigate personalized characteristics of the knee joint. However, in that aim model validation is important, which will be addressed in the following section.

3.2 Development and evaluation of a new procedure for subject-specific tensioning of finite element knee ligaments¹

Abstract Subject-specific tensioning of ligaments is essential for the stability of the knee joint and represents a challenging aspect in the development of finite element models. We aimed to introduce and evaluate a new procedure for the quantification of ligament prestrains from biplanar X-ray and CT data. Subject-specific model evaluation was performed by comparing predicted femorotibial kinematics with the *in vitro* response of six cadaveric specimens. The differences obtained using personalized models were comparable to those reported in similar studies in the literature. This study is the first step towards the use of simplified, personalized knee FE models in clinical context such as ligament balancing.

Keywords: Finite Element Analysis, Ligament Prestrain, Subject-Specific Knee Model, Joint Kinematics, Model Evaluation

3.2.1 Introduction

The knee joint is highly susceptible to frequent injury of ligaments. If it remains untreated, has the probability of limiting joint stability, and can further lead to progression of joint arthritis (Fleming et al., 2005). In such scenario, early stage clinical intervention e.g., ligament repair or replacement is often recommended. For such therapeutic interventions and to properly plan surgical procedures, accurate knowledge of the biomechanical behavior of knee ligaments is fundamental.

Several experiments dealing with main knee ligaments (anterior cruciate ligament (ACL), posterior cruciate ligament (PCL), lateral collateral ligament (LCL) and medial collateral ligament (MCL)) have been carried out in the literature (Aunan et al., 2012; Belvedere et al., 2012; Gardiner, Weiss, and Rosenberg, 2001; Pedersen et al., 2019; Rochcongar et al., 2016). Although these studies have substantially increased knowledge on joint functions, yet the complexity of measurements, lesser availability of cadavers, ethical and cost implications have made data acquisition challenging.

Alternatively, FE models are commonly used as a reliable complementary means to experimental studies providing significant insight into knee joint biomechanics. A variety of modeling techniques have been utilized to model the joint structure, particularly ligaments. Some of the strategies are steered by simplicity, while others concentrate on faithful capture of specimen-specific anatomy with varying levels of joint representation fidelity. For example, some models included 3D geometries of ligaments with complex material behavior (Kiapour et al., 2014; Limbert, Taylor, and Middleton, 2004; Orsi et al., 2016; Pena et al., 2006). Such approach allows to consider ligament wrapping behavior and analysis of local biomechanical response (e.g., 3D stresses and strains across tissue). Nevertheless, higher anatomically complex models require detailed image-based information of the soft tissue

¹Potential copyright issues with direct reuse of the article including figures and contents

structures under consideration. Generation and simulation of such models often require manifold higher time than that for simpler models (Bolcos et al., 2018). Therefore, simpler models may be beneficial for studies where higher number of subjects need to be analyzed and, at the same time, capable of predicting joint mechanics.

In an attempt for model simplification, other authors have proposed to represent ligaments as bundles of springs or tension only cables (Adouni and Shirazi-Adl, 2009; Baldwin et al., 2012; Moglo and Shirazi-Adl, 2005). Although ligaments are exposed to both compressive and tensile states of stress, yet the contribution of tensile stress is substantially higher than others (Pena et al., 2006; Orsi et al., 2016). Therefore, such simplification is considered reasonable and recommended particularly for predicting joint kinematics (Beidokhti et al., 2017). Nevertheless, personalization of ligament properties (stiffness and prestrain), although clinically essential to restore joint stability, represents a challenge for the community. For example, there is a consensus that graft under-tensioning could lead to joint laxity, which is biomechanically analogous to a ligament deficient knee (Sherman et al., 2012). In addition to that, owing to variable morphology, different bundles of a ligament (e.g., two main fiber bundles of ACL) may exhibit variable prestrain by becoming active at different flexion angles (Girgis, Marshall, and JEM, 1975). From a modeling perspective, it has also been reported that incorrectly applied ligament prestrain can have a considerable effect on the kinematics of the knee (Mesfar and Shirazi-Adl, 2006; Rachmat et al., 2016). To tackle this issue, some authors made subject-specific adjustment using inverse methods to calibrate specific ligament constitutive behavior. Models either used laxity tests (Baldwin et al., 2012; Beidokhti et al., 2017) or distraction loading (Zaylor, Stulberg, and Halloran, 2019) to estimate ligament properties by minimizing differences between model-predicted and experimental kinetics. Such calibrations are, however, likely to be computationally expensive.

In light of the above considerations, we proposed an original framework for calibrating subject-specific tensioning of FE knee ligaments based on experimentally acquired data. Subject-specific model evaluation was performed by comparing predicted femorotibial kinematics under passive flexion with the experimental data of six cadaveric specimens. We hypothesized that the employed methodology of building personalized FE models with experiment-based prestrains could predict overall passive kinematics of the knee joint.

3.2.2 Materials and methods

The overall workflow of generating specimen-specific FE mesh is presented in figure 3.7

Experimental data acquisition

We obtained the experimental knee kinematic responses in a previous study (Rochcongar et al., 2016). The experimental procedure is recalled briefly hereafter. Six fresh-frozen lower limb specimens harvested from subjects with age range 47 to 79 years, were tested under passive flexion-extension on a previously validated kinematic test-bench (Azmy et al., 2010; Hsich and Draganich, 1997). Skin and muscles were removed except eight centimeters of

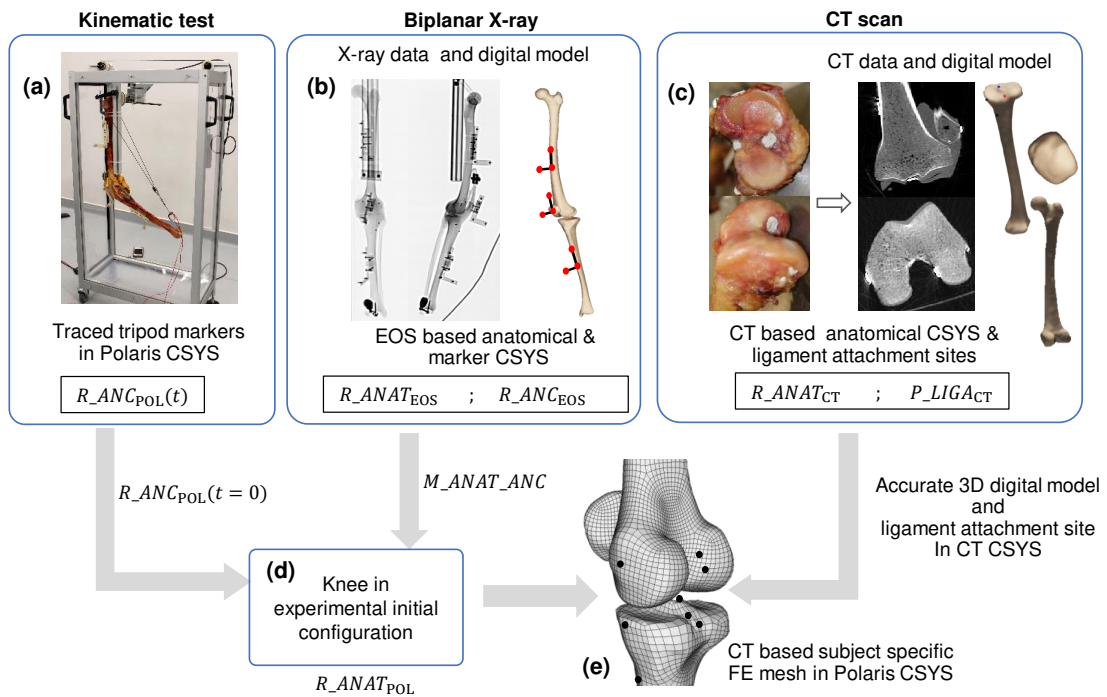


FIGURE 3.7: Schematic illustration for (a) kinematic test: position of tripod markers in Polaris coordinate system (CSYS), (b) biplanar X-ray: 3D digital models of bone and tripod markers giving anatomical and ancillary reference frames in EOS CSYS, (c) CT scan: Accurate 3D digital models of bone and ligament attachment sites giving anatomical reference frames and ligament attachment locations in CT CSYS, (d) knee in experimental initial configuration giving anatomical reference frames in Polaris CSYS, (e) CT based subject-specific FE mesh and ligament attachment sites in experimental initial configuration

quadriceps tendon and popliteus muscle prior to the kinematic data collection. All other relevant joint-soft-tissue structures (such as ligaments, articular capsule) were kept intact during kinematic data acquisition. The femur was kept fixed, and flexion movement was introduced to the tibia by a rope and pulley system. During flexion, the positions of the three marker tripods placed on the femur, tibia, and patella were recorded using an optoelectronic system (Polaris[®], Northern Digital Inc., Canada). These recorded positions allowed establishing ancillary reference frames (referred to as $R_{ANC_{POL}}(t)$) from $t=0$ (before applying flexion load) till the end of flexion (figure 3.7a). Measurement uncertainties with the optoelectronic system was previously assessed. Overall uncertainties of less than 0.5 mm in translational and 1° in rotational DoF were obtained (Azmy et al., 2010).

In addition, two orthogonal radiographs of each specimen were acquired using an EOS biplanar X-ray system (EOS[®], EOS-imaging, France) to obtain 3D digital models of the bones and tripod markers. From the 3D models, anatomical reference frames (referred to as $R_{ANAT_{EOS}}$) for the femur, tibia, and patella were defined (Schlatterer et al., 2009). Ancillary reference frames (referred to as $R_{ANC_{EOS}}$) from the tripod markers were also defined allowing a relationship between anatomical frames and ancillary frames, termed as

M_ANAT_ANC (figure 3.7b). This relation was further used for converting acquired kinematic data, $R_ANC_{POL}(t)$ to relative patellofemoral and tibiofemoral motions in the femur anatomical reference frame with Cardan sequence $ZY'X''$.

After the kinematic data acquisition, each specimen was fully dissected to identify the ligament attachment sites. Absence of trauma and integrity of soft tissue structures was checked during the dissection. An experienced surgeon identified the origin and insertion locations for the following ligaments: anteromedial (AM) and posterolateral (PL) bundles of ACL, posteromedial (PM) and anterolateral (AL) bundles of PCL, superficial (MCLs) and deep (MCLd) bundles of MCL, and LCL. Identified locations were marked with radio-opaque paints, and the bones were scanned using a computed tomography (CT) scanner (Philips, Best, The Netherlands). 3D digital models of each dissected specimen were acquired using MITK-GEM[®] (version 5.0) giving anatomical frames (R_ANAT_{CT}) and ligament attachment sites (P_LIGA_{CT}) in the CT scanner system of reference (figure 3.7c). 3D Digital models and digital footprints of ligament attachment sites were then registered into experimental initial configuration. Registration was performed with biplanar X-ray data. Once the centroidal coordinates of the attachment sites were known, the end-to-end distance of the ligaments origin and insertion site was computed at experimental initial configuration. For the sake of readability, end-to-end distance will be referred to as ligament length hereafter.

Initial bone pose estimation

Relative pose (position and orientation) of tibia and patella with respect to the femur at initial unloaded configuration was obtained using the relation M_ANAT_ANC and experimental kinematic data, $R_ANC_POL(t)$ at time=0 (figure 3.7d)).

Specimen specific FE model

(i) *FE mesh* First, subject-specific FE hexahedral mesh for each bony segment was created based on the subject-specific CT based digital models (figure 3.7e) (Lahkar et al., 2018). Then, only the surface mesh (4-noded shell element) was kept to represent bones and cartilage to reduce computational cost (Germain et al., 2016). Then, mesh smoothing was performed at the articular surfaces to improve the mesh quality (Taubin, 1995).

Mesh quality was assessed using standard ANSYS[®] mesh quality indicators: aspect ratio, parallel deviation, maximum angle, Jacobian ratio, and warping factor. The surface accuracy of specimen specific mesh for each specimen was compared against respective 3D digital model (i.e. segmented 3D geometry from CT data) by registering Hausdorff distance expressed in mean (2RMS) values.

(ii) *Knee joint FE model* Bones were assumed to be isotropic linear elastic with Young's modulus of 12000 MPa (Choi et al., 1990). As the loading pattern in the study is quasi-static,

cartilage was assumed as single-phase linear isotropic material (Eberhardt et al., 1990). Cartilage regions were modeled as cortico-cartilage material and assigned with Young's modulus of 250 MPa to summarize the material properties of cortical bone and cartilage (Germain et al., 2016). A very thin strip of material between bones and cortico-cartilage region were also modeled with intermediate properties (2000 MPa) to limit mechanical discontinuity (Germain et al., 2016) (figure 3.8).

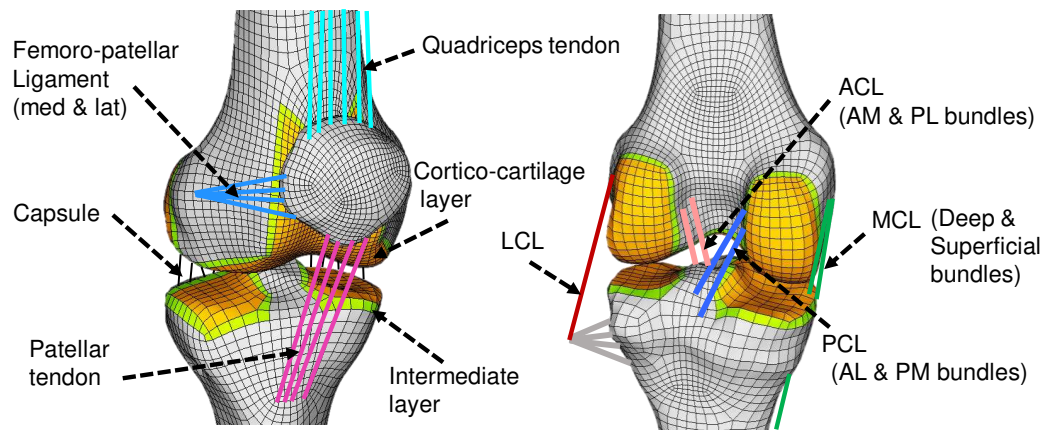


FIGURE 3.8: FE model with soft tissues (only shown for the distal femur and proximal tibia)

Attachment sites for the cruciate and collateral ligaments were based on the already identified locations (Rochcongar et al., 2016). For other ligaments and tendons (femoro-patellar ligament, patellar tendon, quadriceps tendon, posterior capsule), general anatomical sites based on *a priori* knowledge of an anatomist were used. Each cruciate ligament was represented by 2 bundles (Blankevoort and Huiskes, 1991) along with MCL (deep and superficial) (Smith et al., 2016). Posterior capsule and femoropatellar ligaments were each represented by 8 bundles (4 bundles in the medial and lateral side each), while quadriceps and patellar tendon as 4 bundles each (Germain et al., 2016) and LCL as one (Meister et al., 2000). All ligaments and tendons were represented as point-to-point, tension-only cable elements as their contribution in tension is much higher than that in compression (Baldwin et al., 2009; Harris et al., 2016). Three frictionless surface-to-surface contact pairs were considered: tibia-femur cartilage (medial and lateral) and femur-patella cartilage with augmented penalty solution algorithm.

(iii) Ligament material properties Three cases of ligament prestrain values (% ϵ) were considered for cruciate and collateral ligaments. No prestrain values for other ligaments were considered and stiffness (k) values for all the ligaments were adopted or estimated from our previous study (Germain et al., 2016). It is to be noted that constant stiffness values were applied across all specimens.

Case 1: Generic material properties. Prestrain values for ACL (5%), PCL (-3%), MCL (0%) and LCL (0%) were adopted from previous study (Germain et al., 2016).

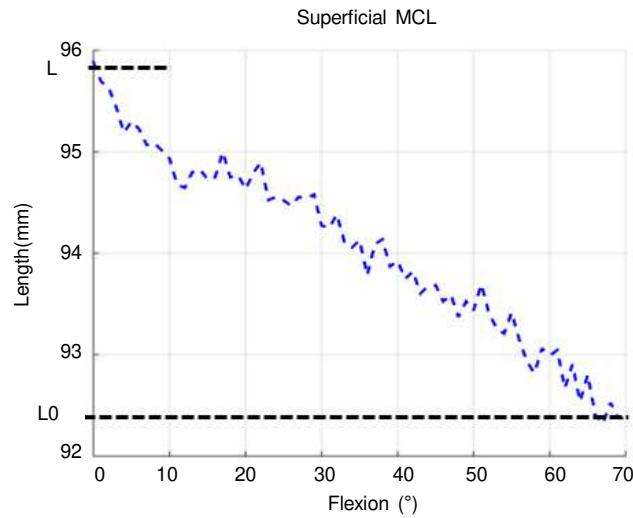


FIGURE 3.9: Experimental ligament length change for superficial MCL throughout the flexion movement. A similar strategy was implemented for other ligaments except for PCL, which is based on literature values)

Case 2: Automatic pre-computation from experimental data. For each specimen, ligament and bundle specific prestrains were automatically computed from the experimental ligament lengths using equation 3.1. This is illustrated for the MCL in figure 3.9.

Case 3: Combination of automatic pre-computation and further manual adjustment. Initial values for the 7 ligament parameters (prestrains) were assigned with precomputed ligament prestrains. The minimum and maximum bounds for each parameter was defined from the literature (Blankevoort and Huijskes, 1996; Baldwin et al., 2009). Each parameter at a time was modified by changing the previously assigned value by roughly 10% and RMS error between numerical and experimental kinematics was observed for each DoF. Based on the error, a new parameter set was assigned. Thus the procedure was repeated till rotational and translational RMS error became steady state. Stopping criteria was chosen as change in RMS error between two consecutive iterations is less than or equal to 0.1° for rotational and 0.1 mm for translation.

$$prestrain = (\delta/L) * 100 = ((L - L_0)/L) * 100 \quad (3.1)$$

where, L is the experimental ligament length at initial configuration (before application of flexion load), and L_0 is the zero-strain length at the end of flexion, with an assumption that ligaments experience no force after the prescribed maximum flexion angle.

(iv) FE model simulation states Three different configurations were defined to represent different simulation states applicable to all the FE models and all cases of ligament properties. As the models are built from the experimental initial configuration, the first state is referred to as (a) **no-load or stress free configuration**. The second state corresponds to

the configuration after attaining equilibrium under prestrain effect, termed as (b) **initial equilibrium configuration** (or reference configuration). The third state corresponds to the deformed states of the model upon application of incremental rotational displacements on the tibial malleolus until 70° of flexion angle (Germain et al., 2016). Knee flexion took place at the third state and referred to as (c) **current deformed configuration**. Remaining degrees of freedom (DoFs) were left unconstrained. Only geometric non-linearity was considered for the model simulations.

(v) **Model evaluation (Knee joint kinematics):** The relative position and orientation of the tibia with respect to femur was computed based on their anatomical reference frames, as described in (Schlatterer et al., 2009) and interpreted in the femur anatomical reference frame. One-to-one model evaluation was performed by comparing predicted femorotibial kinematics to experimental measurements throughout flexion motion for both the cases 2 and 3. Specimen specific RMS differences between model-predicted and experimental measurements were computed based on values at 1° interval for a range of flexion angle 0-60°. Eventually, RMS difference with experimental data was averaged for all the specimens.

3.2.3 Results

Mesh quality

Quality of individual knee joint FE mesh showed no occurrence of error in terms of ANSYS mesh quality indicators.

Surface representation accuracy

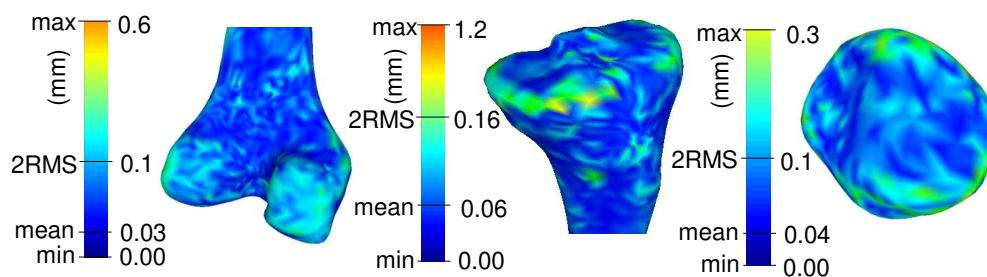


FIGURE 3.10: Surface representation accuracy as a Hausdorff distance for femur, tibia, and patella

FE mesh surface accuracy for the femur, tibia, and patella with respect to corresponding CT surface across all specimens were found less than or equal to (mean (2RMS) in mm) 0.03 (0.1), 0.06 (0.16) and 0.04 (0.1) respectively. For the sake of example, error-values are pictorially shown in figure 3.10 for the specimen 1.

Estimation of subject-specific ligament material properties

(i) **Case 2: Based on automatic pre-computation from experimental data** Estimated ligament stiffness and prestrain values computed according to the procedure described in case

TABLE 3.3: Estimated ligament stiffness values for a single specimen

Ligaments	ACL		PCL		MCL		LCL
Bundles	AM	PL	AL	PM	MCLd	MCLs	
Stiffness (N/mm)	125	105	125	65	45	25	60

TABLE 3.4: Automatically computed ligament prestrains (%) from experimental data (case 2)

Specimens	ACL		PCL		MCL		LCL
	AM	PL	AL	PM	MCLd	MCLs	
Specimen1	8	14	-8	-20	-1	-3	10
Specimen2	6	17	-17	-3	10	5	10
Specimen3	-8	16	-10	-10	3	2	8
Specimen4	4	20	-16	-15	6	2	10
Specimen5	9	20	-15	-6	8	4	7
Specimen6	0	13	-9	4	-3	-2	9

2 are presented in table 3.3 and table 3.4, respectively. Positive prestrain denotes tight condition and negative prestrain slack condition. Ligament prestrains showed both ligament-specific and specimen-specific variability.

TABLE 3.5: Prestrain (%) obtained with a combination of automatic pre-computation and further manual adjustment (case 3)

Specimens	ACL		PCL		MCL		LCL
	AM	PL	AL	PM	MCLd	MCLs	
Specimen1	8	10	-2	-8	8	3	6
Specimen2	6	12	-8	-4	6	3	5
Specimen3	8	10	-8	-8	2	1	4
Specimen4	10	10	-9	-5	2	3	6
Specimen5	10	13	-5	-5	3	2	2
Specimen6	6	6	-3	-3	4	3	3

(ii) Case 3: Combination of automatic pre-computation and further manual adjustment

Estimated ligament prestrain values computed according to the procedure described in case 3 are presented in table 3.5. Ligament stiffness values were kept the same as presented in table 3.3.

One-to-one validation of knee joint kinematics

On implementation of the generic ligament properties (case 1), only two FE models out of six achieved full convergence. Convergence in this study refers to successful attainment of mechanical equilibrium (within a default tolerance value of ANSYS) at each load step.

Predicted kinematics showed large deviation from the experimental both in magnitude and trend (not reported in this manuscript as only two models achieved convergence). Using the ligament material properties computed automatically (case 2, table 3.4), 5 models out of 6 achieved convergence throughout 60° of flexion.

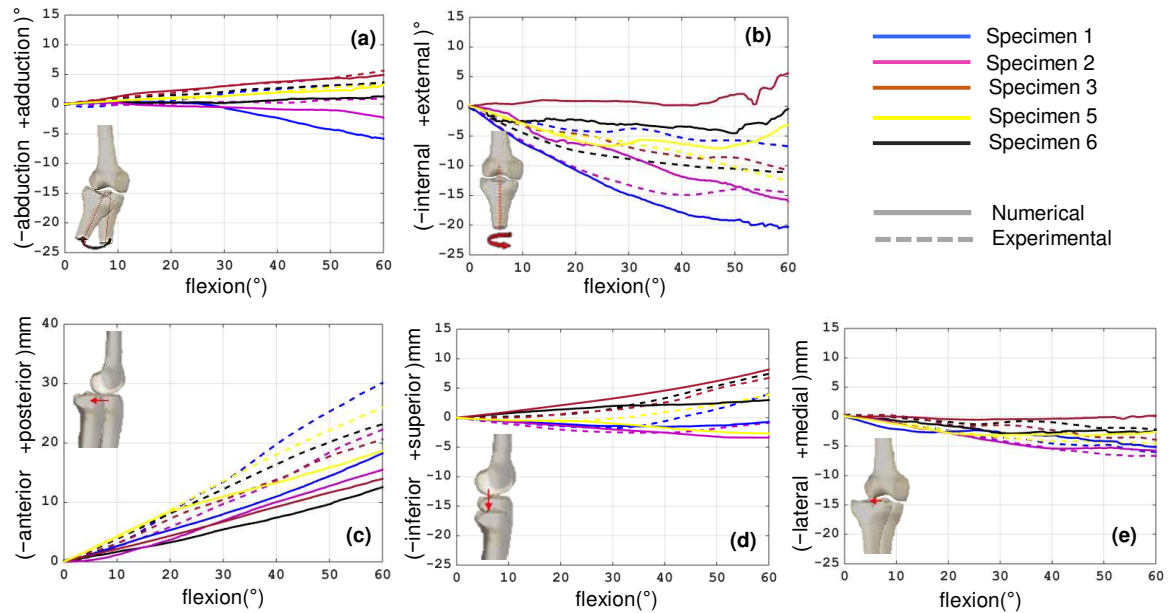


FIGURE 3.11: One-to-one comparison of FE model kinematic predictions against corresponding experimental data for (a) – (b): rotational and for (c) – (e): translational femorotibial kinematics interpreted in femur anatomical reference frame. Results reported are based on the implementation of automatically computed ligament prestrains

Using the ligament material properties computed automatically combined with manual adjustment (case 3, table 3.5), all the FE knee models remained stable throughout the range of flexion. Individual run time was approximately 13 minutes per specimen. One-to-one comparison of model predicted femorotibial kinematics against corresponding *in vitro* results for all specimens are presented in figure 3.11 and figure 3.12 for automatically computed prestrains and adjusted ligament prestrains respectively. For both the cases, model kinematics for all DoF are shown from the reference configuration (state-b) until the end of flexion movement.

TABLE 3.6: Average RMS difference \pm SD between experimental and model-predicted kinematics

Flexion	Case	A/A(°)	I/E(°)	P/A(mm)	I/S(mm)	L/M(mm)
	1	-	-	-	-	-
0-60°	2	2.4 \pm 1.3	6.3 \pm 6.2	5.0 \pm 3.5	1.9 \pm 1.8	1.2 \pm 1.1
	3	1.5 \pm 1.3	5.3 \pm 5.1	3.4 \pm 2.3	1.2 \pm 0.8	2.0 \pm 1.9

A/A: Abduction/Adduction, I/E: Internal/External, P/A: Posterior/ Anterior, I/S: Inferior/Superior, L/M: Lateral/Medial

Table 3.6 summarizes the RMS difference between model-predicted and experimental

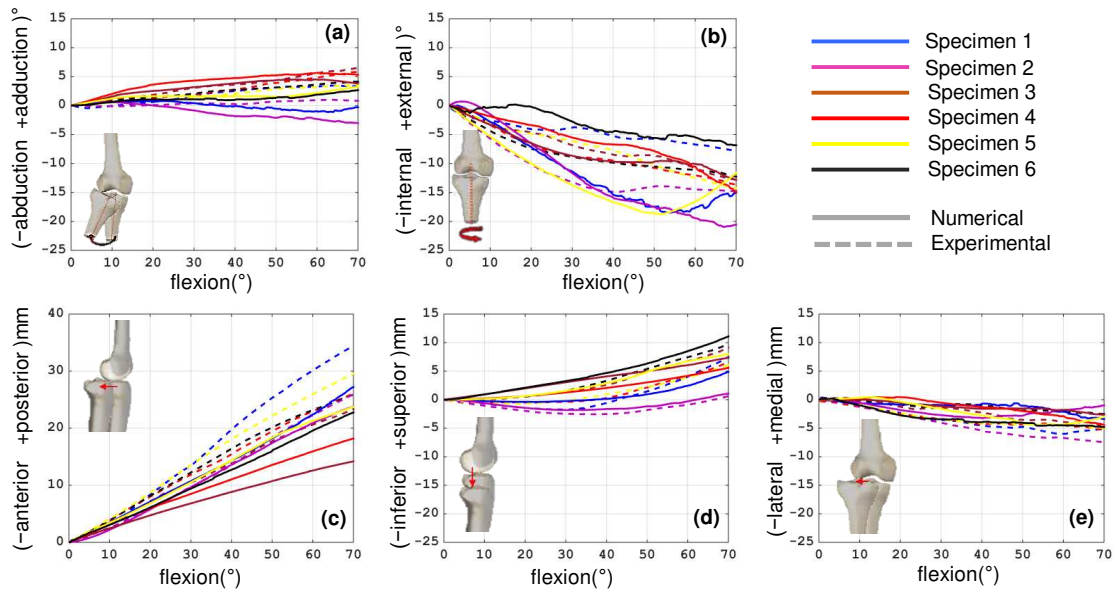


FIGURE 3.12: One-to-one comparison of FE model kinematic predictions against corresponding experimental data for (a) – (b): rotational and for (c) – (e): translational femorotibial kinematics interpreted in femur anatomical reference frame. Results reported obtained using a combination of automatic pre-computation and further manual adjustment

kinematics for the range of flexion angle 0-60° for the two cases (case 2 and case 3) of ligament material properties. Since 5 models out of 6 were converged while applying automatically computed ligament prestrains, differences are presented for 5 models.

3.2.4 Discussion

Subject-specific tensioning of ligaments is essential in developing personalized knee FE models. In this study, we built subject-specific knee FE model with CT-based geometry and evaluated a new procedure for subject-specific calibration of ligaments prestrain from biplanar X-ray data. Predicted femorotibial kinematics of each model was compared to the corresponding *in vitro* response for three different cases of ligament properties (prestrain). First, we investigated whether the FE models with generic prestrain values can capture inter-individual variability of the *in vitro* kinematics. Second, experimentally obtained prestrains were recruited to the FE models and predicted kinematics were observed (case 2). Third, model kinematics were observed with respect to calibrated ligament properties based on the combination of pre-computed prestrains and further adjustment (case 3). For case 2, RMS differences between model-predicted and experimental results for abduction/adduction and external/internal rotation were less than or equal to 2.4° and 6.3° respectively. For translation kinematics, the differences observed were less than or equal to 5.0 mm, 1.9 mm and 1.2 mm respectively for posterior/anterior, superior/inferior, and lateral/medial motions. For case 3, improvement in model kinematics was observed with RMS differences 1.5° and 5.3° for abduction/adduction and external/internal rotation. Differences for posterior/anterior, superior/inferior, and lateral/medial motions were 3.4 mm,

1.2 mm and 2 mm respectively. These results show that the proposed methodology allows us to obtain a first good approximation of the prestrain values with further manual adjustment to improve the kinematic prediction.

As far as the authors are aware of, there are numerous challenges exist in determining ligament prestrain. Challenges are linked to both measurement issues and modeling issues. Measurement challenges are mainly methodological issues related to identification of ligament attachment sites and determination of ligament elongation pattern during motion (Belvedere et al., 2012; Gardiner, Weiss, and Rosenberg, 2001; Woo et al., 1990). Because of such difficulties, FE models in general, adopt prestrain values from other studies available in the literature (Galbusera et al., 2014; Yang et al., 2010). As these values are adopted from other experimental studies and not corresponding to the specimen under consideration, thereby cannot be considered as subject-specific. Optimization methods have also been extensively used to calibrate specific ligament constitutive behavior. These approaches particularly used laxity tests to calibrate their models (Baldwin et al., 2012; Beidokhti et al., 2017). Such approaches are, although shown effective to attain specimen-specific ligament properties, yet computationally expensive.

The current study focused on the development and evaluation of a new procedure for subject-specific tensioning of FE knee ligaments. The proposed procedure builds upon data previously collected during an experimental investigation conducted to identify ligament (cruciate and collateral) attachment sites, and to determine the ligament elongation patterns during passive knee flexion (Rochcongar et al., 2016). The FE model replicates the natural ligament (cruciate and collateral) insertions since these are derived from the radio opaque paint locations painted on the specimens prior to the CT-scan (figure 3.7). The values obtained were consistent with those experimental measurements reported in the literature (Belvedere et al., 2012; Bicer et al., 2010). It is worth mentioning that because of the lack of experimental data for other ligaments, generic insertion sites were employed. Although, it is difficult to directly compare the estimated prestrains with similar studies in literature because of variability in ligament geometry and material property, yet the prestrain values were found within the range confirmed by others (Amiri et al., 2006; Wismans et al., 1980; Zaylor, Stulberg, and Halloran, 2019). Also, most of the ligaments were found in tensed state at full extension except PCL, which is overall in agreement with the literature (Blankevoort and Huijskes, 1991; Guess, Razu, and Jahandar, 2016; Moglo and Shirazi-Adl, 2005). Similarly, predicted kinematic response also showed good correspondence with the experimental results for all the specimens. The experimental-numerical differences found in this study were comparable to similar studies reported in the literature (Beidokhti et al., 2017; Harris et al., 2016). For instance, (Beidokhti et al., 2017) reported an average RMS difference of 3.5° and 2.8° respectively for abduction/adduction and external/internal rotations. For anterior/posterior, superior/inferior and lateral/medial motions the differences were 3 mm, 2.3 mm and 1.6 mm respectively. It is worthwhile to mention that when generic properties were used, most of the models couldn't reach convergence. As previously reported by other research teams (e.g., (Schwartz, Chokhandre, and Erdemir, 2019)) focusing on the medial

collateral ligament), convergence difficulty appeared in this kind of models when material properties were not personalized.

The procedure to compute ligament prestrain directly from experimental data (Case 3) provided satisfactory initial guess, based on which model estimated kinematics were already in good agreement with the experimental data. As this approach appears to be computationally inexpensive (15-20 sec to obtain ligament specific prestrain for a single knee model) and methodologically simple, it may serve as a reliable alternative for estimating subject-specific ligament prestrain values. To be noted that no direct evaluation of the ligament tensions was performed in the present study. The decision to implement the current technique as an alternative has to be conducted with caution. For successful implementation of this technique towards clinics, exhaustive model evaluation under various loading conditions is required including ligament tension and contact stress. Nevertheless, validating joint kinematics as a first step could be valuable to show feasibility of the current approach.

This study contains some considerations and limitations worth highlighting. First, while comparing with experimental kinematics, model-predicted results were shown from reference configuration (state-b). It is an auto-equilibrated configuration under the prestrain effect, which is not concurrent with initial experimental configuration and difficult to calibrate. This results in absolute offset from the experimental kinematics (Baldwin et al., 2012), although masked in relative kinematics. Second, we acknowledge that one of the sources of discrepancies between experimental-numerical kinematics may come from model simplifications and assumptions. It is also to be noted that predicted kinematics with a combination of initial guess from experimental data and further manual adjustment displayed closer correspondence to *in vitro* data. Although the difference is minimal, this may be attributed to the representation of overall joint soft tissue structure with simple ligamentous structures without including cartilage layers and menisci. As the proposed methodology is not based on current state-of-the-art approaches (such as MRI based complex models with detailed soft tissue structures), there was difficulty to obtain subject-specific geometry of cartilage and menisci with available imaging modalities (CT and biplanar X-ray) employed in our study. Such simplification, therefore doesn't hold if we are interested in more detailed local insights, e.g., cartilage contact stress. However, for analysis, such as graft tensioning effect on knee response while reconstructing ACL, such simplification was considered relevant (Pena et al., 2005). Third, exclusion of meniscus may overestimate the role of the ligaments in constraining the joint and providing stability (Harris et al., 2016). However, other studies reported no remarkable influence of meniscus on the assessment of the knee joint kinematics, especially for the flexion range 0°–90° (Amiri et al., 2006; Guess, Razu, and Jahandar, 2016). Fourth, ligaments and tendons were represented as bundles of 1D elements, which may not capture actual ligament length variation, as they do not account for material continuum, fiber twisting or wrapping. Yet, such simplification provides faster solutions and recommended, particularly for the prediction of knee kinematic parameters (Bolcos et al.,

2018; Beidokhti et al., 2017). Fifth, we chose to personalize only ligament prestrains, although stiffness values vary from subject to subject. This consideration was based on sensitivity analyses found in literature, where model predicted kinematics are proclaimed to be highly sensitive to strain state at initial configuration rather than stiffness values (Pena et al., 2005; Wismans et al., 1980). Besides, the models were validated only under passive flexion load, which may not imitate an *in vivo* situation of clinical interest, yet could be a first step of assessing the potential of the models towards complex scenarios. In this contribution, a maximum flexion angle of 70° was considered to calibrate the model as this range covers the most common amplitude of *in vivo* motion under level walking, during which ligaments offer a substantial contribution to knee stability (Butler et al., 2007). However, perspective work will focus on calibrating the model up to 120° of knee flexion. We acknowledge that no influence of experimental uncertainty nor sensitivity of ligament attachment sites on predicted kinematics was performed. Future study is necessary to assess this issue. Finally, the study was limited to six specimens due to time and labor associated with CT segmentation, yet higher in number compared to other similar published studies. This might limit the model at the current state for clinical translation; however, it was imperative to build CT-based models to minimize the impact of geometrical uncertainty in model predictions.

In conclusion, as it was a first study to directly implement prestrain values on models directly from the experiment, which may find scopes in model-based clinical studies, such as planning of ligament balancing or reconstruction as it reduces complexity in model development (especially ligament calibration) as well as computational cost, while maintaining good correspondence with experimental data. In that aim, further model evaluation would be necessary for larger specimen size and in other clinically relevant scenarios.

Overall, this chapter allowed to address two prominent challenges exist in model development and evaluation approaches as elaborated in the literature review. The quasi-automatic methodology employed in the first section helped to generate subject-specific FE mesh of the knee joint with satisfactory mesh quality and surface representation accuracy. Thanks to the EOS system and fast 3D reconstruction techniques.

The second section focused on validation of the subject-specific *in vitro* FE models of the knee joint under passive flexion. A novel methodology to calibrate ligament prestrains based on experimentally acquired values was attempted and evaluated satisfactorily. The overall methodology helped to estimate knee kinematics with low computational cost as no optimization process was involved, and secondly owing to the careful strategy of model simplification. The model validation against *in vitro* experiments, although cannot be considered sufficient (passive loads), however, will serve as an intermediate step prior to translating the models towards *in vivo* loading condition.

Chapter 4

Soft Tissue Artifact correction in motion analysis

The contribution elaborated in the previous chapter allowed to assess feasibility and capability of the FE models to estimate joint kinematics of the knee joint. In order to proceed a step further, i.e., to estimate *in vivo* kinematics, integration of subject-specific physiological boundary conditions to the FE models is paramount. As discussed in the literature review, the widespread approach to apply *in vivo* boundary conditions in models is skin marker-based motion analysis data. Also, it is clearly evident that estimation of joint kinematics based on skin marker data is error prone because of soft tissue artifact (STA). It is also apparent that existing methods for STA compensation are not adequate to take subject-specific joint morphology (in particular for patients with joint lesion) and soft tissue properties into account. This justified the need to propose a different approach for STA compensation which is elaborated in the first section of this chapter. This work has been submitted to *Journal of Biomechanics* entitled "Development and evaluation of a new methodology for Soft Tissue Artifact compensation in the lower limb" and is currently under review.

The second section pertains to experimental quantification of soft tissue deformation, which is often considered essential to effectively compensate for STA.

4.1 Development and evaluation of a new methodology for Soft Tissue Artifact compensation in the lower limb¹

Abstract Skin Marker (SM) based motion capture is the most widespread technique used for motion analysis. Yet, the accuracy is often hindered by Soft Tissue Artifact (STA). This is a major issue in clinical gait analysis where kinematic results are used for decision-making. It also has a considerable influence on the results of rigid body and Finite Element (FE) musculoskeletal models that rely on SM based kinematics to estimate muscle, contact and ligament forces. Current techniques designed to compensate for STA, in particular multi-body optimization methods, assume anatomical simplifications to define joint constraints. These methods, however, cannot adapt to subjects' bone morphology particularly for patients with joint lesions, nor easily can account for subject- and location-dependent STA. In this perspective, we propose to develop a conceptual FE based model of the lower limb for STA compensation and evaluate it for 66 healthy subjects under level walking motor task.

Both hip and knee joint kinematics were analyzed considering 6 degrees of freedom (DoF) joint. Results showed that STA caused underestimation of the hip joint kinematics (up to 2.2°) for all rotational DoF, and overestimation of knee joint kinematics (up to 12°) except in flexion/extension. Joint kinematics, in particular knee joint appeared to be sensitive to soft tissue stiffness parameters (rotational and translational mean difference up to 1.5° and 3.4 mm). Analysis of the results using alternative joint representations highlighted the versatility of the proposed modeling approach. This work paves the way for using personalized models to compensate for STA in healthy subjects as well as in patients with degenerated joints and for different activities.

Keywords: Soft Tissue Artifact, In vivo joint kinematics, Model personalization, Hip and knee joint, Finite Element Analysis

4.1.1 Introduction

Accurate assessment of *in vivo* kinematics is essential for providing insights into normal joint functionality (Akbarshahi et al., 2010) and investigation of lower limb joint pathology (Andriacchi and Alexander, 2000). Skin Marker (SM) based motion capture is the most widespread technique used for estimating skeletal kinematics of the lower limb. However, the accuracy of such technique is affected by the relative movement of soft tissues with respect to the underlying bone, a bias commonly referred to as Soft Tissue Artifact (STA). If not compensated for, STA can lead average kinematic errors up to 16 mm in translation and 13° in rotation for the knee joint (Benoit et al., 2006). Such errors may have a significant influence on the assessment of pathology or the treatment effects in clinical gait analysis (Seffinger and Hruby, 2007).

Different methods have been proposed in the literature to reduce the effect of STA on bone pose estimation (e.g., single-body optimization (Cheze, Fregly, and Dimnet, 1995),

¹Potential copyright issues with direct reuse of the article including figures and contents

double anatomical landmark calibration (Cappello et al., 1997), point cluster technique (Andriacchi et al., 1998), and Multi-body Optimisation (MBO) (Lu and O'connor, 1999). Amongst these, MBO, which relies on a predefined kinematic model with specific joint constraints, is increasingly used.

Initially, simple kinematic constraints such as hinge or spherical joints were considered to represent hip and knee articulation (Charlton et al., 2004; Lu and O'connor, 1999; Reinbolt et al., 2005). Later, anatomical joint constraints (parallel mechanism, coupling curves, ligament length variation, elastic joint etc.) were introduced providing encouraging 3D kinematics as they allowed joint displacements (Bergamini et al., 2011; Duprey, Cheze, and Dumas, 2010; Gasparutto et al., 2015; Richard et al., 2016). However, regardless of the joint constraints imposed, generic (unpersonalized) model-derived kinematics were shown inaccurate (knee kinematic error up to 17° and 8 mm) as these models could not adapt to patient-specific geometry, particularly in pathological conditions (Clément et al., 2017). On the other hand, personalization of model geometry based on medical images were shown promising in improving the accuracy of joint kinematics (Assi et al., 2016; Clément et al., 2015; Nardini et al., 2020).

Joint simplification has indirect consequences on the predictive accuracy of both rigid body musculoskeletal (MSK) models and FE based MSK models. Studies that used FE-MSK models to predict local joint mechanics using *in vivo* joint kinematics (Shu et al., 2018; Xu et al., 2016), assumed the knee joint as 1 DoF. This might result in propagation of uncertainties on the predicted kinematics and would affect the joint reaction as well as muscle and ligament forces.

In light of the aforementioned contexts, reliable estimation of skeletal kinematics with SM based motion data is still a major challenge (Richard, Cappozzo, and Dumas, 2017). Furthermore, extensive time and complexity associated with customization of models to subjects' geometry prohibit large sample size. In that context, methods for 3D reconstruction of bony segments from medical imaging modalities, in particular biplanar X-ray imaging is promising in research and clinical routine (Chaibi et al., 2012). Also, there is a need for adaptable modeling approaches that can account for subject-, task-, and location-dependent STA.

In a previous study, a conceptual FE model was proposed for STA compensation (Skalli et al., 2018). The objective of the current study was to develop the conceptual model for the lower limb and to implement it on healthy volunteers considering subject-specific models.

4.1.2 Materials and methods

First, the conceptual model is presented. Then implementation of the model is illustrated within an IRB approved (CEHDF285) study. Finally, the consistency and versatility of the model were investigated through sensitivity of various parameters, including the joints representation.

Conceptual FE model of the lower limb

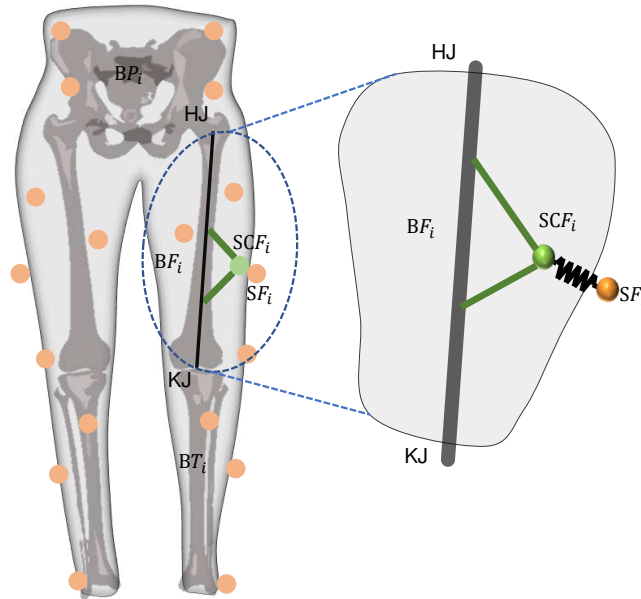


FIGURE 4.1: Schematic illustration of the conceptual lower limb FE model. Detailed illustration shown only for the femur segment. BP_i , BF_i and BT_i denote pelvis, femur and tibia bone nodes. SF_i and SCF_i are the skin and subcutaneous markers respectively for the femur segment. HJ and KJ denote the hip and knee joint respectively.

The conceptual model the lower limb consists of bone segments, nodes representing skin markers and subcutaneous markers, joint elements, and elements that connect the skin markers to the corresponding bones. Bone segments are represented by a set of high stiffness beams. The joints between the segments are represented by rigid links, allowing free rotations at the joint and controlled displacements. To simplify the soft tissue modeling, all the soft tissue deformation effect is reported to the subcutaneous level. Therefore the connection between a skin marker and corresponding bone segment is represented by a combination of spring connecting the skin marker to the subcutaneous marker and beams connecting the subcutaneous markers to the bone segments (figure 4.1).

The measured skin marker displacements throughout gait cycle are considered as input to the FE model, yielding bone and subcutaneous marker locations and joints kinematics.

Skin markers are denoted by S , differentiating between those of the pelvis (SP), femur (SF) and tibia (ST). The number of markers for the pelvis (NMP), femur (NMF) and tibia (NMT) is variable and depends on the protocol being considered. Each skin marker is therefore referred to using the corresponding subscript: SP_i , SF_i and ST_i respectively for the pelvis (SP_1 to SP_{NMP}), femur (SF_1 to SP_{NMF}) and tibia (ST_1 to ST_{NMT}). Using the same convention, subcutaneous markers are denoted SC (SCP_i , SCF_i and SCT_i for the pelvis, femur and tibia respectively) and the bone points are denoted as B (differentiating between those of the pelvis (BP), femur (BF) and tibia (BT)). Hip and knee joints are denoted by HJ and KJ respectively.

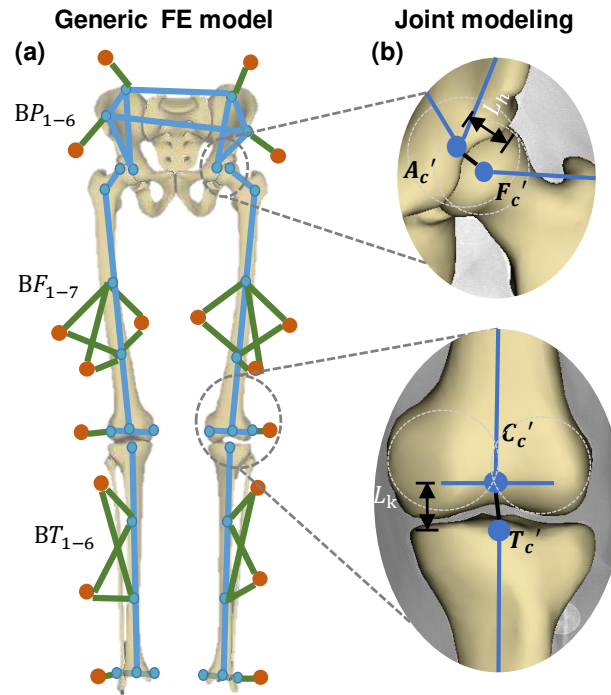


FIGURE 4.2: (a) Detailed representation of the lower limb FE model with generic anatomical bony landmarks. Anatomical landmarks for the pelvis (BP_1 to BP_6): right antero-superior iliac spine, right postero-superior iliac spine, left antero-superior iliac spine, left postero-superior iliac spine, and right and left acetabulum centers. For the femur (BF_1 to BF_7): femur head center, greater trochanter, two diaphyseal points, medial and lateral condyle centers and center of the two condyles. For the tibia (BT_1 to BT_6): center of the two plateaus, two diaphyseal points, medial and lateral malleoli and center of the two malleoli. (b) joint modeling of the hip (L_h) and knee joint (L_k) with rigid links allowing free rotation and controlled relative displacement.

As illustrated further in figure 4.2a, the pelvis bone was represented by 6 nodes (BP_1 to BP_6): right antero and postero superior iliac spine, left antero and postero superior iliac spine, and right and left acetabulum centers. The femur was represented by 7 nodes (BF_1 to BF_7): femoral head center, greater trochanter, centers of lateral and medial femoral condyles, center of the two condyles (equidistant from the condyle centers) and two other diaphyseal nodes along the femoral longitudinal axis placed approximately at the lower third of the segment as recommended in the conventional Davis protocol (Davis III et al., 1991). Similarly, the tibia was represented by 6 nodes (BT_1 to BT_6) consisting of center of the two plateaus, lateral and medial malleoli, center of the two malleoli and two other diaphyseal nodes along the tibial longitudinal axis placed approximately at the tibial tuberosity and lower third of the segment respectively. Beam elements with elastic modulus (E) of 12 GPa were used to connect the nodes for each bone segment (Choi et al., 1990).

Modeling of the skin marker-bone connection: Each pelvis skin marker (SP_1 to SP_4) was linked to the pelvis bone by a combination of spring element that connects the skin marker to the corresponding subcutaneous marker (SCP_1 to SCP_4), and a beam element that connects the subcutaneous marker to the bone. The springs were assigned with stiffness (k) values in the range 5 kN/m to 65 kN/m in agreement with orders of magnitudes reported in the

literature (Dumas and Jacquelin, 2017; Gittoes, Brewin, and Kerwin, 2006; McLean, Su, and Bogert, 2003), whereas the beams were considered highly stiff and assigned the same elastic modulus as that of the bones. The same combination of elements was used to connect the skin markers to the bone segments for the femur and tibia.

Modeling of the joints: As a first option, hip and knee joints were represented each by a rigid link allowing free rotation while controlling the relative displacements (through the length of the link). For the hip joint, the rigid link connected the acetabulum center and femur head center. For the knee joint, the rigid link was defined in the line joining the centroid of the two femoral condyle centers to the centroid of the two tibial plateau centers (figure 4.2b).

Model implementation

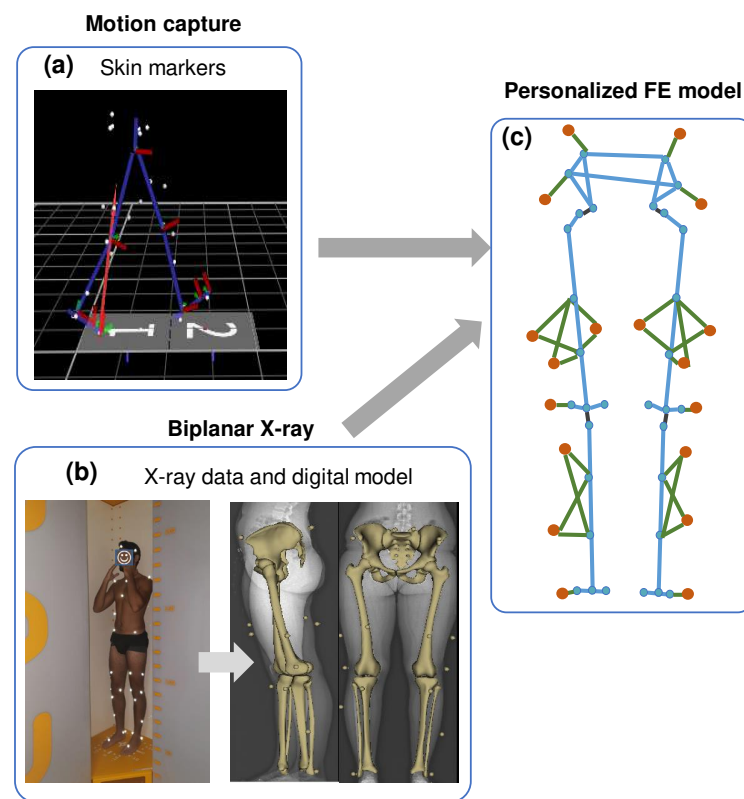


FIGURE 4.3: Schematic illustration of FE model personalization (a) the locations of the skin markers throughout gait cycle obtained from motion capture and (b) 3D digital models of the pelvis, femur and tibia built from two orthogonal radiographs (c) anatomical landmarks were identified from the 3D digital models resulting the nodal coordinates of each bone.

(i) Data acquisition 66 healthy volunteers were included (age range: 18-60 years; weight: 71.3 ± 15 Kg; height: 170 ± 10 cm) in this study. The only exclusion criteria were previous records of orthopedic surgery of the lower limbs.

Quantitative Movement Analysis was performed on an optoelectronic analysis system comprising 7 video-cameras (Vicon Motion System Ltd., Oxford Metrics, UK). The optoelectronic markers were positioned following the Plug-in Gait[®] method (Davis III et al., 1991), and participants were asked to perform level walking at self-selected speed (figure 4.3a). Biplanar radiographs were then acquired using the EOS system (EOS Imaging, France). 3D digital models of bones were obtained using a 3D reconstruction algorithm validated by previous studies (figure 4.3b) (Chaibi et al., 2012). The location of skin markers was also computed from biplanar X-Rays.

(ii) Subject-specific FE model development and simulation From the 3D digital models of the bones, subject-specific anatomical landmarks were identified, resulting in nodal coordinates of each bone, as represented in figure 4.3c. The distance between skin and subcutaneous markers were arbitrarily chosen as 1 mm (i.e., spring length). Based on the mean translational displacement of the knee joint found in our previous in vitro experimental work (Germain et al., 2016), the joint length for the knee (L_k) was fixed to 20 mm. For the hip (L_h), the joint length was fixed to 1 mm based on an unpublished data on the hip translational displacement quantified using biplanar X-rays. For simplicity, stiffness parameter of the springs was kept constant across all segments and assigned 50 kN/mm.

The measured marker displacements from the motion capture were incrementally introduced to the model as a prescribed boundary condition, and resulting bone and subcutaneous marker positions throughout the gait cycle were computed using commercial FE package ANSYS[®]. The resolution was performed via an implicit scheme and taking into account geometric non-linearity.

(iii) Kinematic computation The positions of the resulting bone segments and subcutaneous markers were used to define a set of virtual markers (figure 4.4). These virtual markers hereafter will be termed as corrected markers (CF_i) and were defined with the same consideration as those of the subcutaneous markers, i.e., rigid links with the bone segment. The positions of the corrected markers were used to compute STA Compensated (STAC) joint kinematics. Hip and knee joint rotational kinematics were expressed in the pelvis and femur anatomical reference frames (EOS-based) respectively, and with Cardan sequence $YX'Z''$. Hip joint translation was defined as the relative displacement between points A'_c and F'_c expressed in the pelvis anatomical reference frame. Similarly, knee joint translation was defined as a relative displacement between points C'_c and T'_c expressed in the femur anatomical reference frame. Anatomical reference frames were defined as described in (Schlatterer et al., 2009) for the femur and tibia, and in (Dubois, 2014) for the pelvis. A customized Matlab[®] (Mathworks, Massachusetts, United States) routine was used for both SM-based and STAC kinematic processing.

Joint kinematics (mean \pm 1SD) for the hip and knee joint were plotted for all 6 DoF over time normalized gait cycle. Difference in range of motions ($dROM$) was also computed between SM-based and STAC kinematics.

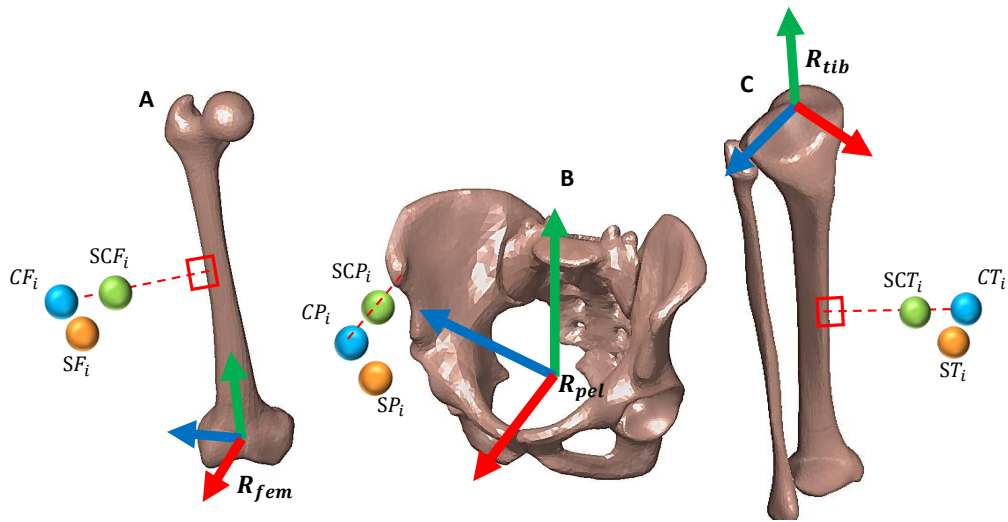


FIGURE 4.4: Illustration of corrected markers (CF_i, CP_i, CT_i) and anatomical reference frames ($R_{fem}, R_{pel}, R_{tib}$) for the (A) femur, (B) pelvis and (C) tibia respectively. Corrected markers are obtained from the subcutaneous marker in a direction orthogonal to the bone segment and 1mm away from subcutaneous marker. Anatomical reference frames for the femur and tibia were defined as described in (Schlatterer et al., 2009) and for pelvis (Dubois, 2014).

Illustration of versatility

(i) *Sensitivity of spring stiffness and joint length* Two different stiffness values for the subcutaneous springs were implemented (5 kN/m and 65 kN/m) to investigate the influence of stiffness parameters on joint kinematics. Segment specific stiffness values were also considered by assigning different stiffness values to pelvis (5 kN/m), femur (10 kN/m) and tibia (55 kN/m).

Furthermore, two different knee joint lengths ($L_k = 21 \text{ mm}$ and 31 mm) were arbitrarily considered to investigate the impact of joint lengths on estimated kinematics. Implemented knee joint lengths were based on the minimum and maximum value found in the population. In this case, spring stiffnesses were kept constant with a value 65 kN/m .

Joint kinematics (mean \pm 1SD) for the hip and knee joint were computed for all 6 DoF over time normalized gait cycle. Differences in range of motions ($dROM$) were also computed for the kinematics computed with different stiffness values and different joint lengths.

(ii) *Alternative joint representation* Two other alternative joint models were considered to illustrate the versatility of the lower limb FE model. These alternative joint models considered were:

Parallel Mechanism: Two rigid links connecting the center of the medial and lateral condyles to the corresponding tibial plateaus were considered to model the knee joint approximating the femur-tibia contact behavior. The hip joint model was left unaltered (single-link model).

Spherical joint: Spherical joint model at the hip and knee joint was considered allowing free rotations while restricting the displacements. The location of the joint constraint was placed on the femur head center for the hip joint and the mid-point of the two femoral condyles for the knee joint.

Joint kinematics (mean \pm 1SD) for the hip and knee joint were compared among the single link, parallel mechanism and spherical joint model. Spring stiffness value 65 kN/mm were assigned for all the joint models.

Model comparison with multi-body optimization

As no reference kinematics (artifact-free motion) was available, the FE model results were compared to a classical STA compensation MBO method with spherical joint modeling for both the hip and knee joints (Lu and O'Connor, 1999). The joint constraints and locations incorporated in the MBO were in accordance with the FE model. To compare the kinematic results of the subject-specific FE models with MBO, the same anatomical reference frames were defined for the MBO bone segments.

Differences between the two methods were also analyzed with a Student's t-test or Wilcoxon sign-rank test depending on the outcomes of the Shapiro-Wilk test of normality, using a customized Matlab routine. For all the tests, the significance level was set 0.05 *a priori*.

4.1.3 Results

Each FE model with 6-DoF joints required less than 45 sec of run time on a single processor desktop PC to simulate a complete gait cycle of approximately 200–300 frames. All results are synthesized in Table 4.1.

Joint kinematics

Both rotational and translational kinematics estimated with skin marker measurements and FE model embedding the 6 DoF joint model are illustrated in figures 4.5 and 4.6 for the hip and knee joints respectively. The joint kinematics are plotted over time-normalized gait cycle.

Overall, for the hip joint, STAC and SM-based kinematics exhibited qualitatively similar pattern. However, differences in range of motion (*dROM*) varied across all DoF, with a maximum value of -2.2° for Abduction/Adduction (Abd/Add) followed by -1.6° and -0.3° for Flexion/Extension (Flex/Ext) and Internal/External (Int/Ext) rotation respectively. Maximum joint displacement up to 1 mm was observed for STAC kinematics while showing up to 41.5 mm for SM-based kinematics in Posterior/Anterior (Post/Ant) direction. In the Medial/Lateral (Med/Lat) and Inferior/Superior (Inf/Sup) direction, joint displacement exhibited less than 1 mm, whereas SM-based kinematics showed up to 28 mm.

TABLE 4.1: Difference in mean ROM ($dROM$) presented for SM Vs STAC, different spring stiffness, different joint lengths and alternative joint models. Singed difference is presented only for SM Vs STAC and FE Vs MBO

		A/A(°)	I/E(°)	F/E(°)	P/A(mm)	I/S(mm)	L/M(mm)
Hip	SM Vs STAC	-2.2	-0.3	-1.6	40.5	23.5	27.5
	Spring stiffness	0.1	0.1	0.3	0.8	0.2	0.6
	Joint length	0.4	0.6	0.2	0.8	0.1	2.0
	Sph Vs SL	1.0	0.8	0.2	-	-	-
	Sph Vs PM	1.7	1.4	0.7	-	-	-
	SL Vs PM	0.8	0.6	0.5	2.7	0.4	4.0
	FE Vs MBO	1.5	-1.6	-2.0	-	-	-
Knee	SM Vs STAC	1.5	12.5	-6.3	10.2	16.3	8.0
	Spring stiffness	1.0	1.4	0.1	3.4	1.0	1.1
	Joint length	0.5	0.3	0.3	2.1	1.6	0.5
	Sph Vs SL	0.2	1.3	1.2	-	-	-
	Sph Vs PM	0.6	3.4	0.8	-	-	-
	SL Vs PM	0.4	2.6	0.5	7.6	0.9	0.4
	FE Vs MBO	1.4	0.7	1.9	-	-	-

SM: skin marker, STAC: soft tissue artifact corrected, Sph: spherical, SL: single link, PM: parallel mechanism, FE: finite element, MBO: multibody optimization, A/A: Abduction/Adduction, I/E: Internal/External, F/E: Flexion/Extension, P/A: Posterior/Anterior, I/S: Inferior/Superior, L/M: Lateral/Medial

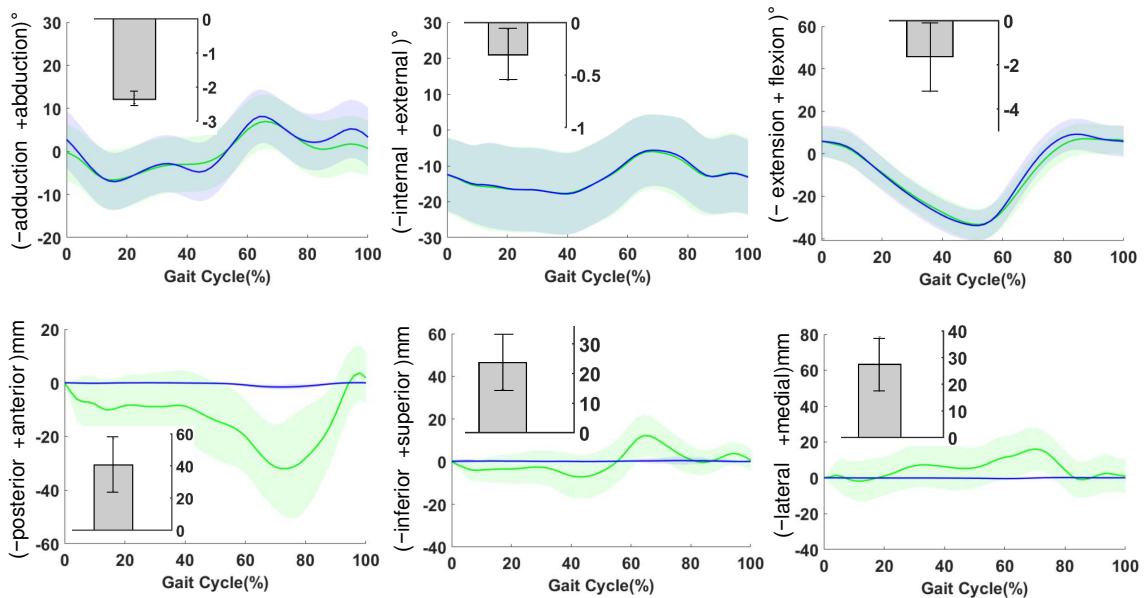


FIGURE 4.5: Hip joint kinematics during gait presented as Mean \pm 1SD. Mean values for skin marker-based (green) and FE model predicted results (blue) are shown as solid lines, while standard deviation in lighter shades. Differences in ROM ($dROM$) between SM-based and STAC results are depicted as insets for all DoFs

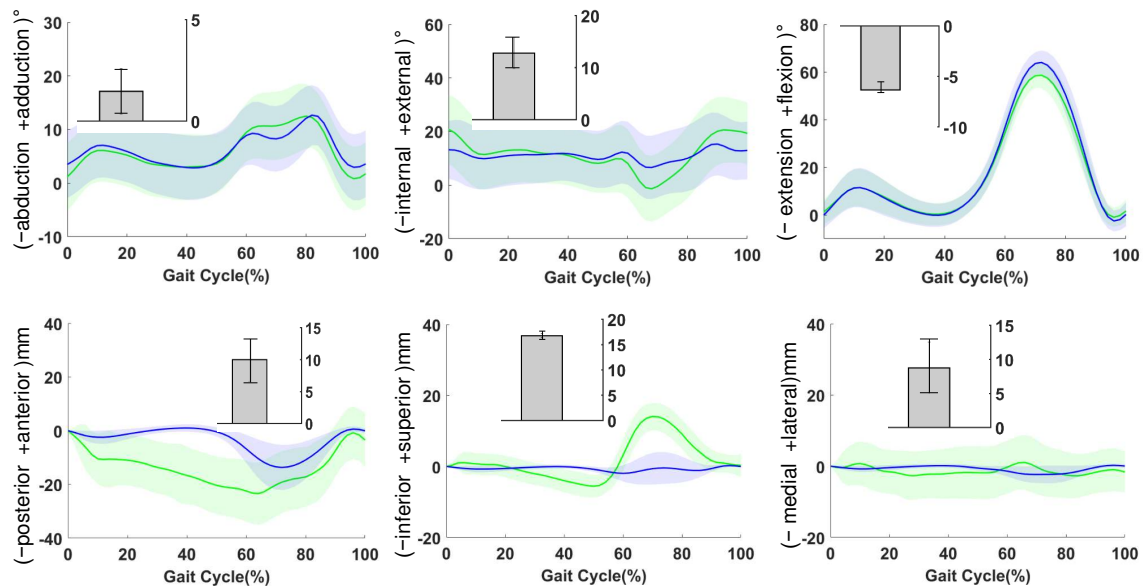


FIGURE 4.6: Knee joint kinematics during gait presented as Mean \pm 1SD. Mean values for skin marker-based (green) and FE model predicted results (blue) are shown as solid lines, while standard deviation in lighter shades. Differences in ROM ($dROM$) between SM-based and STAC results are depicted as insets for all DoFs.

For the knee joint, maximum $dROM$ value (12.5°) was observed for Int/Ext followed by Flex/Ext (-6.3°) and Abd/Add (1.5°) rotation respectively. A maximum of 20 mm of joint displacement was noted in (Post/Ant) direction, while remaining DoFs showed up to 9 mm (Med/Lat) and 3 mm (Inf/Sup) for STAC kinematics. These results showed up to 30.5 mm, 12.5 mm and 21 mm respectively for SM-based kinematics.

Sensitivity study

(i) **Spring stiffness parameters and joint length** With two different values of spring stiffness parameters ($5kN/mm$ and $65kN/mm$), less than a degree of $dROM$ was noted for the hip joint rotational kinematics. Similarly, very small variability (submillimeter) was observed for the translational motions. As for the knee joint kinematics, less than 1.5° of $dROM$ across all rotational DoFs and 1 mm in Inf/Sup and Lat/Med motion were observed. The effect on Ant/Post translations was higher up to 3.4 mm during the swing phase of the knee joint.

Different knee joint lengths influenced both hip and knee joint rotational kinematics exhibiting less than a degree of $dROM$. Hip translational kinematics displayed higher variability for Lat/Med motions (by 2mm) while showing less than 1 mm change for remaining DoFs. As for knee translational kinematics, $dROM$ showed a change in the range of 0.5 to 2.1 mm.

(ii) **Influence of alternative joint models on kinematics** Different joint representations displayed varying kinematic changes across all DoFs for the hip and knee joints. Up to 1°

of $dROM$ was observed for hip Add/Abd when the joint model was changed to spherical from the single-link. This value changed till 1.7° when the joint model was further switched to parallel mechanism from single-link. Maximum $dROM$ of 4 mm was observed for the hip Lat/Med motion followed by Post/Ant motion (2.7 mm) and Inf/Sup motion (0.4 mm) when changing knee joint model from single-link to parallel mechanism. Similarly, knee joint kinematics exhibited up to 3.4° in $dROM$ for Int/Ext rotation when joint model was altered, while Add/Abd and Flex/Ext displayed up to 0.6° and 1.2° respectively. Knee Post/Ant motion displayed up to 7.6 mm of $dROM$, whereas less than 1 mm of $dROM$ was noted for the remaining DoFs.

FE Model comparison with MBO

Statistically significant differences between MBO-based and FE-based STA compensation for the hip and knee joints were found ($p < 0.05$). Those differences, however, were always in the range of 0.7° to 2° .

4.1.4 Discussion

Soft Tissue Artifact compensation is essential for accurate estimation of in vivo joint kinematics in both research and clinical routine; however, personalization and versatility of current model-based methods still represents a challenge. The purpose of this study was to develop and evaluate a conceptual FE model of the lower limb for STA compensation. The proposed method was successfully tested on a population of 66 subjects. This model is computationally fast (less than 45 sec run time), and its main advantage is versatility allowing a wide range of parameters and joint representations to be considered.

Qualitatively similar kinematic patterns were observed between SM-based and FE-based STA compensated (STAC) kinematic results for both the hip and knee joints, with differences in range ROM across all DoFs. SM-based kinematics were comparable to the literature (D'Isidoro, Brockmann, and Ferguson, 2020; Fiorentino et al., 2017). Results obtained showed that overall rotational ROM was underestimated by SM-based results up to 2.2° for the hip joint, thus confirming similar observations reported in studies that compared SM-based ROM to dual fluoroscopic measurements (Fiorentino et al., 2020). For the knee joint, SM-based ROM was smaller by 6.3° for the Flex/Ext only. For the other DoFs, SM-based ROM was higher up to 12° as compared to STAC kinematics. For translational kinematics of the knee joint, SM-based results were higher (up to 30.5 mm of ROM) as compared to STAC kinematics showing up to 20 mm. STAC knee kinematics were comparable to studies reported in the literature that reported either bone-pin-based or fluoroscopy-based kinematics (Benoit et al., 2006; Kozanek et al., 2009; Myers et al., 2012). Nevertheless, we observed overall higher $dROM$ values between SM-based and STAC as compared to the studies that reported in the range 4.4° – 5.3° for rotational kinematics and up to 13mm for translational kinematics (Benoit et al., 2006; Leardini et al., 2005). These discrepancies may arise from the experimental protocol such as number of markers, cluster configuration and location.

While comparing FE model predicted results to those of MBO-based, statistically significant differences were observed. However, mean differences were minor (less than or equal to 2°).

The distinguished advantage of the current approach as opposed to the MBO is the model versatility. First, the introduction of springs to account for all soft tissue deformation facilitated to compensate for STA by adjusting the stiffness parameters. Sensitivity study showed that joint kinematics (particularly the knee joint) were sensitive to spring stiffness exhibiting dROM value up to 1.5° for the rotational kinematics and up to 4.5 mm for translational kinematics. Given the subject-specific nature of the soft tissue deformation, spring parameters can be calibrated in the presence of reference kinematics. Moreover, the model allows to easily tune individual spring parameters, which could be helpful to account for location-specific soft tissue behavior (Akbarshahi et al., 2010; Gao and Zheng, 2008). Second, the FE model allows easy implementation of alternatives joint models and joint lengths. Joint models can be further customized to reproduce specific joint angular and translational displacements quantified in specific sub-groups and for specific motor tasks (Kim et al., 2019). Although we cannot confirm the accuracy of the results in the absence of a gold standard, our findings revealed that joint representations have considerable influence on the estimated kinematics, establishing similar remarks as reported in the literature (Duprey, Cheze, and Dumas, 2010; Richard, Cappozzo, and Dumas, 2017). Furthermore, the study (Richard, Cappozzo, and Dumas, 2017) concluded that none of the joint constraints (kinematic or anatomical) could significantly improve the estimation of joint kinematics, and therefore image-based (CT, MRI, biplanar X-ray etc.) model personalization was recommended (Clément et al., 2017; Nardini et al., 2020). In that context, the current FE model has the potential to implement a wide range of joint models, from the most simplified (with spherical constraint) to the anatomically detailed (with articular surfaces).

This study has some limitations. First, there was no reference kinematics to compare the results to. Therefore, the joint kinematics exhibited by the FE models were compared to those computed with the MBO method. Nevertheless, as we cannot consider MBO as a fully reliable solution for STA compensation (Richard, Cappozzo, and Dumas, 2017), such comparison is only for assessing the qualitative performance of the FE model. Second, STA parameters implemented in the model were arbitrary as there is lack of data in the literature. Personalization of such parameters is, however, essential to encompass different range of subjects (young, adult, patients with cerebral palsy and osteoarthritis). Third, joint representation in this model is still simplified, which could be insufficient for investigating local joint mechanics for healthy or degenerated joints (Adouni, Shirazi-Adl, and Shirazi, 2012; Lenhart et al., 2015; Shu et al., 2018; Valente et al., 2014). Nevertheless, as a preliminary step, the current contribution only focused on exploring and facilitating personalization of the parameters that are important for STA compensation. Moreover, even with simplified joint representation, the model could limit the effect of STA in joint kinematics. Fourth, although the proposed approach may give the impression that it complicates the process of STA compensation in gait analysis, the perspectives are numerous, as already highlighted.

Finally, the study was based on a single motor task, i.e., level walking. Therefore, the results may vary with other motor tasks (hopping, cutting, stand-to-sit etc.) and hence the interpretations.

The proposed approach may serve in two major fields of applications: i) in gait analysis for research, where model personalization using medical imaging (e.g., CT, MRI, biplanar X-ray) is usually not performed. However, compensating for STA with classical model scaling techniques is possible, while being able to differentiate soft tissue stiffness parameters between different sub-groups. ii) in clinical gait analysis, where image-based model personalization could capture anatomical details of the healthy or degenerated joints.

In conclusion, we presented a conceptual FE model of the lower limb for STA compensation and successfully tested it in a population of 66 subjects with varying morphologies. The model appeared to be satisfactory in compensating STA and versatile, facilitating parameters that are necessary for model personalization. The methodology developed and evaluated in this study may improve the accuracy of kinematic predictions, which is instrumental for MSK models as well as making clinical decisions.

In this section of Chapter 4, we observed that the proposed FE-based model of the lower limb could effectively compensate for STA and the observed results were in-line with the literature. However, while developing the model, arbitrary stiffness values to the springs were assigned as no information on soft tissue deformation at each marker location was available. This led to experimentally investigate soft tissue deformation pattern at the lower limb during movement. This contribution is included in the following chapter.

4.2 Experimental quantification of soft tissue deformation in quasi-static single leg flexion using biplanar imaging¹

Abstract Soft tissue deformation (STD) causes the most prominent source of error in skin marker (SM) based motion analysis, commonly referred to as Soft Tissue Artifact (STA). To compensate for its effect and to accurately assess *in vivo* joint kinematics, quantification of STD in three-dimension (3D) is essential. In the literature, different invasive and radiological approaches have been employed to study how STA propagates in joint kinematics. However, there is limited reference data extensively reporting distribution of the artifact itself in 3D.

The current study was thus aimed at quantifying STD in 10 subjects along three anatomical directions. Biplanar X-ray system was used to determine true bone and SM positions while the subjects underwent quasi-static single leg flexion.

STD exhibited inter-subject similarity. A non-uniform distribution was observed at the pelvis, thigh and shank displaying maximum at the thigh (up to 18.5 mm) and minimum at the shank (up to 8 mm). STD at the pelvis and thigh displayed inter-marker similarity. STD at the pelvis was found direction independent, showing similar distribution in all the 3 directions. However, the thigh and shank exhibited higher STD in the proximal-distal direction of the bone embedded anatomical reference frame. These findings may provide more insights while interpreting motion analysis data as well to effectively strategize STA compensation methods.

Keywords: Soft tissue deformation, Skin marker-based motion analysis, Biplanar X-ray

4.2.1 Introduction

Skin Marker (SM) based motion analysis is the most common non-invasive method for estimating skeletal position and orientation in 3D space. Accuracy of such method is mainly limited by relative movement between soft tissues and the underlying bone, commonly known as Soft Tissue Artifact (STA). In order to compensate for it and to accurately estimate *in vivo* skeletal position during motion, knowledge of Soft Tissue Deformation (STD) pattern during motion is critical (Benoit et al., 2006; Stagni et al., 2005).

Several invasive (e.g., bone pins (Benoit et al., 2006; Reinschmidt et al., 1997) and radiological studies (e.g., fluoroscopy (D'Isidoro, Brockmann, and Ferguson, 2020; Stagni et al., 2005), biplanar X-ray (Südhoff et al., 2007; Tashman and Anderst, 2002), MRI (Akbarshahi et al., 2010; Sangeux et al., 2006)) have been proposed to characterize STD during different motor tasks. Most of the studies concluded that STD is dependent on an individual subject, type of performed activity, marker configuration as well as locations. For instance, few studies have found that kinematic error due to STD is greater at the thigh than the shank, suggesting location- and segment- specific scheme to compensate for the artefact (Akbarshahi et al.,

¹Potential copyright issues with direct reuse of the article including figures and contents (article under preparation)

2010; Stagni et al., 2005; Benoit et al., 2006). Nevertheless, these studies primarily focused on quantifying the kinematic errors caused by STD rather than STD itself.

As far as the authors are aware of, only one study exists in the literature dealing with quantification of STD at different marker locations and directions in 20 healthy volunteers (Gao and Zheng, 2008). But, due to technical limitations preventing access to the bone position, STA quantification was reported as inter-marker movement instead of marker movement relative to true bone positions. Hence, there is still a lack of reference data on subject-, location- and direction-specific STD, which may provide insight for effective STA compensation strategies for SM based motion analysis.

Amongst the different methods devised for compensating STA, multi-body optimization (MBO) method is increasingly used. It generally assigns a weight matrix reflecting the STA error distribution among the markers adhered to a segment (Lu and O'connor, 1999). Moreover, FE based novel approach to compensate for STA of the lower limb and successfully evaluated in a population of 66 subjects (section 4.1). The FE model facilitates to incorporate STA correction stiffness at each marker location, and stiffness can be calibrated based on information of local STD at each marker location and along each anatomical direction. However, owing to lack of STD data, arbitrary values were assigned for the stiffness parameters.

The current study was thus aimed at quantifying soft tissue deformation on the pelvis, thigh and shank at each marker location and in three anatomical directions during single-leg quasi-static knee flexion using low dose biplanar radiography.

4.2.2 Materials and methods

Data collection

The retrospective data included in the study recruited ten volunteers (age range: 23-40 years; weight range: 63-89 kg, height range: 1.7-1.9 m), 6 months after ACL reconstruction following approval of a relevant ethical committee. Patients with a large osteochondral defect ($>1\text{cm}^2$), operated for a meniscal suture and multi-ligament knee injury, or diagnosed with a neuromuscular disorder which could impair motion, were excluded from this study. The mean IKDC (International Knee Documentation Committee) score for the subjects was 79.7 ± 7.2 . This score ranges from 0 to 100, with higher scores representing lower levels of symptoms and higher levels of function and sports activity (Irrgang et al., 2001).

Subjects were equipped with a total of 20 retro-reflective skin markers (pelvis: 4, thigh: 8 and shank: 8) according to the Plug-in Gait[®] method (Davis III et al., 1991). Three pairs of biplanar radiographs (EOS Imaging, France) were acquired in three configurations for each subject (figure 4.7). First, a pair of radiograph was taken in the free-standing position. Then, two sequential pairs of radiographs at approximately 20° and 40° of knee flexion were acquired while each subject performed a quasi-static single-leg knee flexion. For the sake of

Biplanar X-ray data and 3D models

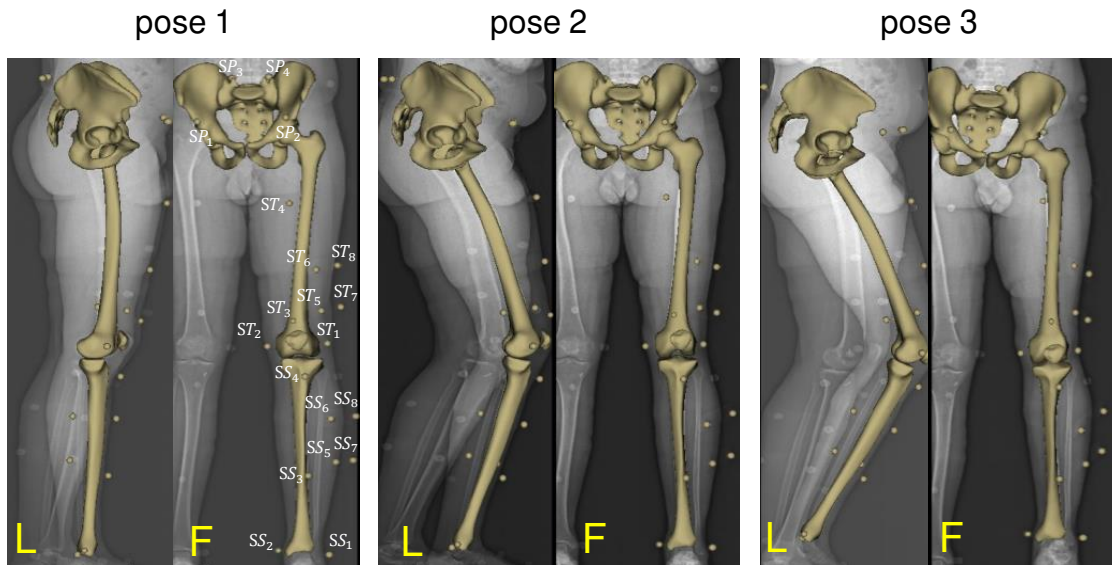


FIGURE 4.7: 3D digital models of the pelvis, femur and tibia and their respective skin adhered markers at positions: pose 1 (free-standing), pose 2 (20° knee flexion) and pose 3 (40° knee flexion) built from orthogonal radiographs. Marker nomenclature is shown at pose 1 for the pelvis: SP_1 to SP_4 , for the thigh ST_1 to ST_8 and for the shank: SS_1 and SS_8 . L: lateral and F: frontal view

clarity, three sequential postures will be hereafter termed as respectively pose 1, pose 2 and pose 3 for free-standing, 20° and 40° of knee flexion.

3D digital models of bones (pelvis, femur and tibia) were first obtained at free-standing position using a 3D reconstruction algorithm developed previously by (Chaibi et al., 2012) for the femur and tibia and (Mitton et al., 2006) for the pelvis. The 3D models were then projected on the frontal and lateral radiographs. The positions of the bony contours were manually adjusted until the contours exactly matched those of the radiographs at each pose. 3D locations of skin markers at each pose were also computed from biplanar radiographs using the same procedure. Anatomical reference (R_{anat}) frames for the femur and tibia was defined following the definition reported in (Schlatterer et al., 2009), and for the pelvis, in (Dubois, 2014). x , y and z axes of the R_{anat} frames are along antero-posterior, proximal-distal and medial-lateral direction respectively.

Quantification of STD

STD quantification on the pelvis, thigh and shank was performed based on two different schemes in line with the literature.

First, as a Soft Tissue Element (STE) deformation at each marker location as introduced in the previous section 4.1. The overall procedure is briefly explained and illustrated in figure 4.8.

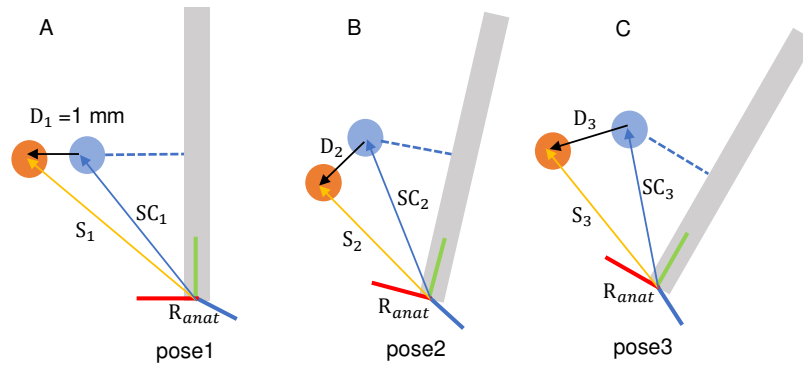


FIGURE 4.8: Scheme 1: Schematic representation of Soft Tissue Element (STE) deformation. Skin S_i ($i = 1, 2, 3$) and subcutaneous marker (SC_i) locations are expressed in bone R_{anat} frames in all the poses. Element deformations are presented as D_2 and D_3 between skin and subcutaneous marker at pose 2 and pose 3 respectively. Pose 1 corresponds to free-standing position. Shown only for a single marker.

3D position of the skin markers (S_i) in all the poses were first computed from the biplanar X-ray data and expressed in the respective bone R_{anat} frames. From the skin markers, a set of virtual markers referred to as subcutaneous markers (SC_i), were defined 1 mm beneath the skin marker following the methodology elaborated in section 4.1 and illustrated in figure 4.8(A). All the soft tissue deformation effect at the marker level is reported to the STE, which connects the S_i to the corresponding SC_i . The connection between the SC_i and the corresponding bone segment was assumed to be rigid. Due to the rigidity assumption, the locations of the subcutaneous markers in R_{anat} frame remained the same in all the poses ($SC_1 = SC_2 = SC_3$). Thus the absolute differences between skin and subcutaneous marker locations at pose 2 and pose 3 were computed and expressed in R_{anat} frames along x , y and z direction (figure 4.8(B) and 4.8(C)). Eventually, from the directional components, Euclidean distances were computed using equation 4.1.

$$D_{i+1}(dx_{i+1}, dy_{i+1}, dz_{i+1}) = \|S_{i+1} - SC_i\|; \quad i = 1, 2 \quad (4.1)$$

Second, STD was computed as a relative displacement of the skin markers at pose 2 and pose 3 with respect to pose 1 (reference pose) as illustrated in figure 4.9. From the directional components, Euclidean distances were computed using equation 4.2.

$$D_{i+1}(dx_{i+1}, dy_{i+1}, dz_{i+1}) = \|S_{i+1} - S_1\|; \quad i = 1, 2 \quad (4.2)$$

where S_i is the 3D location of the skin marker at pose i obtained from biplanar X-ray data and expressed in bone R_{anat} frames. D_{i+1} is the relative displacement of the skin markers at pose $(i+1)$.

STA quantification in both the schemes was performed using a customized MATLAB[®] routine (Mathworks, Massachusetts, United States).

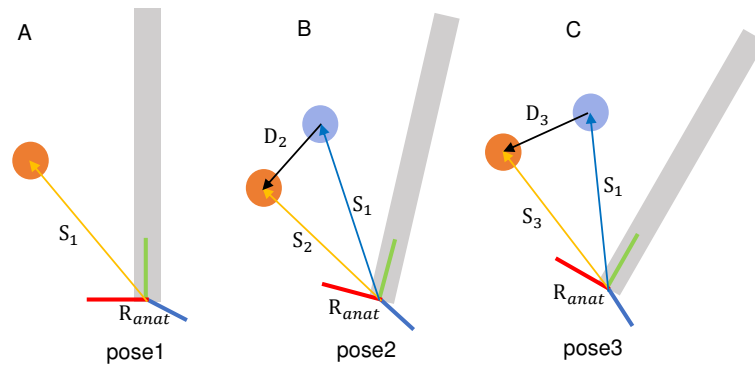


FIGURE 4.9: Scheme 2: STD as a skin marker relative displacement at pose 2 and pose 3 with respect to pose 1. Schematic representation of skin marker S_i ($i = 1, 2, 3$) locations expressed in bone R_{anat} frames in all the poses. Shown only for a single marker.

Statistical analysis

Statistical analysis on the collected data was performed using both the schemes to test 4 hypotheses.

STD is subject-specific: Deformation data at all marker locations were pooled together per subject per pose to check inter-individual similarity/variability.

STD is segment-specific: Deformation data for all the subjects and at all marker locations per segment per pose were pooled together to check inter-segment variability/similarity among pelvis, thigh and shank.

STD is location-specific: Deformation data for all the subjects per marker location per pose within a segment were pooled together to check inter-marker location variability/similarity within segments.

STD is direction-specific: Deformation component in a particular anatomical direction (x , y or z) per pose, for all the subjects and at all marker locations within a segment were pooled together to check if deformation is dependent on anatomical directions within segments.

Normality of the distributions were first assessed using the Shapiro-Wilk test. According to the outcomes of normality test, ANOVA or nonparametric Kruskal-Wallis (KW) test was performed to observe intergroup differences using the built-in MATLAB[®] functions. We also performed pairwise comparisons with Student t-test or nonparametric Man-Whitney U test (with Bonferroni's correction). For all the tests, the significance level was set to 0.05 (*) and 0.01 (**) *a priori*.

4.2.3 Results

Results obtained with both the schemes were similar, with mean differences between the schemes less than 1 mm (Appendix C). Therefore, the results of the statistical analysis are shown only for scheme 1, where deformation at each marker location is presented as STE deformation.

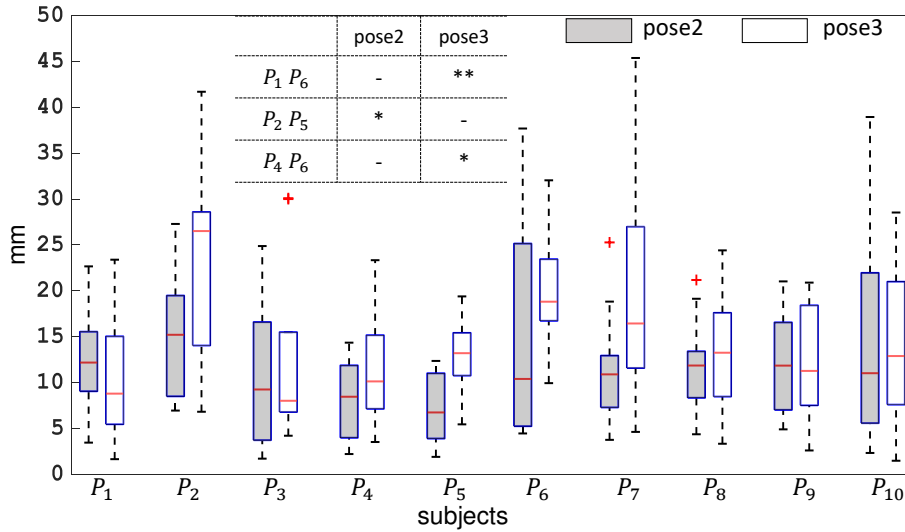


FIGURE 4.10: Boxplot for subject-specific STD presented at pose 2 and pose 3. P_1 to P_{10} are number of subjects. Only significant parameters are presented in the table.

Figure 4.10 illustrates STD (i.e., median, quartiles, minimum, maximum and outliers) per subject (P_1 to P_{10}) per pose. Results of the KW test showed, the null hypothesis that STD for each subject comes from the same distribution cannot be accepted ($p < 0.05$). The pairwise test showed that there is a significant difference in STD between subjects P_2 and P_5 at pose 2. Similarly, subjects P_1 and P_6 , and P_4 and P_6 displayed significantly dissimilar STD at pose 3 only. Subjects $P_1 - P_4$ and $P_7 - P_{10}$ showed inter-subject similarity among them. Overall, higher STD was observed for the subjects P_2 , P_6 and P_7 at pose 3, exhibiting maximum value up to 45 mm for P_7 .

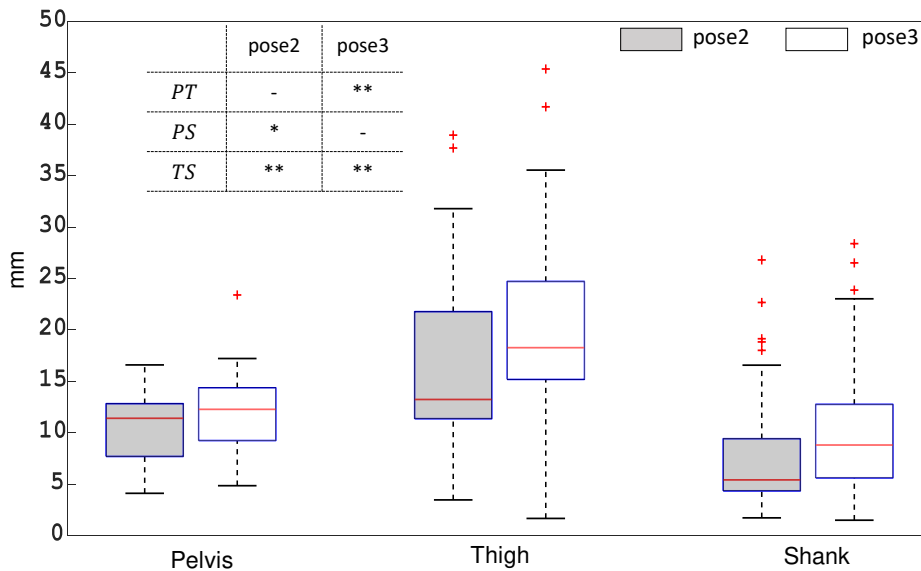


FIGURE 4.11: Boxplot for segment-specific STA presented at pose 2 and pose 3. Only significant parameters are presented in the table. P : Pelvis, T : Thigh and S : Shank.

Figure 4.11 represents STD per segment per pose for all the subjects. KW test revealed

that STD across all the segments was distinctly different ($p < 0.05$). Among the segments, STD for the thigh was observed significantly higher at both the poses with values (median) 13.5 mm and 18.5 respectively. Lowest STD (median: 5 mm) was observed for the shank at pose 2. STD at the pelvis was found around 13 mm (median). Few outliers were observed at both the poses, particularly for the thigh and shank.

Figure 4.12 depicts STD at each marker location (left column figures) and per anatomical direction (right column figures) within a segment. In the case of location-specific analysis, STD at each marker location of pelvis appeared similar ($p > 0.05$) for both the poses with values (median) within 11 mm to 13 mm. Similarly, for the shank, no significant difference in STD among different locations were seen ($p > 0.05$). For the thigh, only ST_1 and ST_4 displayed significantly dissimilar STD at both the poses, with the highest STD (median: 26 mm) for ST_4 and the lowest (median: 15 mm) for ST_1 at pose 3.

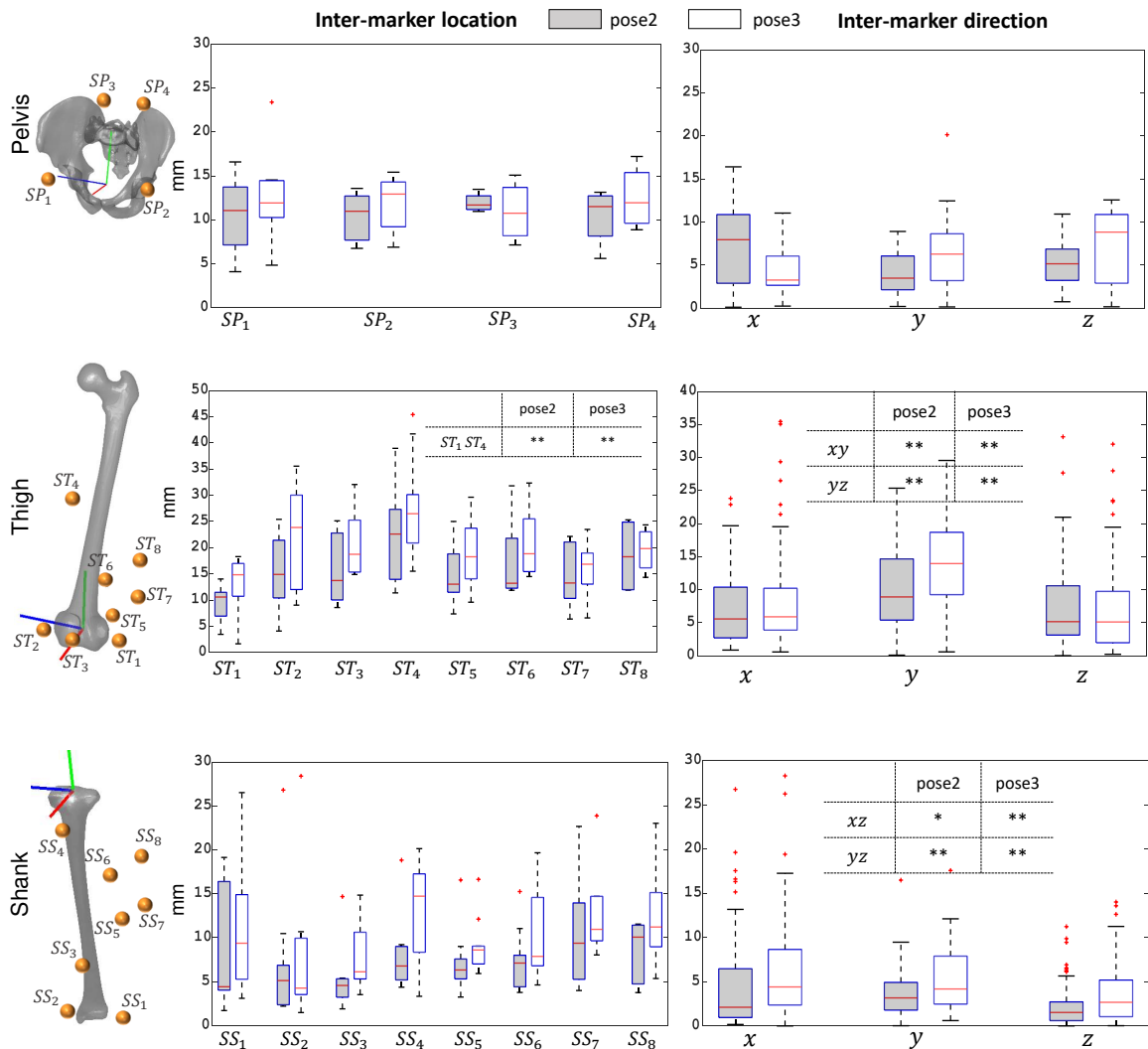


FIGURE 4.12: Boxplot for location-specific (left column) and direction-specific (right column) STD presented at pose 2 and pose 3 for the pelvis, thigh and shank. Only significant parameters are presented in the tables. Anatomical reference frames (R_{anat}) are also highlighted on the bone segments in different colours according to different axes. Green: proximal-distal direction, red: anter-posterior direction, blue: lateral-medial direction.

In the case of direction-specific analysis, a similar ($p>0.05$) STD was observed across the three anatomical directions of the pelvis R_{anat} frame. STD along proximal-distal direction of the thigh was observed distinctly higher in both the poses, while showing similar values along antero-posterior and lateral-medial direction. STD at the shank was appeared similar along antero-posterior and proximal-distal direction, while revealing significantly lower values along the medial-lateral direction. Overall analysis showed higher STD at pose 3 as compared to pose 2.

4.2.4 Discussion

In order to compensate for STA and to interpret SM-based motion analysis data, knowledge of Soft Tissue Deformation (STD) pattern in three dimension (3D) is essential. Yet, there is a paucity of reference data in the literature comprehensively showing variability of STD among individuals, segments, marker locations and along the three anatomical directions. The purpose of this study was to quantify STD in 3D at the pelvis, thigh and shank for 10 subjects. Two schemes were employed to quantify STD, although exhibited similar results.

The rationale behind employing two schemes is that both of them may serve two different communities; first, those particularly deal with compensation methods, and second those deal with STD quantification. The first scheme intends to address conventional STA compensation methods (such as MBO) that generally minimizes measured and model determined marker position. The subcutaneous markers are analogous to the model determined markers. This approach could also be helpful for FE-based STA compensation method, where a deformable element connecting the skin and subcutaneous marker accounts for all soft tissue deformation (as detailed in section 4.1). The second scheme pertains to STD quantification methods, where soft tissue deformation is considered as a relative displacement of skin markers at different poses with respect to the reference pose.

Overall, soft tissue deformation displayed inter-subject similarity in most of the subjects showing a similar STD pattern. Although such observation is in contrast to the current prevailing idea of STD as subject-specific, yet found in accordance with one study which explained overshadowing of similarity by dissimilarity for few subjects (Gao and Zheng, 2008). Secondly, segment-specific STD was observed exhibiting the highest deformation at the thigh followed by the pelvis and the shank (Akbarshahi et al., 2010; Walker, 2015). A similar observation was also reported in studies that measured higher kinematic error at the thigh (Sangeux et al., 2006; Stagni et al., 2005).

STD at the pelvis and shank exhibited no inter-marker variability. For the thigh, the marker (ST_4) placed towards the hip joint showed significantly higher STD, where muscle thickness is higher (Rouhandeh and Joslin, 2018). Except ST_4 , other markers at the displayed similar STD.

STA occurred in all the three directions of the bone embedded anatomical frames, however not uniform for the thigh and shank in particular. Soft tissue deformation in proximal-distal direction of the thigh and shank was distinctly higher. This is probably due to the

orientation of the muscular structure of the thigh and shank, which contracts and relaxes during movement along its length. Deformation in the medial-lateral direction was noticed the lowest. A similar observation was also reported in the literature (Gao and Zheng, 2008).

This study, to the authors' knowledge, is the second attempt to use EOS low dose system, allowing to quantify STD in 3D. Previously, our group used EOS to investigate motion of lower limb attachment systems with respect to the underlying bone (Südhoff et al., 2007). It is to be noted that because of the limited acquisition volume within the EOS, markers present in the radiographs were not consistent throughout the subjects. Few markers couldn't be located in the radiographs of some subjects either in the orthogonal views or in the consecutive poses. Moreover, both due to limited acquisition volume and ethical reasons, the number of poses had to be limited. Also, we acknowledge that STD reported in this study doesn't include inertial effects, as the movement under consideration was quasi-static. Quantified STD is a consequence of both muscle contraction and skin sliding. Currently, other existing methods, such as invasive attachments and fluoroscopic measurements, have been shown useful to quantify soft tissue deformation. But, invasive methods are prone to alter free soft tissue movement and therefore, may impact its results. Fluoroscopy is also not effective for capturing the entire lower limb, although efficient for local observations in dynamics. Hence, EOS in conjunction with skin markers can serve as a gold standard to locate actual bone positions as well to quantify STD for a limited range of motion.

The findings in the study may open up effective STA compensation strategies for SM-based motion analysis. Instead of assigning arbitrary STA correction stiffness, subjects with similar STD patterns can be grouped together to assign the same correction stiffness. Moreover, for such quasi-static activities, all the markers at the pelvis can be grouped together to assign the same stiffness values. Similar is the case for the shank. For the thigh, marker locations where STD was observed highest can be assigned with the lowest stiffness and vice versa. To be noted that while assigning stiffness values for the thigh and shank, different stiffness values need to be defined along different anatomical direction. In conclusion, although the STD data provided in this study may be beneficial for future STA compensation approaches, further study would be required in different dynamic activities.

Chapter 5

Clinical application: Preliminary investigation

The contribution in the previous chapter allowed to develop and evaluate a novel FE-based approach for soft tissue artifact (STA) compensation of the lower limb (first section). The STA compensated kinematics revealed that the personalized FE models (geometry and boundary condition) could effectively compensate for STA, although direct validation was not possible. This work further led to proposing an effective STA compensation strategy that would allow personalizing soft tissue stiffness properties based on experimentally acquired soft tissue deformation pattern (second section).

It is noteworthy to mention that the personalization of the FE models was based on the morphology of healthy population. Given the effectiveness of the model for STA compensation, it is also essential to develop and evaluate models replicating patients' morphology, which may eventually lead to investigation of various surgical scenarios and outcomes. In that direction, this chapter briefly describes a preliminary investigation on the utility of the biplanar X-ray system in evaluating Total Knee Arthroplasty (TKA) implant alignment.

5.1 Utility of EOS system in evaluating TKA implant pose¹

Abstract Total knee Arthroplasty (TKA) is a frequently performed surgical procedure in terminal stage osteoarthritis (OA). However, patients still remain dissatisfied because of either patient related factors (e.g., age, health) or surgical factors (e.g., implant design, alignment) leading to a revised TKA. Out of several factors affecting functional outcome of TKA, implant alignment is considered as a major contributor. To preoperatively plan for TKA implantation, surgeons normally use CT-scan images to align the implant components with respect to the 3D alignment of femur and tibia. There are several standard alignment options available, from which a surgeon chooses one based on subjective assessment. However, there is no complete agreement on a particular procedure that can provide better functional outcome and implant survivorship. It is now well known that apart from low dose irradiation, biplanar X-ray imaging allows image acquisition in weight-bearing positions unlike CT scans. This facility could be advantageous in the sense that patients' position may significantly impact lower limb alignment and thereby may affect the implant alignment process. In this regard, biplanar X-ray may ease the process of implant alignment as it is routinely used in clinics. The objective of this study is therefore to evaluate the utility of the biplanar X-ray system in evaluating TKA implant alignment. In a first step, reproducibility of the TKA implant alignment process is evaluated in the current contribution.

12 patients operated with TKA were included in the study. All subjects underwent biplanar radiography postoperatively and digital models of the implants were manually positioned on the postoperative radiographs. The process was performed by 3 operators and inter operator reproducibility study was carried out on 3 rotational and 3 translation parameters following the guidelines of the ISO 5725-2 standard.

Reproducibility of manual positioning for translation was less than 1 mm for both the implant components. For rotational parameters, less than or equal to 1.5° was observed for the femoral component while revealing less than 3° for the tibial component. Overall, EOS imaging system showed a good reproducibility for evaluating knee prosthesis position. This study may contribute to further investigation of global alignment of the TKA implant with respect to both lower limb and upper limb skeleton in order to provide an effective surgery planning.

Keywords: Biplanar X-ray, TKA implant alignment, surgery planning

5.1.1 Introduction

To regain functional mobility and relieve pain, Total Knee Arthroplasty (TKA) is often recommended at the later stage of Osteoarthritis (OA). An increase in 33% (more than 80000) TKA cases were registered in the period 2008-2013 in France (Colas et al., 2016). In the United States, it is expected to surpass 3 million TKA cases by the year 2030, with a hospital cost of more than 2 billion dollars (Kurtz et al., 2007). With such increase in trends, number of dissatisfied patients have been rising accordingly. Two studies reported that up to 20% of the patients experienced sub-optimal satisfaction 1 year postoperatively, and 30-34% of

¹Potential copyright issues with direct reuse of the article including figures and contents (article under preparation)

patients suffered pain in 3 months to 5 years post TKA (Beswick et al., 2012; Bourne et al., 2010).

The source of patient dissatisfaction and survival of TKA implant is highly variable. A part of the source is often attributed to patient related factors such as age and general health status, whereas the other part constitutes mainly surgical factors such as, implant design and alignment (Choong, Dowsey, and Stoney, 2009). Even with the technically sound implant design and alignment, outcome may vary patient to patient because of patient-specific variabilities in joint loading, soft tissue properties and muscle strength (Fitzpatrick, Clary, and Rullkoetter, 2012). One study also found that patient dissatisfaction is also related to neuromotor deficits, which could be a result of injury to the joint capsule and loss of cruciate ligaments during surgery (Ardestani et al., 2017).

Among the several reasons, implant malalignment has been reported as a major reason for revision in 7% of revised TKA (Schroer et al., 2013). Implant malposition causes increased mechanical loads at the prosthesis leading to accelerated polyethylene wear and laxation of the implant, which eventually results in decreased implant survivorship (Ritter et al., 1996).

Several investigators asserted the use radiological approaches to assess the alignment of implants in regards to the bone. To increase implant survival, one popular principle is to position the implant components by aligning to the mechanical axis of the knee joint within $180\pm 3^\circ$ (Jeffery, Morris, and Denham, 1991). Other studies also recommended to place the femoral component in 2-8° coronal valgus to femoral anatomical axis, and tibial component in neutral coronal alignment (Ritter et al., 2011; Kim et al., 2014). Overall, there is a large variety of alignment methodologies can be observed. Although different methods are in use, but there is little convincing evidence that these techniques improve function and patient experience (Sodhi et al., 2018).

Biplanar low dose X-Ray system (EOS[®], EOS-imaging, France) is frequently used in pre-operative planning and postoperative monitoring of patients (Melhem et al., 2016). It allows fast and simultaneous acquisition of antero-posterior and lateral images of the whole body with no projection bias and less radiation (Radtke et al., 2010). From the calibrated images, 3D surface reconstruction of the bones can be achieved with a precision comparable to CT (Chaibi et al., 2012; Girinon, Rouch, and Skalli, 2018). In clinical perspective, such 3D models may particularly help clinicians to examine bone alignment in weight bearing position and to properly plan implant positioning. In this context, our group had previously showed the usability of EOS system to evaluate precision of implemented skeletal landmark for TKA implantations (Schlatterer et al., 2009).

In modeling perspective, to develop subject-specific FE models of the TKA implanted knee, proper positioning of the implant is essential so as to avoid artificial malalignment of the implant during modeling. Any artificial misalignment or deviation from the actual implant position can manifest erroneous outcomes and attributing such outcome to surgical malalignment would be misleading.

The objective of this current study was therefore to evaluate the reproducibility of TKA implants positioning using EOS imaging system.

5.1.2 Materials and methods

Population

Twelve adult patients (gender: 4 men and 8 women, age range: 58-70 years, height range: 1.7-1.8 m) underwent TKA implantation operated by a senior orthopaedic surgeon at the hôpital Salpêtrière in Paris. Out of 12 patients, 1 patient underwent TKA implantation at both the knees resulting a total of 13 knee implants (5 for left knee and 8 for the right knee). A subvastus¹ approach was used with dependent tibial and femoral bone cuts. The prosthesis used was the FHK[®] model (FH Orthopedics, France), a posterior stabilized prosthesis with a fixed Polyethylene (PE) plateau. Postoperative frontal and lateral radiographs of the lower limb was acquired with EOS[®] system in a calibrated environment.

TKA implant alignment

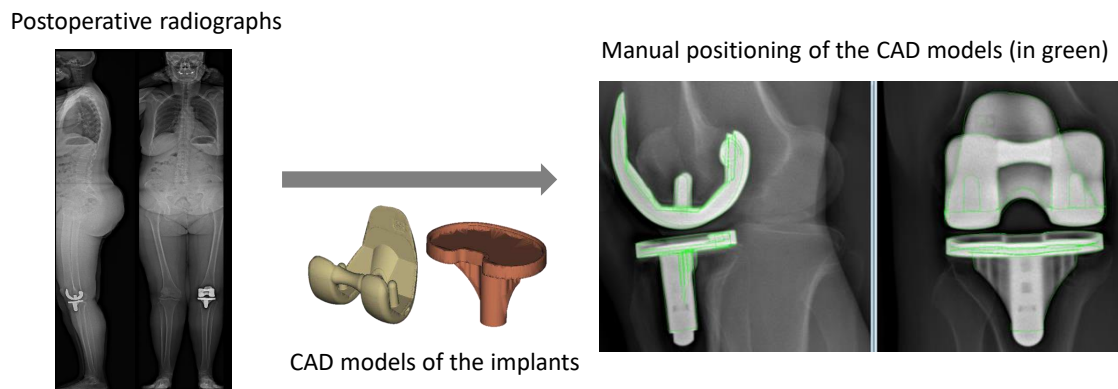


FIGURE 5.1: Superposition of the digital CAD models (in green) on corresponding postoperative radiographs

There are seven variants of the prosthesis of different sizes for both the femur and tibia. For each patient, the corresponding femoral and tibial digital CAD models were first imported onto post-op radiographs using an in-house lab developed software. The CAD models of the prosthesis were then manually positioned on the anteroposterior (AP) and lateral views, such that geometric contours of the prosthesis superimposed to the radio-opaque edges of the prosthesis already existing in the radiographs (figure 5.1). Once the 3D models of the prosthesis sufficiently confirm the radiographs, they were exported so that their position and orientation retained for the reproducibility study.

¹a quadriceps sparing technique, where the capsule below the quad muscle is divided allowing the extensor mechanism to be displaced providing exposure of the knee joint for the replacement operation.

Inter-operator reproducibility study of implant alignment

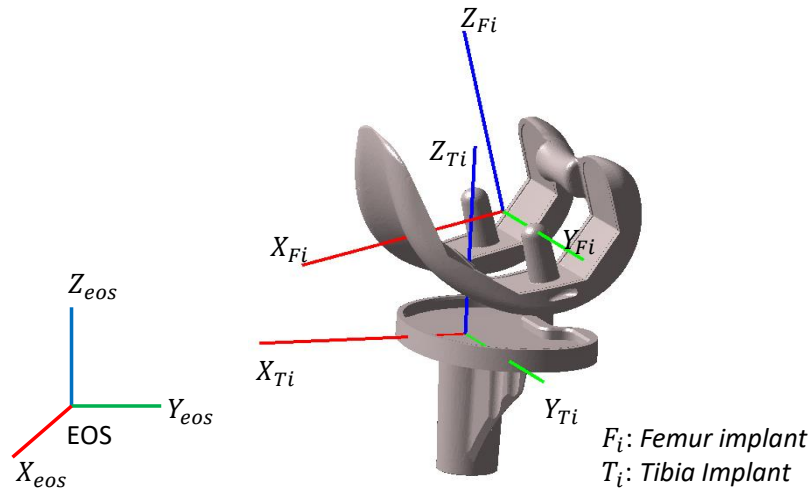


FIGURE 5.2: Definition of implant CSYS for the femoral and tibial component

For each knee, implant alignment was performed twice by 3 different operators: 1 qualified (surgeon) and 2 engineers. Inter operator reproducibility study was carried out on 3 rotational (R_x , R_y and R_z) and 3 translation (T_x , T_y , T_z) parameters following the guidelines of the ISO 5725-2 standard. The rotational and translation parameters were computed based on the coordinate systems (CSYS) of the femoral and tibial components. This was done by computing 3D angles and translations of both the implant models with respect to the global EOS CSYS. The three rotational parameters characterized the successive rotations according to Cardan sequence $YZ'X''$. The procedure for defining implant CSYS for the femoral and tibial component is adopted from (Schlatterer et al., 2009) as pictorially presented in figure 5.2 (detailed in Appendix D). The X-axis is directed anteriorly, Y-axis medially and Z-axis proximally for both the components.

5.1.3 Results

Inter-operator reproducibility of implant alignment on post operative biplanar radiographs are summarized in table 5.1 and pictorially illustrated in figures 5.3 and 5.4.

For the femoral component, 95% CI of rotational parameters (R_x , R_y and R_z) are less than or equal to 1.5° and for the translation (T_x , T_y , T_z) less than 1 mm.

For the tibial component, 95% CI of rotational parameters (R_x , R_y and R_z) are less than 3° and for the translation (T_x , T_y , T_z) less than 1 mm.

5.1.4 Discussion

The objective of the current study was to assess inter-operator reproducibility of TKA implant alignment on postoperative radiographs. Alignment was performed by 3 operators for 13 TKA implants. Reproducibility for the translation parameters was highly satisfactory for

TABLE 5.1: Inter-operator reproducibility of TKA implant within 95% confidence interval

Implant	Rotation (95% CI)			Translation (95% CI)		
	Rx	Ry	Rz	Tx	Ty	Tz
Femoral component	1°	1.7°	1.5°	0.5 mm	0.6 mm	0.5 mm
Tibial component	0.9°	1.3°	2.9°	0.5 mm	0.7 mm	0.5 mm

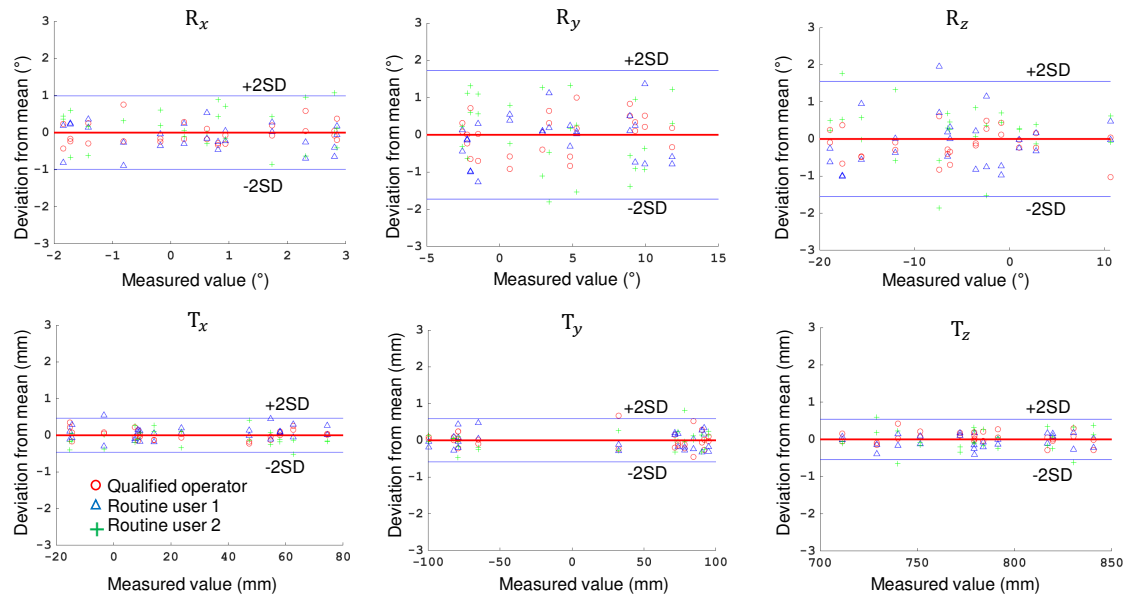


FIGURE 5.3: Bland-Altman plots representing 95% CI values for the femoral component

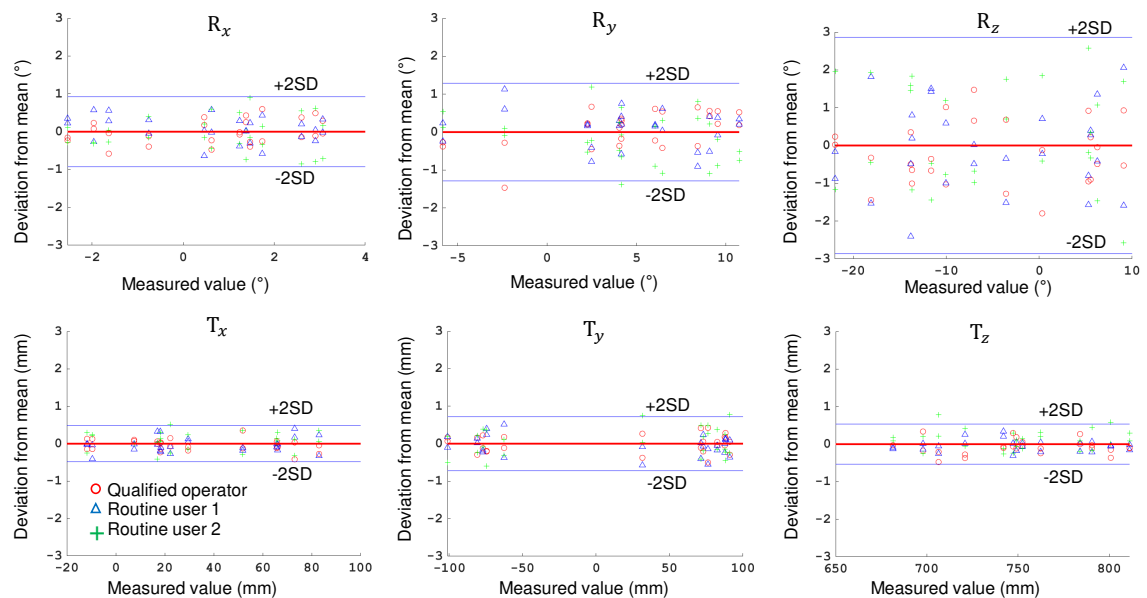


FIGURE 5.4: Bland-Altman plots representing 95% CI values for the tibial component

both the femoral and tibial implants (error less than 1 mm within 95% CI). For the rotational parameters, 95% CI values were less than 2° for femoral component in all the directions.

For the tibial component, more variation can be observed up to 2.9° , particularly about the Z-axis, which represents rotation in the axial plane.

The reproducibility achieved on the postoperative radiographs are comparable to the study of (Schlatterer et al., 2009), who performed alignment of the TKA using the bony landmarks of the preoperative radiographs. The methodology they implemented was advantageous to select the skeletal landmarks as the preoperative radiographs do not contain any bone cuts. Nevertheless, the reproducibility obtained in our study is in agreement with them who reported less than less than 3° (95% CI) for the rotational parameters and less than 1 mm (95% CI) for the translation parameters. Another study evaluated the reliability of implant adjustment on the radiographs, which reported mean error less than 1° and a maximum error of 1.1° (Langlois, 2003). Overall, the EOS system and the in-house lab developed software for 3D reconstruction and implant readjustment can be considered highly reliable.

Such high degree of reproducibility will be advantageous for building personalized FE models representing patients with TKA and to evaluate implant performance post-surgery. This will open further opportunities to study the effect of different implant alignment methodologies on the implant performance by observing passive response. Nevertheless, further studies will be necessary to correlate implant orientations with those of the bone segments such as mechanical or anatomical axis of the knee joint.

General conclusion and perspectives

The musculoskeletal (MSK) system of the lower limb, the knee joint in particular, is a complex system constituting bony structures, cartilages, ligaments, muscles and other connective tissues. It has a fundamental role to support the weight of the body and to produce controlled and precise movement by inter-dependently coordinating among the constituents. Repeated activities of daily life or any high impact exertion can inflict aberrant loads in the joint, causing injuries to the bones and other soft tissues. Such mechanical burden disturbs the overall stability of the entire limb and can further introduce joint degeneration (e.g., osteoarthritis), leading to partial or complete loss of functional activities.

In the clinical context, we observed that to restore the stability and mobility of the system, various surgical management methods have been traditionally performed depending on the degree of severity. One of the widespread surgical procedures for end-stage osteoarthritis is Total Knee Arthroplasty (TKA). To perform TKA implantation, clinicians mostly prefer geometric alignment techniques based on radiographic images as a preoperative planning. Although implant positioning procedure has been improved with advanced surgical tools, there is no complete unanimity on a particular method that works the best, and the implant is still likely to fail under abnormal mechanical loads. As the knee joint elements do not inherently function in isolation, understanding their interaction and their influence at the joint seems logical for better surgical planning. In this aspect, we observed that personalized FE modeling could be a promising avenue for assessing patient-specific joint mechanics for different treatment scenarios. It was also apparent that to assess functional outcomes after surgical intervention, assessing the knee joint under *in vivo* loading conditions is crucial. Further, we observed the importance of gait analysis to feed physiological boundary conditions to the models. While prescribing physiological loading conditions in the models based on skin marker-based motion data, the most prominent source of error in estimating joint kinematics appeared as soft tissue artifact (STA). Such conclusions on broader clinical context led to study relevant literature on FE modeling strategies, gait analysis and associated musculoskeletal models, and various STA compensation strategies in the context of current challenges and opportunities.

In the literature, a large body of work on FE models, FE-MSK models could be seen to estimate various quantities of interests that cannot be easily obtained with experimental studies. Nevertheless, numerous challenges appeared in the model development and evaluation approaches. One of the critical challenges we observed was obtaining fast and accurate

finite element mesh from medical images. Another prominent challenge appeared as adopting a computationally inexpensive approach for subject-specific FE model development and validation focusing on personalized geometry and ligament material properties. The third key challenge was devising an effective STA compensation strategy. Owing to such hurdles, translating models to clinically relevant tools remains a major bottleneck, and therefore the existing models could hardly be seen used in routine clinics. This motivated the need for developing a FE-MSK modeling framework by taking the aforementioned challenges into account.

Based on the identified challenges, the first phase of the thesis focused on fast subject-specific finite element mesh generation of the knee joint from biplanar X-ray images. This study enabled to generate hexahedral mesh for the femur, tibia and patella from the 3D reconstruction of 11 cadaveric specimens. The whole procedure from 3D reconstruction to mesh generation took 12 minutes of computational time per specimen. Mesh quality and surface representation accuracy were highly satisfactory. This contribution paved the way to reliably investigate inter-individual variability of the knee joint passive elements and its effect on joint kinematics.

In estimating subject-specific knee joint kinematics under passive flexion, this study confronted a significant challenge of personalizing soft-tissue properties, particularly the ligaments. As the existing optimization approaches are computationally expensive, a new procedure to estimate specimen-specific ligament material property (prestrain) was proposed and evaluated on 6 cadaveric specimens. Subject- and ligament-specific prestrain values were directly computed from the experimental study and implemented in the corresponding FE models to estimate joint kinematics. Subject-specific model evaluation was performed by comparing predicted femorotibial kinematics with the *in vitro* response of the corresponding specimens. The experimental-numerical agreement was found highly satisfactory and in-line with the literature. *In vitro* validation of the FE models served as an intermediate step necessary for further transforming the model towards *in vivo* loads. This contribution opened up gateways to use simplified yet relevant model development strategies towards personalized FE modeling.

The second phase of the PhD focused on development and evaluation of a novel FE-based STA compensation approach. In this context, a conceptual FE model of the lower limb was proposed to showcase the model's capability to minimize STA. The model was implemented on 66 subjects, and the results of the personalized FE models revealed promising and in agreement with the literature. The model's unique feature was its versatility to take subject-, task-, and marker location-specific soft tissue deformation into account, thus emphasizing the need for a proper understanding of soft tissue deformation at different marker locations so as to facilitate better compensation strategies.

Therefore, in a continuation of the aforementioned work, experimental quantification of soft tissue deformation was performed using biplanar imaging. This contribution enhanced

the knowledge of the distribution of soft tissue deformation among individuals and different marker locations. When integrated into the STA compensation scheme, such insightful information on soft tissue deformation may provide more reliable and clinically relevant results.

The third phase of the thesis was dedicated to clinical application, in which utility of the biplanar X-ray system in positioning the Total Knee Arthroplasty (TKA) implant was briefly explored. The implemented methodology, although manual, was found highly reproducible. This contribution opened ways to develop subject-specific knee joints FE models with TKA implants and study how implant alignment influences joint mechanics. In a step forward, the interaction of the implant with other elements of the knee joint during daily activities can be studied.

In conclusion, the objectives undertaken during the PhD appeared to be necessary for developing a comprehensive framework of FE-MSK modeling. Nevertheless, to develop a full-fledged FE-MSK model, integrating muscles to the existing model is essential to drive the model with actuated muscles following the pipeline of inverse and forward dynamics. In that direction future work will be necessary and the framework developed for the FE-MSK modeling in the current study will provide a strong base.

Appendix A

Sources of errors in gait analysis

Only the first two sources of errors are described here, as because the third source of error (STA) is explained in the main text elaborately.

The *instrumental error* arises as a result of instrumental noise and volume calibration inaccuracies. Using different filtering methods, number of cameras, and volume calibration algorithms, contribution of this error to the total error can substantially be decreased and often considered negligible (Surer and Kose, 2011).

The second source of error arises from difficulty in placing the markers accurately in regards to specific anatomical landmarks. This needs proper expertise, and at many times the landmarks are not easily palpable for patients with musculoskeletal disorders and even for healthy subjects with excessive soft tissues. For instance, conventional gait models (CGM) establish the medial-lateral axis of the knee based on markers placed on medial and lateral epicondyles, or sometimes from the position of knee alignment devices (KAD) (Davis and DeLuca, 1996). Any discrepancy between marker position and bony landmarks eventually leads to erroneous estimation of joint centers and other kinematic parameters. Both functional and predictive methods have been proposed to circumvent this problem. Functional methods aim at the estimation of subject-specific joint centers/axes by using movement data of adjacent segments relative to marker cluster motion. Conversely, predictive methods (regression-based approaches) have been recommended in situations when the range of motion is restricted, particularly for patients with cerebral palsy (Assi et al., 2016). Nevertheless, accuracy of both the approaches been greatly enhanced by the use biplanar X-ray system (EOS, EOS imaging, France), as it allows accurate static calibration between bones and skin markers at patient's standing position (Assi et al., 2016; Pillet et al., 2014; Sauret et al., 2016). Using 3D reconstructions acquired from biplanar images, an average accuracy of 2.9 mm was achieved (Pillet et al., 2014) in comparison to non-image-based methods reporting 13 mm to 30 mm of accuracy in locating hip joint center (Sangeux, Peters, and Baker, 2011). With such advancement in techniques and medical imaging facilities, this source of error has been substantially reduced.

Appendix B

Various TKA alignment state-of-the-art approaches

Table B.1 presents an overview of some of the mostly used state-of-the-art approaches for TKA implant alignment and current controversies.

Amount of corrections for osteotomy, optimal implant size and type, and alignment of implant components are important surgical factors that a clinician must determine for a successful surgery. Normally, two main types of implants: constrained (or hinged) and unconstrained are used (Lemaire and Witvoet, 2002). Constrained implants are used for patients with damaged ligaments, where the femur and the tibial components are linked together with a hinge mechanism. Unconstrained implants offer nearly physiological movements (e.g., varus/valgus and internal/external rotation). Depending on the type and size of the implant, preoperative assessment of the knee in the three spatial planes is normally performed for successful implant positioning.

One popular principle is to position the implant components by aligning to the mechanical axis of the knee joint within $180\pm 3^\circ$ (Jeffery, Morris, and Denham, 1991). For mechanical alignment of the femur, normally intramedullary (IM) guide is used, yet there is controversy between intramedullary and extramedullary (EM) methods for the tibial alignment (Bansal et al., 2020). One study found IM guide to be more accurate on 103 primary TKA cases (Cashman et al., 2011), whereas comparable results were obtained between those two techniques by another study performed on 350 TKA (Zeng et al., 2015). Nevertheless, all these studies considered mechanical alignment as a gold standard. Conversely, no association between mechanical alignment and implant survival was observed in a study on 398 primary TKA cases (Parratte et al., 2010). Another study also recommended anatomical alignment of implants, which reported better implant durability for 3048 primary cases (Kim et al., 2014). The concept of mechanical alignment has also been challenged by another study (Howell et al., 2001). This study observed encouraging implant survivorship (up to 10 years) and functional outcomes on kinematically aligned knees performed on 220 cases. Moreover, studies based on kinematic alignment claimed that it can restore native knee alignment by aligning rotational axes of the implant components to the kinematic axes of the knee joint (Dossett et al., 2014). Patient specific instrumentation (PSI) has also been recently used as

Appendix B. Various TKA alignment state-of-the-art approaches

TABLE B.1: Non-exhaustive synthesis of mostly used TKA implantation methods and outcomes

Author, year	Objective (cases)	Methodology	Assessment criteria	Remarks
Parratte et al., 2010	To evaluate if mechanical limb alignment can improve implant survival (398 primary TKA cases)	Mechanical alignment	Radiographic limb alignment	- No association between mechanical malalignment and implant survivorship
Cashman et al., 2011	To evaluate alignment accuracy of correct tibial positioning (103 primary TKA cases)	Mechanical alignment through Intramedullary (IM) and Extramedullary (EM) technique	Radiographs and WOMAC score	- IM guide is more accurate - Mechanical alignment serves as gold standard
Kim et al., 2014	To evaluate relationship between postoperative anatomical alignment and implant survival (3048 primary TKA cases)	Anatomical alignment	Radiographs	- Overall knee anatomic alignment at 3-3.7° varus is necessary
Yaffe et al., 2014	To evaluate clinical, functional and radiographic outcomes for TKA performed with patient specific instrumentation (122 TKA cases)	Patient specific instrumentation	Knee Society Functional Score	- Patient specific instrumentation improved component positioning
Zeng et al., 2015	To evaluate accuracy of correct tibial positioning (350 primary TKA cases)	Mechanical alignment through Intramedullary (IM) and Extramedullary (EM) technique	Radiographic limb alignment	- Accuracy of IM and EM are comparable. - Use of IM results in less time
Zhu et al., 2015	Evaluation of clinical and functional outcomes for TKA performed with patients specific instrumentation (90 TKA cases)	Patient specific instrumentation	Oxford Knee Score, Knee Society Function Score	- No significant difference in outcomes performed with patient specific instrumentation and conventional instrumentation
Howell et al., 2018	To evaluate if varus alignment adversely affect implant survival (222 primary TKA cases)	Kinematic alignment	Radiographs and WOMAC score	- Kinematically aligned knee restores natural alignment of limb - Recommends kinematic alignment as an alternative
Bansal et al., 2020	To evaluate functional and radiological outcome (400 primary TKA cases)	Mechanical alignment through Intramedullary (IM) and Extramedullary (EM) technique	Radiographs and Oxford knee score	- Less accuracy for tibial alignment for EM - Mechanical alignment still serves as gold standard
Fuji et al., 2020	Comparative study of weight bearing and non-weight bearing alignment	Knee alignment in supine position and weight bearing position	Radiographs	- Patient position significantly effects lower limb alignment

a modern technique to facilitate proper implantation (Yaffe et al., 2014; Zhu et al., 2017). This technique uses customized cutting blocks generated from 3D models of the preoperative images to avoid errors in alignment and planning. It also facilitates the surgeon to preoperatively adjust the depth of cut and, coronal and rotational orientation of the resection. Using this technique, (Yaffe et al., 2014) observed improvement in implant positioning and functional outcome 6 months after surgery in comparison to standard TKA. On the

other hand, no significant improvement in clinical and functional outcome was found between PSI and standard instrumentation in another study (Zhu et al., [2017](#)). Patient position was also found to have significant influence on alignment accuracy, reporting differences in alignment between weight bearing and supine position (Fujii et al., [2020](#)).

Appendix C

Soft Tissue Deformation (STD) with both the schemes

C.0.1 Scheme1

TABLE C.1: STD at pose 2 and pose 3 presented as Mean \pm 1SD at each marker location and along x, y and z direction of R_{anat} frame

Segment	Marker	Pose2			Pose3		
		x	y	z	x	y	z
Pelvis	SP1	7.9 \pm 6.1	2.2 \pm 2.1	4.3 \pm 2.9	3.8 \pm 1.8	7.1 \pm 6.5	8.9 \pm 3.3
	SP2	5.6 \pm 3.5	5.2 \pm 2.5	5.9 \pm 1.6	3.6 \pm 2.3	6.4 \pm 4.2	7.6 \pm 4.2
	SP3	8.5 \pm 5.5	4.3 \pm 1.6	5.9 \pm 2.9	6.9 \pm 4.4	5.9 \pm 2.8	4.6 \pm 4.1
	SP4	7.8 \pm 4.3	4.7 \pm 2.1	4.5 \pm 4.3	6.7 \pm 5.5	6.2 \pm 2.9	6.7 \pm 5.7
Thigh	ST1	4.6 \pm 2.7	7.1 \pm 3.3	2.4 \pm 2.1	7.5 \pm 4.5	9.9 \pm 4.7	1.6 \pm 1.3
	ST2	13.2 \pm 7.1	3.6 \pm 2.6	5.9 \pm 3.1	20.0 \pm 10.4	5.4 \pm 4.1	6.3 \pm 2.3
	ST3	3.4 \pm 2.2	11.0 \pm 6.0	9.8 \pm 5.6	7.3 \pm 8.2	16.7 \pm 4.2	5.2 \pm 3.9
	ST4	4.3 \pm 3.6	13.7 \pm 6.4	17.0 \pm 8.9	7.2 \pm 5.2	18.1 \pm 6.8	17.8 \pm 8.6
	ST5	5.4 \pm 3.6	11.4 \pm 5.4	7.3 \pm 3.4	3.3 \pm 1.7	16.8 \pm 5.6	6.2 \pm 6.2
	ST6	7.7 \pm 4.8	11.9 \pm 5.8	8.2 \pm 6.8	7.1 \pm 4.3	16.5 \pm 5.4	8.5 \pm 6.2
	ST7	8.7 \pm 4.6	11.8 \pm 5.4	1.5 \pm 1.3	5.0 \pm 2.4	14.2 \pm 6.9	2.6 \pm 3.0
	ST8	11.6 \pm 7.5	13.8 \pm 4.2	2.4 \pm 1.5	6.9 \pm 3.8	17.0 \pm 3.4	4.5 \pm 5.2
Shank	SS1	6.8 \pm 6.8	2.9 \pm 1.6	4.1 \pm 3.7	8.1 \pm 7.5	5.1 \pm 2.7	2.9 \pm 2.0
	SS2	5.0 \pm 7.9	1.9 \pm 2.1	1.6 \pm 1.6	6.6 \pm 8.2	1.9 \pm 1.0	1.8 \pm 1.8
	SS3	3.3 \pm 4.5	2.9 \pm 1.5	1.5 \pm 2.0	4.7 \pm 4.4	4.0 \pm 1.6	4.0 \pm 1.8
	SS4	1.6 \pm 2.2	6.7 \pm 4.7	4.0 \pm 1.6	3.5 \pm 2.9	8.0 \pm 4.9	8.0 \pm 5.1
	SS5	4.2 \pm 5.0	3.7 \pm 1.7	1.8 \pm 2.4	6.4 \pm 3.2	4.8 \pm 3.1	2.7 \pm 1.9
	SS6	5.1 \pm 4.9	3.3 \pm 2.1	1.5 \pm 1.2	6.3 \pm 5.5	4.5 \pm 3.1	4.5 \pm 4.2
	SS7	6.4 \pm 7.4	4.9 \pm 3.1	4.1 \pm 4.6	6.9 \pm 5.7	8.5 \pm 3.9	4.8 \pm 3.2
	SS8	4.0 \pm 4.4	5.8 \pm 2.9	2.5 \pm 2.6	5.4 \pm 8.1	9.9 \pm 3.0	1.5 \pm 0.9

C.0.2 Scheme2

TABLE C.2: STD at pose 2 and pose 3 presented as Mean \pm 1SD at each marker location and along x, y and z direction of R_{anat} frame

Segment	Marker	Pose2			Pose3		
		x	y	z	x	y	z
Pelvis	SP1	7.7 \pm 6.0	2.2 \pm 1.9	4.3 \pm 2.9	3.5 \pm 2.1	7.3 \pm 6.6	8.9 \pm 3.3
	SP2	5.6 \pm 3.3	5.8 \pm 2.4	6.0 \pm 1.5	3.5 \pm 2.0	6.7 \pm 4.7	7.7 \pm 4.0
	SP3	7.7 \pm 5.3	4.2 \pm 1.4	5.9 \pm 3.4	6.4 \pm 3.8	5.7 \pm 2.8	4.6 \pm 4.7
	SP4	7.0 \pm 4.3	4.6 \pm 2.3	4.2 \pm 4.0	6.7 \pm 4.5	6.1 \pm 2.7	6.5 \pm 5.5
Thigh	ST1	4.5 \pm 2.8	7.1 \pm 3.3	3.0 \pm 2.5	7.7 \pm 4.7	9.9 \pm 4.7	2.0 \pm 1.4
	ST2	13.7 \pm 7.2	3.7 \pm 2.7	5.2 \pm 3.0	20.6 \pm 10.4	5.5 \pm 4.1	5.5 \pm 2.4
	ST3	3.0 \pm 2.1	11.1 \pm 6.0	9.9 \pm 5.6	7.1 \pm 8.7	16.7 \pm 4.2	5.3 \pm 3.4
	ST4	5.1 \pm 3.7	13.8 \pm 6.4	17.1 \pm 8.9	7.8 \pm 5.4	18.2 \pm 6.8	17.8 \pm 8.7
	ST5	4.9 \pm 3.6	11.4 \pm 5.4	7.8 \pm 3.5	3.1 \pm 1.7	16.8 \pm 5.6	6.5 \pm 6.3
	ST6	7.3 \pm 4.5	11.9 \pm 5.8	8.4 \pm 6.9	6.9 \pm 3.8	16.5 \pm 5.5	8.8 \pm 6.3
	ST7	8.4 \pm 4.8	11.7 \pm 5.4	1.8 \pm 1.5	4.7 \pm 2.6	14.1 \pm 6.9	3.1 \pm 3.2
	ST8	11.3 \pm 7.6	13.7 \pm 4.2	2.6 \pm 1.8	6.5 \pm 3.9	17.0 \pm 3.4	4.9 \pm 5.5
Shank	SS1	7.1 \pm 6.9	2.9 \pm 1.6	3.5 \pm 3.5	8.2 \pm 7.7	5.1 \pm 2.7	3.3 \pm 2.3
	SS2	5.1 \pm 8.1	1.9 \pm 2.1	1.8 \pm 2.0	6.7 \pm 8.4	1.9 \pm 1.0	1.2 \pm 1.5
	SS3	3.0 \pm 4.1	2.9 \pm 1.5	1.4 \pm 1.9	4.4 \pm 4.1	4.0 \pm 1.6	3.9 \pm 1.8
	SS4	2.6 \pm 2.2	6.6 \pm 4.7	3.7 \pm 1.7	4.3 \pm 3.2	8.0 \pm 4.9	7.9 \pm 4.9
	SS5	4.3 \pm 4.9	3.8 \pm 1.7	2.0 \pm 1.9	6.4 \pm 3.5	4.8 \pm 3.1	2.6 \pm 1.6
	SS6	5.2 \pm 4.9	3.4 \pm 2.1	1.2 \pm 0.8	6.6 \pm 5.6	4.5 \pm 3.1	4.0 \pm 4.2
	SS7	6.7 \pm 7.6	4.9 \pm 3.0	3.9 \pm 4.2	7.0 \pm 5.5	8.5 \pm 3.9	5.4 \pm 3.4
	SS8	3.9 \pm 4.6	5.8 \pm 2.9	2.2 \pm 2.0	5.5 \pm 7.9	9.9 \pm 3.0	1.7 \pm 1.2

Appendix D

Definition of TKA implant coordinate system (CSYS)

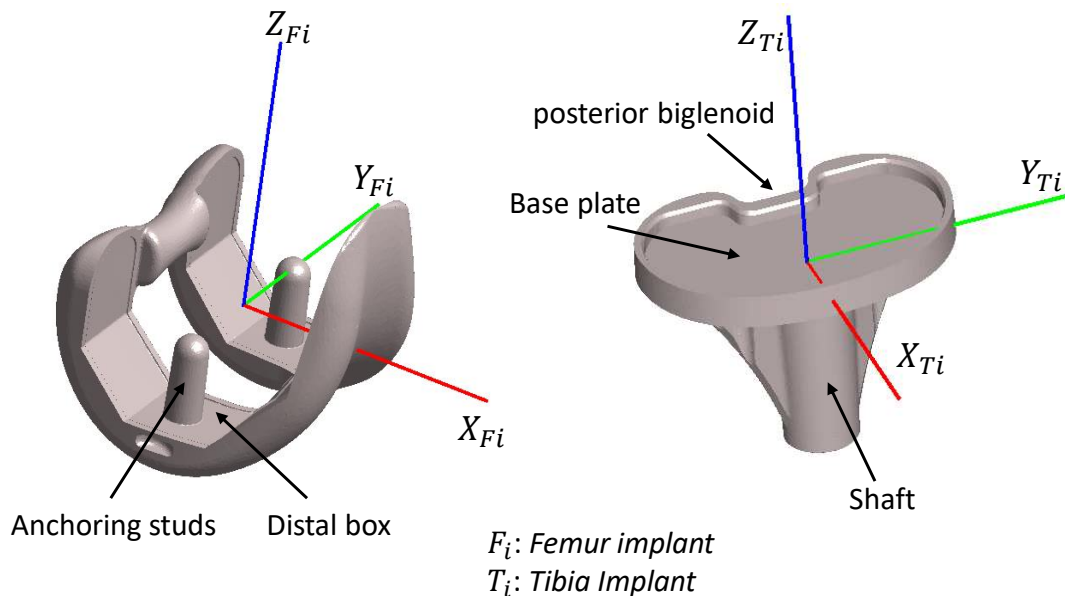


FIGURE D.1: Definition of implant CSYS for the femoral and tibial components

Femoral component:

Center: mid-point of the two anchoring studs.

Z axis: perpendicular to the distal box (directed proximally).

Y axis: line joining the summit of the two anchoring studs (directed medially).

X axis: vector product of Z and Y axes (directed forward).

Tibial component:

Center: Intersection point between the tibial base plate and the inertial axis of the shaft

Z axis: perpendicular to the base plate (directed proximally).

Appendix D. Definition of TKA implant coordinate system (CSYS)

Y axis: Parallel to the posterior biglenoid and perpendicular to Z axis (directed medially).

X axis: vector product of Z and Y axes (directed forward).

Bibliography

- Abulhasan, Jawad F and Michael J Grey (2017). "Anatomy and physiology of knee stability". In: *Journal of Functional Morphology and kinesiology* 2.4, p. 34.
- Adouni, M and A Shirazi-Adl (2009). "Knee joint biomechanics in closed-kinetic-chain exercises". In: *Computer Methods in Biomechanics and Biomedical Engineering* 12.6, pp. 661–670.
- Adouni, M, A Shirazi-Adl, and R Shirazi (2012). "Computational biodynamics of human knee joint in gait: from muscle forces to cartilage stresses". In: *Journal of biomechanics* 45.12, pp. 2149–2156.
- Akbarshahi, Massoud et al. (2010). "Non-invasive assessment of soft-tissue artifact and its effect on knee joint kinematics during functional activity". In: *Journal of biomechanics* 43.7, pp. 1292–1301.
- Ali, Azhar A et al. (2016). "Validation of predicted patellofemoral mechanics in a finite element model of the healthy and cruciate-deficient knee". In: *Journal of biomechanics* 49.2, pp. 302–309.
- Amiri, Shahram et al. (2006). "Mechanics of the passive knee joint. Part 1: the role of the tibial articular surfaces in guiding the passive motion". In: *Proceedings of the Institution of Mechanical Engineers, Part H: Journal of Engineering in Medicine* 220.8, pp. 813–822.
- Anderson, Frank C and Marcus G Pandy (2003). "Individual muscle contributions to support in normal walking". In: *Gait & posture* 17.2, pp. 159–169.
- Andriacchi, Thomas P and Eugene J Alexander (2000). "Studies of human locomotion: past, present and future". In: *Journal of biomechanics* 33.10, pp. 1217–1224.
- Andriacchi, TP et al. (1998). "A point cluster method for in vivo motion analysis: applied to a study of knee kinematics". In:
- Ardestani, Marzieh M et al. (2017). "TKA patients with unsatisfying knee function show changes in neuromotor synergy pattern but not joint biomechanics". In: *Journal of Electromyography and Kinesiology* 37, pp. 90–100.
- Assi, Ayman et al. (2016). "Validation of hip joint center localization methods during gait analysis using 3D EOS imaging in typically developing and cerebral palsy children". In: *Gait & Posture* 48, pp. 30–35.
- Ateshian, Gerard A, Benjamin J Ellis, and Jeffrey A Weiss (2007). "Equivalence between short-time biphasic and incompressible elastic material responses". In:
- Aunan, Eirik et al. (2012). "A new method to measure ligament balancing in total knee arthroplasty: laxity measurements in 100 knees". In: *Archives of orthopaedic and trauma surgery* 132.8, pp. 1173–1181.

- Azmy, C et al. (2010). "EOS® orthopaedic imaging system to study patellofemoral kinematics: Assessment of uncertainty". In: *Orthopaedics & Traumatology: Surgery & Research* 96.1, pp. 28–36.
- Baker, Richard (2006). "Gait analysis methods in rehabilitation". In: *Journal of neuroengineering and rehabilitation* 3.1, p. 4.
- Baldwin, Mark A et al. (2009). "Verification of predicted specimen-specific natural and implanted patellofemoral kinematics during simulated deep knee bend". In: *Journal of biomechanics* 42.14, pp. 2341–2348.
- Baldwin, Mark A et al. (2012). "Dynamic finite element knee simulation for evaluation of knee replacement mechanics". In: *Journal of biomechanics* 45.3, pp. 474–483.
- Bansal, Mohit R et al. (2020). "Tibial alignment technique and its influence on clinical and functional outcomes following total knee arthroplasty". In: *Journal of Clinical Orthopaedics and Trauma*.
- basic medical. URL: <https://basicmedicalkey.com/lower-limb-2/>.
- Beidokhti, Hamid Naghibi et al. (2017). "The influence of ligament modelling strategies on the predictive capability of finite element models of the human knee joint". In: *Journal of biomechanics* 65, pp. 1–11.
- Belvedere, Claudio et al. (2012). "Geometrical changes of knee ligaments and patellar tendon during passive flexion". In: *Journal of biomechanics* 45.11, pp. 1886–1892.
- Bendjaballah, MZea, A Shirazi-Adl, and DJ Zukor (1997). "Finite element analysis of human knee joint in varus-valgus". In: *Clinical biomechanics* 12.3, pp. 139–148.
- Benoit, Daniel L et al. (2006). "Effect of skin movement artifact on knee kinematics during gait and cutting motions measured in vivo". In: *Gait & posture* 24.2, pp. 152–164.
- Bergamini, Elena et al. (2011). "Tibio-femoral joint constraints for bone pose estimation during movement using multi-body optimization". In: *Gait & posture* 33.4, pp. 706–711.
- Beswick, Andrew David et al. (2012). "What proportion of patients report long-term pain after total hip or knee replacement for osteoarthritis? A systematic review of prospective studies in unselected patients". In: *BMJ open* 2.1.
- Bicer, Elcil Kaya et al. (2010). "Current knowledge in the anatomy of the human anterior cruciate ligament". In: *Knee surgery, sports traumatology, arthroscopy* 18.8, pp. 1075–1084.
- Blagojevic, M et al. (2010). "Risk factors for onset of osteoarthritis of the knee in older adults: a systematic review and meta-analysis". In: *Osteoarthritis and cartilage* 18.1, pp. 24–33.
- Blankevoort, L. and R. Huiskes (1991). "Ligament-Bone Interaction in a Three-Dimensional Model of the Knee". In: *Journal of Biomechanical Engineering* 113.3, pp. 263–269.
- Blankevoort, Leendert and Rik Huiskes (1996). "Validation of a three-dimensional model of the knee". In: *Journal of biomechanics* 29.7, pp. 955–961.
- Bolcos, Paul O et al. (2018). "Comparison between kinetic and kinetic-kinematic driven knee joint finite element models". In: *Scientific reports* 8.1, pp. 1–11.
- Bourne, Robert B et al. (2010). "Patient satisfaction after total knee arthroplasty: who is satisfied and who is not?" In: *Clinical Orthopaedics and Related Research®* 468.1, pp. 57–63.
- Brand, Richard A (1989). "Can biomechanics contribute to clinical orthopaedic assessments?" In: *The Iowa Orthopaedic Journal* 9, p. 61.

- Brand, Richard A (1997). "Hip osteotomies: a biomechanical consideration". In: *JAAOS- Journal of the American Academy of Orthopaedic Surgeons* 5.5, pp. 282–291.
- Brandt, KD et al. (2006). *Yet more evidence that osteoarthritis is not a cartilage disease*.
- Burgess, Matthew D and Forshing Lui (2019). "Anatomy, Bony Pelvis and Lower Limb, Pelvic Bones". In: *StatPearls [Internet]*. StatPearls Publishing.
- Burr, DB (2016). *The use of finite element analysis to estimate the changing strength of bone following treatment for osteoporosis*.
- Butler, Robert J et al. (2007). "The effect of a subject-specific amount of lateral wedge on knee mechanics in patients with medial knee osteoarthritis". In: *Journal of orthopaedic research* 25.9, pp. 1121–1127.
- Cameron, Hugh U and Ian Macnab (1972). "The structure of the meniscus of the human knee joint". In: *Clinical Orthopaedics and Related Research*® 89, pp. 215–219.
- Capkin, Sercan et al. (2017). "An anatomic study of the lateral patellofemoral ligament". In: *Acta Orthopaedica et Traumatologica Turcica* 51.1, pp. 73–76.
- Cappello, Angelo et al. (1997). "Multiple anatomical landmark calibration for optimal bone pose estimation". In: *Human movement science* 16.2-3, pp. 259–274.
- Cashman, James P et al. (2011). "Intramedullary versus extramedullary alignment of the tibial component in the Triathlon knee". In: *Journal of orthopaedic surgery and research* 6.1, pp. 1–4.
- Chaibi, Y et al. (2012). "Fast 3D reconstruction of the lower limb using a parametric model and statistical inferences and clinical measurements calculation from biplanar X-rays". In: *Computer methods in biomechanics and biomedical engineering* 15.5, pp. 457–466.
- Charlton, Iain W et al. (2004). "Repeatability of an optimised lower body model". In: *Gait & posture* 20.2, pp. 213–221.
- Cheze, L, BJ Fregly, and J Dimnet (1995). "A solidification procedure to facilitate kinematic analyses based on video system data". In: *Journal of biomechanics* 28.7, pp. 879–884.
- Choi, K et al. (1990). "The elastic moduli of human subchondral, trabecular, and cortical bone tissue and the size-dependency of cortical bone modulus". In: *Journal of biomechanics* 23.11, pp. 1103–1113.
- Choong, Peter F, Michelle M Dowsey, and James D Stoney (2009). "Does accurate anatomical alignment result in better function and quality of life? Comparing conventional and computer-assisted total knee arthroplasty". In: *The Journal of arthroplasty* 24.4, pp. 560–569.
- Clément, Julien et al. (2015). "Soft tissue artifact compensation in knee kinematics by multi-body optimization: Performance of subject-specific knee joint models". In: *Journal of biomechanics* 48.14, pp. 3796–3802.
- (2017). "Can generic knee joint models improve the measurement of osteoarthritic knee kinematics during squatting activity?" In: *Computer methods in biomechanics and biomedical engineering* 20.1, pp. 94–103.
- Colas, S et al. (2016). "Étude de l'utilisation de prothèses de la hanche en France entre 2008 et 2013". In: *Revue d'Épidémiologie et de Santé Publique* 64, S23.

- Correa, Tomas A and Marcus G Pandy (2011). "A mass-length scaling law for modeling muscle strength in the lower limb". In: *Journal of biomechanics* 44.16, pp. 2782–2789.
- Dagneaux, Louis et al. (2015). "Sequential 3D analysis of patellofemoral kinematics from biplanar x-rays: In vitro validation protocol". In: *Orthopaedics & Traumatology: Surgery & Research* 101.7, pp. 811–818.
- Davis, R and P DeLuca (1996). "Clinical gait analysis: current methods and future directions". In: *Human motion analysis: current applications and future directions*, pp. 17–42.
- Davis III, Roy B et al. (1991). "A gait analysis data collection and reduction technique". In: *Human movement science* 10.5, pp. 575–587.
- Delp, Scott L, Abraham V Komattu, and Richard L Wixson (1994). "Superior displacement of the hip in total joint replacement: Effects of prosthetic neck length, neck-stem angle, and anteversion angle on the moment-generating capacity of the muscles". In: *Journal of orthopaedic research* 12.6, pp. 860–870.
- Delp, Scott L, Kimberly Statler, and Norris C Carroll (1995). "Preserving plantar flexion strength after surgical treatment for contracture of the triceps surae: a computer simulation study". In: *Journal of Orthopaedic Research* 13.1, pp. 96–104.
- Delp, Scott L and Felix E Zajac (1992). "Force-and moment-generating capacity of lower-extremity muscles before and after tendon lengthening". In: *Clinical Orthopaedics and Related Research*® 284, pp. 247–259.
- Delp, Scott L et al. (1996). "How superior placement of the joint center in hip arthroplasty affects the abductor muscles". In: *Clinical Orthopaedics and Related Research*® 328, pp. 137–146.
- Dhaher, Yasin Y, Tae-Hyun Kwon, and Megan Barry (2010). "The effect of connective tissue material uncertainties on knee joint mechanics under isolated loading conditions". In: *Journal of biomechanics* 43.16, pp. 3118–3125.
- D'Isidoro, Fabio, Clara Brockmann, and Stephen J Ferguson (2020). "Effects of the soft tissue artefact on the hip joint kinematics during unrestricted activities of daily living." In: *Journal of Biomechanics*, p. 109717.
- Dossett, HG et al. (2014). "A randomised controlled trial of kinematically and mechanically aligned total knee replacements: two-year clinical results". In: *The bone & joint journal* 96.7, pp. 907–913.
- Dubois, Guillaume (2014). "Contribution 'a personalized musculoskeletal modeling of the lower limb combining st 'e r é oradiography and ultrasound." PhD thesis.
- Dubousset, Jean et al. (2010). "EOS: a new imaging system with low dose radiation in standing position for spine and bone & joint disorders". In: *Journal of Musculoskeletal Research* 13.01, pp. 1–12.
- Dumas, Raphaël and Eric Jacquelin (2017). "Stiffness of a wobbling mass models analysed by a smooth orthogonal decomposition of the skin movement relative to the underlying bone". In: *Journal of Biomechanics* 62, pp. 47–52.
- Duprey, Sonia, Laurence Cheze, and Raphaël Dumas (2010). "Influence of joint constraints on lower limb kinematics estimation from skin markers using global optimization". In: *Journal of biomechanics* 43.14, pp. 2858–2862.

- Dyrby, Chris O and Thomas P Andriacchi (2004). "Secondary motions of the knee during weight bearing and non-weight bearing activities". In: *Journal of Orthopaedic Research* 22.4, pp. 794–800.
- Eberhardt, AW et al. (1990). "An analytical model of joint contact". In: *Journal of biomechanical engineering* 112.4, pp. 407–413.
- Eltoukhy, Moataz et al. (2017). "Prediction of ground reaction forces for Parkinson's disease patients using a kinect-driven musculoskeletal gait analysis model". In: *Medical Engineering & Physics* 50, pp. 75–82.
- Erdemir, Ahmet et al. (2007). "Model-based estimation of muscle forces exerted during movements". In: *Clinical biomechanics* 22.2, pp. 131–154.
- Fiorentino, Niccolo M et al. (2017). "Soft tissue artifact causes significant errors in the calculation of joint angles and range of motion at the hip". In: *Gait & posture* 55, pp. 184–190.
- Fiorentino, Niccolo M et al. (2020). "Soft Tissue Artifact Causes Underestimation of Hip Joint Kinematics and Kinetics in a Rigid-Body Musculoskeletal Model". In: *Journal of Biomechanics*, p. 109890.
- Fitzpatrick, Clare K, Chadd W Clary, and Paul J Rullkoetter (2012). "The role of patient, surgical, and implant design variation in total knee replacement performance". In: *Journal of biomechanics* 45.12, pp. 2092–2102.
- Fleming, Braden C et al. (2005). "Ligament injury, reconstruction and osteoarthritis". In: *Current opinion in orthopaedics* 16.5, p. 354.
- Fregly, Benjamin J, Michael L Boninger, and David J Reinkensmeyer (2012). "Personalized neuromusculoskeletal modeling to improve treatment of mobility impairments: a perspective from European research sites". In: *Journal of neuroengineering and rehabilitation* 9.1, p. 18.
- Fridén, Jan and Richard L Lieber (2002). "Tendon transfer surgery: clinical implications of experimental studies." In: *Clinical Orthopaedics and Related Research (1976-2007)* 403, S163–S170.
- Fujii, Toshihide et al. (2020). "A comparative study of weight-bearing and non-weight-bearing 3-dimensional lower extremity alignment in knee osteoarthritis". In: *Journal of Orthopaedic Science*.
- Galbusera, Fabio et al. (2014). "Material models and properties in the finite element analysis of knee ligaments: a literature review". In: *Frontiers in bioengineering and biotechnology* 2, p. 54.
- Gao, Bo and Naiquan Nigel Zheng (2008). "Investigation of soft tissue movement during level walking: translations and rotations of skin markers". In: *Journal of Biomechanics* 41.15, pp. 3189–3195.
- Gardiner, John C, Jeffrey A Weiss, and Thomas D Rosenberg (2001). "Strain in the human medial collateral ligament during valgus loading of the knee". In: *Clinical Orthopaedics and Related Research*® 391, pp. 266–274.

- Gasparutto, Xavier et al. (2015). "Validation of a multi-body optimization with knee kinematic models including ligament constraints". In: *Journal of biomechanics* 48.6, pp. 1141–1146.
- George, Michael S, Warren R Dunn, and Kurt P Spindler (2006). "Current concepts review: revision anterior cruciate ligament reconstruction". In: *The American journal of sports medicine* 34.12, pp. 2026–2037.
- Gérard, Jean-Michel et al. (2006). "A 3D dynamical biomechanical tongue model to study speech motor control". In: *arXiv preprint physics/0606148*.
- Germain, F et al. (2016). "Role of ligaments in the knee joint kinematic behavior: Development and validation of a finite element model". In: *Computational biomechanics for medicine*. Springer, pp. 15–26.
- Girgis, Fakhry G, John L Marshall, and ARS Al MONA JEM (1975). "The cruciate ligaments of the knee joint: anatomical. functional and experimental analysis". In: *Clinical Orthopaedics and Related Research®* 106, pp. 216–231.
- Girion, François, Phillipe Rouch, and Wafa Skalli (2018). "Modélisation musculo-squelettique tridimensionnelle des membres inférieurs à partir de radiographies biplanes". In: *Doctoral Thesis at École nationale supérieure d'arts et métiers*.
- Gittoes, Marianne JR, Mark A Brewin, and David G Kerwin (2006). "Soft tissue contributions to impact forces simulated using a four-segment wobbling mass model of forefoot–heel landings". In: *Human movement science* 25.6, pp. 775–787.
- Goodfellow, John and John O'Connor (1978). "The mechanics of the knee and prosthesis design". In: *The Journal of bone and joint surgery. British volume* 60.3, pp. 358–369.
- Gray, Henry (2009). *Gray's anatomy*. Arcturus Publishing.
- Guess, Trent M, Swithin Razu, and Hamidreza Jahandar (2016). "Evaluation of knee ligament mechanics using computational models". In: *The journal of knee surgery* 29.02, pp. 126–137.
- Halloran, Jason P, Anthony J Petrella, and Paul J Rullkoetter (2005). "Explicit finite element modeling of total knee replacement mechanics". In: *Journal of biomechanics* 38.2, pp. 323–331.
- Halloran, JP et al. (2012). "Multiscale mechanics of articular cartilage: potentials and challenges of coupling musculoskeletal, joint, and microscale computational models". In: *Annals of biomedical engineering* 40.11, pp. 2456–2474.
- Halonon, Kimmo S et al. (2016). "Importance of patella, quadriceps forces, and depthwise cartilage structure on knee joint motion and cartilage response during gait". In: *Journal of biomechanical engineering* 138.7.
- Halonon, KS et al. (2014). "Deformation of articular cartilage during static loading of a knee joint—experimental and finite element analysis". In: *Journal of biomechanics* 47.10, pp. 2467–2474.
- Harris, Michael D et al. (2016). "A combined experimental and computational approach to subject-specific analysis of knee joint laxity". In: *Journal of biomechanical engineering* 138.8.

- Hashemi, Javad et al. (2008). "The geometry of the tibial plateau and its influence on the biomechanics of the tibiofemoral joint". In: *The Journal of Bone and Joint Surgery. American volume*. 90.12, p. 2724.
- Haut Donahue, Tammy L et al. (2002). "A finite element model of the human knee joint for the study of tibio-femoral contact". In: *J. Biomech. Eng.* 124.3, pp. 273–280.
- Herrmann, Ariel M and Scott L Delp (1999). "Moment arm and force-generating capacity of the extensor carpi ulnaris after transfer to the extensor carpi radialis brevis". In: *The Journal of hand surgery* 24.5, pp. 1083–1090.
- Howell, Stephen M et al. (2001). "The relationship between the angle of the tibial tunnel in the coronal plane and loss of flexion and anterior laxity after anterior cruciate ligament reconstruction". In: *The American journal of sports medicine* 29.5, pp. 567–574.
- Hsich, Y-F and LF Draganich (1997). "Knee kinematics and ligament lengths during physiologic levels of isometric quadriceps loads". In: *The Knee* 4.3, pp. 145–154.
- Hume, Donald R et al. (2018). "The interaction of muscle moment arm, knee laxity, and torque in a multi-scale musculoskeletal model of the lower limb". In: *Journal of biomechanics* 76, pp. 173–180.
- Hunt, KD et al. (1998). "Ultrasonic determination of the elastic modulus of human cortical bone". In: *Medical and biological engineering and computing* 36.1, pp. 51–56.
- Irrgang, James J et al. (2001). "Development and validation of the international knee documentation committee subjective knee form". In: *The American journal of sports medicine* 29.5, pp. 600–613.
- Jeffery, Robert S, Richard W Morris, and Robin A Denham (1991). "Coronal alignment after total knee replacement". In: *The Journal of bone and joint surgery. British volume* 73.5, pp. 709–714.
- Joldes, Grand Roman, Adam Wittek, and Karol Miller (2009). "Non-locking tetrahedral finite element for surgical simulation". In: *Communications in Numerical Methods in Engineering* 25.7, pp. 827–836.
- Kang, KT et al. (2018). "A computational simulation study to determine the biomechanical influence of posterior condylar offset and tibial slope in cruciate retaining total knee arthroplasty". In: *Bone & joint research* 7.1, pp. 69–78.
- Keyak, JH et al. (2001). "Prediction of fracture location in the proximal femur using finite element models". In: *Medical engineering & physics* 23.9, pp. 657–664.
- Khurana, Bharti et al. (2014). "Pelvic Ring Fractures: What the Orthopedic Surgeon Wants to Know". In: *Radiographics* 34.5, pp. 1317–1333.
- Kiapour, Ali et al. (2014). "Finite element model of the knee for investigation of injury mechanisms: development and validation". In: *Journal of biomechanical engineering* 136.1.
- Kidziński, Łukasz et al. (2020). "Deep neural networks enable quantitative movement analysis using single-camera videos". In: *Nature communications* 11.1, pp. 1–10.
- Kim, Young-Hoo et al. (2014). "The relationship between the survival of total knee arthroplasty and postoperative coronal, sagittal and rotational alignment of knee prosthesis". In: *International orthopaedics* 38.2, pp. 379–385.

- Kim, Youngwoo et al. (2019). "Stand-to-Sit Kinematics of the Pelvis Is Not Always as Expected: Hip and Spine Pathologies Can Have an Impact". In: *The Journal of arthroplasty* 34.9, pp. 2118–2123.
- Koo, Seungbum, Jonathan H Rylander, and Thomas P Andriacchi (2011). "Knee joint kinematics during walking influences the spatial cartilage thickness distribution in the knee". In: *Journal of biomechanics* 44.7, pp. 1405–1409.
- Kozanek, Michal et al. (2009). "Tibiofemoral kinematics and condylar motion during the stance phase of gait". In: *Journal of biomechanics* 42.12, pp. 1877–1884.
- Kurtz, Steven et al. (2007). "Projections of primary and revision hip and knee arthroplasty in the United States from 2005 to 2030". In: *Jbjs* 89.4, pp. 780–785.
- Lahkar, Bhriugu et al. (2018). "Fast Subject Specific Finite Element Mesh Generation of Knee Joint from Biplanar X-ray Images". In: *15th International Conference in Computer Methods in Biomechanics and Biomedical Engineering*.
- Langlois, Laurent Nod 'e (2003). "Three-dimensional analyzes of angular deviations of the axes of the lower limb, in pr 'e per and postop é ratory". PhD thesis. Paris, ENSAM.
- Laville, A, S Laporte, and W Skalli (2009). "Parametric and subject-specific finite element modelling of the lower cervical spine. Influence of geometrical parameters on the motion patterns". In: *Journal of biomechanics* 42.10, pp. 1409–1415.
- Leardini, Alberto et al. (2005). "Human movement analysis using stereophotogrammetry: Part 3. Soft tissue artifact assessment and compensation". In: *Gait & posture* 21.2, pp. 212–225.
- Lemaire, Roger and Jacques Witvoet (2002). "Prothèses totales du genou". In: *Cahiers d'enseignement de la SOFCOT* 81.
- Lenhart, Rachel L et al. (2015). "Prediction and validation of load-dependent behavior of the tibiofemoral and patellofemoral joints during movement". In: *Annals of biomedical engineering* 43.11, pp. 2675–2685.
- Limbirt, G, M Taylor, and J Middleton (2004). "Three-dimensional finite element modelling of the human ACL: simulation of passive knee flexion with a stressed and stress-free ACL". In: *Journal of biomechanics* 37.11, pp. 1723–1731.
- Logterman, Stephanie L, Frank B Wydra, and Rachel M Frank (2018). "Posterior cruciate ligament: anatomy and biomechanics". In: *Current reviews in musculoskeletal medicine* 11.3, pp. 510–514.
- Löhner, Rainald and Paresh Parikh (1988). "Generation of three-dimensional unstructured grids by the advancing-front method". In: *International Journal for Numerical Methods in Fluids* 8.10, pp. 1135–1149.
- Lu, T-W and JJ O'connor (1999). "Bone position estimation from skin marker co-ordinates using global optimisation with joint constraints". In: *Journal of biomechanics* 32.2, pp. 129–134.
- MacInnes, Scott J, Andrew Gordon, and J Mark Wilkinson (2012). "Risk factors for aseptic loosening following total hip arthroplasty". In: *Recent advances in arthroplasty* 10, p. 26975.

- McLean, Scott G, Anne Su, and Antonie J van den Bogert (2003). "Development and validation of a 3-D model to predict knee joint loading during dynamic movement". In: *J. Biomech. Eng.* 125.6, pp. 864–874.
- Meister, Brad R et al. (2000). "Anatomy and kinematics of the lateral collateral ligament of the knee". In: *The American journal of sports medicine* 28.6, pp. 869–878.
- Melhem, Elias et al. (2016). "EOS® biplanar X-ray imaging: concept, developments, benefits, and limitations". In: *Journal of children's orthopaedics* 10.1, pp. 1–14.
- Mesfar, W and A Shirazi-Adl (2005). "Biomechanics of the knee joint in flexion under various quadriceps forces". In: *The knee* 12.6, pp. 424–434.
- (2006). "Biomechanics of changes in ACL and PCL material properties or prestrains in flexion under muscle force-implications in ligament reconstruction". In: *Computer methods in biomechanics and biomedical engineering* 9.4, pp. 201–209.
- Miller, Mark D and Brian J Cole (2004). *Textbook of arthroscopy*. Vol. 355. Gulf Professional Publishing.
- Mitton, David et al. (2006). "3D reconstruction of the pelvis from bi-planar radiography". In: *Computer methods in biomechanics and biomedical engineering* 9.1, pp. 1–5.
- Moglo, KE and A Shirazi-Adl (2005). "Cruciate coupling and screw-home mechanism in passive knee joint during extension–flexion". In: *Journal of biomechanics* 38.5, pp. 1075–1083.
- Molini, L et al. (2011). "Hip: Anatomy and US technique". In: *Journal of ultrasound* 14.2, pp. 99–108.
- Morgan, Elise F, Ginu U Unnikrisnan, and Amira I Hussein (2018). "Bone mechanical properties in healthy and diseased states". In: *Annual review of biomedical engineering* 20, pp. 119–143.
- Murray, Wendy M et al. (2002). "The influence of elbow position on the range of motion of the wrist following transfer of the brachioradialis to the extensor carpi radialis brevis tendon". In: *JBJS* 84.12, pp. 2203–2210.
- Myers, Casey A et al. (2012). "In vivo tibiofemoral kinematics during 4 functional tasks of increasing demand using biplane fluoroscopy". In: *The American journal of sports medicine* 40.1, pp. 170–178.
- Nardini, Fabrizio et al. (2020). "An Anatomical-Based Subject-Specific Model of In-Vivo Knee Joint 3D Kinematics From Medical Imaging". In: *Applied Sciences* 10.6, p. 2100.
- Navacchia, Alessandro et al. (2019). "A computationally efficient strategy to estimate muscle forces in a finite element musculoskeletal model of the lower limb". In: *Journal of Biomechanics* 84, pp. 94–102.
- Neptune, Richard R, Felix E Zajac, and Steven A Kautz (2009). "Author's Response to Comment on "Contributions of the individual ankle plantar flexors to support, forward progression and swing initiation during walking"(Neptune et al., 2001) and "Muscle mechanical work requirements during normal walking: The energetic cost of raising the body's center-of-mass is significant"()". In: *Journal of biomechanics* 42.11, p. 1786.

- Onishi, Y and K Amaya (2014). "A locking-free selective smoothed finite element method using tetrahedral and triangular elements with adaptive mesh rezoning for large deformation problems". In: *International Journal for Numerical Methods in Engineering* 99.5, pp. 354–371.
- Orsi, Alexander D et al. (2016). "The effects of knee joint kinematics on anterior cruciate ligament injury and articular cartilage damage". In: *Computer methods in biomechanics and biomedical engineering* 19.5, pp. 493–506.
- Parratte, Sebastien et al. (2010). "Effect of postoperative mechanical axis alignment on the fifteen-year survival of modern, cemented total knee replacements". In: *JBJS* 92.12, pp. 2143–2149.
- Payen, Daniel Jose and Klaus-Jürgen Bathe (2011). "Improved stresses for the 4-node tetrahedral element". In: *Computers & structures* 89.13-14, pp. 1265–1273.
- Pedersen, Dennis et al. (2019). "A novel non-invasive method for measuring knee joint laxity in four dof: In vitro proof-of-concept and validation". In: *Journal of biomechanics* 82, pp. 62–69.
- Pena, E et al. (2005). "A finite element simulation of the effect of graft stiffness and graft tensioning in ACL reconstruction". In: *Clinical Biomechanics* 20.6, pp. 636–644.
- Pena, E et al. (2006). "A three-dimensional finite element analysis of the combined behavior of ligaments and menisci in the healthy human knee joint". In: *Journal of biomechanics* 39.9, pp. 1686–1701.
- Petersen, Wolf and Thore Zantop (2007). "Anatomy of the anterior cruciate ligament with regard to its two bundles". In: *Clinical Orthopaedics and Related Research®* 454, pp. 35–47.
- Piazza, Stephen J and Scott L Delp (1996). "The influence of muscles on knee flexion during the swing phase of gait". In: *Journal of biomechanics* 29.6, pp. 723–733.
- Pillet, Hélène et al. (2014). "A reference method for the evaluation of femoral head joint center location technique based on external markers". In: *Gait & posture* 39.1, pp. 655–658.
- Pillet, Hélène et al. (2016). "Femur, tibia and fibula bone templates to estimate subject-specific knee ligament attachment site locations". In: *Journal of Biomechanics* 49.14, pp. 3523–3528.
- Quijano, S et al. (2013). "Three-dimensional reconstruction of the lower limb from biplanar calibrated radiographs". In: *Medical engineering & physics* 35.12, pp. 1703–1712.
- Rachmat, HH et al. (2016). "In-situ mechanical behavior and slackness of the anterior cruciate ligament at multiple knee flexion angles". In: *Medical engineering & physics* 38.3, pp. 209–215.
- Radtke, Kerstin et al. (2010). "Effect of limb rotation on radiographic alignment in total knee arthroplasties". In: *Archives of orthopaedic and trauma surgery* 130.4, pp. 451–457.
- Ramos, A and JA Simoes (2006). "Tetrahedral versus hexahedral finite elements in numerical modelling of the proximal femur". In: *Medical engineering & physics* 28.9, pp. 916–924.
- Reinbolt, Jeffrey A et al. (2005). "Determination of patient-specific multi-joint kinematic models through two-level optimization". In: *Journal of biomechanics* 38.3, pp. 621–626.

- Reinschmidt, Christoph et al. (1997). "Effect of skin movement on the analysis of skeletal knee joint motion during running". In: *Journal of biomechanics* 30.7, pp. 729–732.
- Richard, Vincent, Aurelio Cappozzo, and Raphaël Dumas (2017). "Comparative assessment of knee joint models used in multi-body kinematics optimisation for soft tissue artefact compensation". In: *Journal of biomechanics* 62, pp. 95–101.
- Richard, Vincent et al. (2016). "Knee kinematics estimation using multi-body optimisation embedding a knee joint stiffness matrix: a feasibility study". In: *PloS one* 11.6, e0157010.
- Ritter, Merrill A et al. (1996). "Patellofemoral complications following total knee arthroplasty: effect of a lateral release and sacrifice of the superior lateral geniculate artery". In: *The Journal of arthroplasty* 11.4, pp. 368–372.
- Ritter, Merrill A et al. (2011). "The effect of alignment and BMI on failure of total knee replacement". In: *JBJS* 93.17, pp. 1588–1596.
- Rochcongar, Goulven et al. (2016). "A new method for the evaluation of the end-to-end distance of the knee ligaments and popliteal complex during passive knee flexion". In: *The Knee* 23.3, pp. 420–425.
- Rohan, P-Y et al. (2017). "Finite element models of the human tongue: a mixed-element mesh approach". In: *Computer Methods in Biomechanics and Biomedical Engineering: Imaging & Visualization* 5.6, pp. 390–400.
- Rouhandeh, Azadeh and Chris Joslin (2018). "Soft-tissue Artefact Assessment and Compensation in Motion Analysis by Combining Motion Capture Data and Ultrasound Depth Measurements." In: *VISIGRAPP (4: VISAPP)*, pp. 511–521.
- Rupin, Fabienne et al. (2008). "Experimental determination of Young modulus and Poisson ratio in cortical bone tissue using high resolution scanning acoustic microscopy and nanoindentation". In: *The Journal of the Acoustical Society of America* 123.5, pp. 3785–3785.
- Sabet, Fereshteh A et al. (2016). "Modelling of bone fracture and strength at different length scales: a review". In: *Interface focus* 6.1, p. 20150055.
- Sangeux, M et al. (2006). "Quantification of the 3D relative movement of external marker sets vs. bones based on magnetic resonance imaging". In: *Clinical Biomechanics* 21.9, pp. 984–991.
- Sangeux, Morgan, Alana Peters, and Richard Baker (2011). "Hip joint centre localization: Evaluation on normal subjects in the context of gait analysis". In: *Gait & posture* 34.3, pp. 324–328.
- Saraswat, Prabhav, Michael S Andersen, and Bruce A MacWilliams (2010). "A musculoskeletal foot model for clinical gait analysis". In: *Journal of biomechanics* 43.9, pp. 1645–1652.
- Sauret, Christophe et al. (2016). "On the use of knee functional calibration to determine the medio-lateral axis of the femur in gait analysis: comparison with EOS biplanar radiographs as reference". In: *Gait & Posture* 50, pp. 180–184.
- Scheys, Lennart et al. (2008a). "Calculated moment-arm and muscle-tendon lengths during gait differ substantially using MR based versus rescaled generic lower-limb musculoskeletal models". In: *Gait & posture* 28.4, pp. 640–648.

- Scheys, Lennart et al. (2008b). "Personalized MR-based musculoskeletal models compared to rescaled generic models in the presence of increased femoral anteversion: effect on hip moment arm lengths". In: *Gait & posture* 28.3, pp. 358–365.
- Scheys, Lennart et al. (2011). "Calculating gait kinematics using MR-based kinematic models". In: *Gait & posture* 33.2, pp. 158–164.
- Schlatterer, B et al. (2009). "Skeletal landmarks for TKR implantations: evaluation of their accuracy using EOS imaging acquisition system". In: *Orthopaedics & Traumatology: Surgery & Research* 95.1, pp. 2–11.
- Schmidt, Deanna J et al. (1999). "Length changes of the hamstrings and adductors resulting from derotational osteotomies of the femur". In: *Journal of Orthopaedic Research* 17.2, pp. 279–285.
- Schroer, William C et al. (2013). "Why are total knees failing today? Etiology of total knee revision in 2010 and 2011". In: *The Journal of arthroplasty* 28.8, pp. 116–119.
- Schwartz, Ariel, Snehal Chokhandre, and Ahmet Erdemir (2019). "What we said, what we did: Understanding subjective decisions during development of knee models". In: *16th International Conference in Computer Methods in Biomechanics and Biomedical Engineering*.
- Seffinger, Michael A and Raymond J Hrubby (2007). *Evidence-based manual medicine: a problem-oriented approach*. Elsevier Health Sciences.
- Sharifi, M, A Shirazi-Adl, and H Marouane (2017). "Computational stability of human knee joint at early stance in Gait: Effects of muscle coactivity and anterior cruciate ligament deficiency". In: *Journal of biomechanics* 63, pp. 110–116.
- Sherman, Seth L et al. (2012). "Graft tensioning during knee ligament reconstruction: principles and practice". In: *JAAOS-Journal of the American Academy of Orthopaedic Surgeons* 20.10, pp. 633–645.
- Shin, Choongsoo S, Ajit M Chaudhari, and Thomas P Andriacchi (2007). "The influence of deceleration forces on ACL strain during single-leg landing: a simulation study". In: *Journal of biomechanics* 40.5, pp. 1145–1152.
- Shirazi, R, A Shirazi-Adl, and M Hurtig (2008). "Role of cartilage collagen fibrils networks in knee joint biomechanics under compression". In: *Journal of biomechanics* 41.16, pp. 3340–3348.
- Shu, Liming et al. (2018). "A subject-specific finite element musculoskeletal framework for mechanics analysis of a total knee replacement". In: *Journal of biomechanics* 77, pp. 146–154.
- Skalli, Wafa et al. (2018). "A subject-specific finite element based method for soft tissue artefact reduction in motion analysis". In: *8th World Congress of Biomechanics*. URL: <https://app.oxfordabstracts.com/events/123/program-app/submission/24056>.
- Smale, Kenneth B et al. (2019). "Effect of implementing magnetic resonance imaging for patient-specific OpenSim models on lower-body kinematics and knee ligament lengths". In: *Journal of biomechanics* 83, pp. 9–15.
- Smith, Colin R et al. (2016). "The influence of component alignment and ligament properties on tibiofemoral contact forces in total knee replacement". In: *Journal of biomechanical engineering* 138.2.

- Snell, Richard S (2010). *Clinical neuroanatomy*. Lippincott Williams & Wilkins.
- Sodhi, Nipun et al. (2018). "The learning curve associated with robotic total knee arthroplasty". In: *The journal of knee surgery* 31.01, pp. 017–021.
- Stagni, Rita et al. (2005). "Quantification of soft tissue artefact in motion analysis by combining 3D fluoroscopy and stereophotogrammetry: a study on two subjects". In: *Clinical Biomechanics* 20.3, pp. 320–329.
- Stanaway, Jeffrey D et al. (2019). "The global burden of typhoid and paratyphoid fevers: a systematic analysis for the Global Burden of Disease Study 2017". In: *The Lancet Infectious Diseases* 19.4, pp. 369–381.
- Südhoff, Ingrid et al. (2007). "Comparing three attachment systems used to determine knee kinematics during gait". In: *Gait & posture* 25.4, pp. 533–543.
- Surer, Elif and Alper Kose (2011). "Methods and technologies for gait analysis". In: *Computer Analysis of Human Behavior*. Springer, pp. 105–123.
- Tanska, Petri, Mika E Mononen, and Rami K Korhonen (2015). "A multi-scale finite element model for investigation of chondrocyte mechanics in normal and medial meniscectomy human knee joint during walking". In: *Journal of biomechanics* 48.8, pp. 1397–1406.
- Tashman, S and W Anderst (2002). "Skin motion artifacts at the knee during impact movements". In: *Gait & Posture* 16, pp. 11–12.
- Taubin, Gabriel (1995). "Curve and surface smoothing without shrinkage". In: *Proceedings of IEEE international conference on computer vision*. IEEE, pp. 852–857.
- Tautges, Timothy J, Ted Blacker, and Scott A Mitchell (1996). "The whisker weaving algorithm: a connectivity-based method for constructing all-hexahedral finite element meshes". In: *International Journal for Numerical Methods in Engineering* 39.19, pp. 3327–3349.
- Tocks, Gregory A et al. (2018). *Biomechanics of the knee*, pp. 85–93.
- Trochu, François (1993). "A contouring program based on dual kriging interpolation". In: *Engineering with computers* 9.3, pp. 160–177.
- Vaienti, Enrico et al. (2017). "Understanding the human knee and its relationship to total knee replacement". In: *Acta Bio Medica: Atenei Parmensis* 88.Suppl 2, p. 6.
- Valente, Giordano et al. (2014). "Are subject-specific musculoskeletal models robust to the uncertainties in parameter identification?" In: *PLoS One* 9.11, e112625.
- Valente, Giordano et al. (2015). "Effect of lower-limb joint models on subject-specific musculoskeletal models and simulations of daily motor activities". In: *Journal of biomechanics* 48.16, pp. 4198–4205.
- Veldpaus, FE, HJ Woltring, and LJMG Dortmans (1988). "A least-squares algorithm for the equiform transformation from spatial marker co-ordinates". In: *Journal of biomechanics* 21.1, pp. 45–54.
- Viala, Pierre et al. (2016). "Imaging of the postoperative knee". In: *Diagnostic and interventional imaging* 97.7-8, pp. 823–837.
- Walker, Peter S (2015). "The design and pre-clinical evaluation of knee replacements for osteoarthritis". In: *Journal of Biomechanics* 48.5, pp. 742–749.

- Wedegaertner, U et al. (2003). "Multislice CT (MSCT) in the detection and classification of pelvic and acetabular fractures; Multislice CT (MSCT) in der Detektion und Klassifikation von Becken-und Azetabulumfrakturen". In: *RoeFo - Fortschritte auf dem Gebiete der Roentgenstrahlen und der Neuen Bildgebenden Verfahren* 175 (1).
- Wismans, JAC et al. (1980). "A three-dimensional mathematical model of the knee-joint". In: *Journal of biomechanics* 13.8, pp. 677–685.
- Woo, Savio L.-Y. et al. (1990). "Measurement of Changes in Ligament Tension with Knee Motion and Skeletal Maturation". In: *Journal of Biomechanical Engineering* 112.1, pp. 46–51.
- Xie, Xin et al. (2017). "Effect of rotational prosthetic alignment variation on tibiofemoral contact pressure distribution and joint kinematics in total knee replacement". In: *Proceedings of the Institution of Mechanical Engineers, Part H: Journal of Engineering in Medicine* 231.11, pp. 1034–1047.
- Xu, Chun et al. (2016). "An integrated musculoskeletal-finite-element model to evaluate effects of load carriage on the tibia during walking". In: *Journal of Biomechanical Engineering* 138.10.
- Yaffe, Mark et al. (2014). "Clinical, functional, and radiographic outcomes following total knee arthroplasty with patient-specific instrumentation, computer-assisted surgery, and manual instrumentation: a short-term follow-up study". In: *International journal of computer assisted radiology and surgery* 9.5, pp. 837–844.
- Yang, NH et al. (2010). "Protocol for constructing subject-specific biomechanical models of knee joint". In: *Computer methods in biomechanics and biomedical engineering* 13.5, pp. 589–603.
- Yerry, Mark A and Mark S Shephard (1984). "Automatic three-dimensional mesh generation by the modified-octree technique". In: *International Journal for Numerical Methods in Engineering* 20.11, pp. 1965–1990.
- Yu, Chung-Huang, Peter S Walker, and Michael E Dewar (2001). "The effect of design variables of condylar total knees on the joint forces in step climbing based on a computer model". In: *Journal of biomechanics* 34.8, pp. 1011–1021.
- Zaylor, William, Bernard N Stulberg, and Jason P Halloran (2019). "Use of distraction loading to estimate subject-specific knee ligament slack lengths". In: *Journal of biomechanics* 92, pp. 1–5.
- Zeng, Huan Bei et al. (2015). "Extramedullary versus intramedullary tibial alignment technique in total knee arthroplasty: A meta-analysis of randomized controlled trials". In: *Clinics* 70.10, pp. 714–719.
- Zheng, Yongping and Arthur FT Mak (1999). "Effective elastic properties for lower limb soft tissues from manual indentation experiment". In: *IEEE Transactions on Rehabilitation Engineering* 7.3, pp. 257–267.
- Zhu, Meng et al. (2017). "Outcomes following total knee arthroplasty with CT-based patient-specific instrumentation". In: *Knee Surgery, Sports Traumatology, Arthroscopy* 25.8, pp. 2567–2572.

Bibliography

Zlotnicki, Jason P et al. (2016). "Basic biomechanic principles of knee instability". In: *Current reviews in musculoskeletal medicine* 9.2, pp. 114–122.

CONTRIBUTION À LA MODÉLISATION MUSCULOSQUELETTIQUE PERSONNALISÉE DU MEMBRE INFÉRIEUR PAR ELEMENTS FINIS

RESUME : Le trouble musculosquelettique du membre inférieur est l'un des fardeaux de santé les plus courants pouvant entraîner une déficience fonctionnelle chez un individu. Bien que diverses options de gestion opérationnelle soient disponibles, il ne semble pas y avoir unanimité sur une procédure particulière qui servirait au mieux les intérêts de tous. Pour évaluer objectivement les troubles et planifier efficacement les interventions chirurgicales, il est essentiel de comprendre la biomécanique des membres inférieurs dans des conditions de charge physiologique. Avec cette motivation, ce travail de thèse vise à développer un cadre complet de modélisation musculosquelettique du membre inférieur basé sur les éléments finis. La première phase du travail de thèse est axée sur le développement et l'évaluation de modèles personnalisés d'éléments finis en flexion passive. De nouvelles approches sont proposées et évaluées pour le développement rapide de modèles axés sur la géométrie et les propriétés des ligaments. Dans la deuxième phase, une nouvelle approche basée sur les éléments finis pour la compensation des artefacts des tissus mous est proposée et évaluée. Cette contribution a permis de compenser efficacement les artefacts des tissus mous dans l'analyse du mouvement en tenant compte de la spécificité du sujet. La troisième phase du travail de thèse est consacrée à l'application clinique, où l'utilité du système radiographique biplan dans l'évaluation de l'alignement des implants de l'arthroplastie totale du genou est brièvement explorée.

Dans l'ensemble, ce travail de thèse peut aider à estimer et à comprendre avec précision la biomécanique des membres inférieurs dans des conditions de charge cliniquement pertinentes, et à rapprocher le modèle de la routine clinique.

Mots clés : Modélisation personnalisée, Éléments finis, Articulation du genou, Artefact des tissus mous, Biomécanique, Radiographie biplanaire

CONTRIBUTION TO PERSONLIZED FINITE ELEMENT BASED MUSCULOSKELETAL MODELING OF THE LOWER LIMB

ABSTRACT : Musculoskeletal disorder of the lower limb is one of the most common health burdens that may lead to functional impairment in an individual. Although various operative management options are available, there seems no unanimity on a particular procedure that serves the best. To objectively assess disorders and effectively plan surgeries, it is essential to understand lower limb biomechanics under physiological loading conditions. With that motivation, this PhD aims to develop a comprehensive finite element based musculoskeletal modeling framework of the lower limb. The first phase of the PhD focuses on the development and evaluation of subject-specific finite element models under passive flexion. Novel approaches are proposed and evaluated for fast model development focusing on geometry and ligament properties. In the second phase, a novel finite element based approach for soft tissue artifact compensation is proposed and evaluated. This contribution allowed to effectively compensate for soft tissue artifact in motion analysis by taking subject specificity into account. The third phase of the PhD is dedicated to clinical application, where the utility of the biplanar X-ray system in evaluating Total Knee Arthroplasty implant alignment is briefly explored.

Overall, this PhD may help to accurately estimate and understand lower limb biomechanics under clinically relevant loading conditions, and bring the model a step closer to clinical routine.

Keywords : Subject-specific modeling, Finite Element analysis, Knee joint, Soft Tissue Artifact, Biomechanics, Biplanar X-ray